DROP TEST SIMULATION OF A MUNITION WITH FOAMS AND
PARAMETRIC STUDY ON FOAM GEOMETRY AND MATERIAL

A THESIS SUBMITTED TO
THE GRADUATE SCHOOL OF NATURAL AND APPLIED SCIENCES
OF
MIDDLE EAST TECHNICAL UNIVERSITY

BY

BORA GERÇEKER

IN PARTIAL FULFILLMENT OF THE REQUIREMENTS
FOR
THE DEGREE OF MASTER OF SCIENCE
IN
MECHANICAL ENGINEERING

SEPTEMBER 2012

Approval of the Thesis:

DROP TEST SIMULATION OF A MUNITION WITH FOAMS AND OPTIMIZATION OF FOAM GEOMETRY TO PROVIDE SURVAVIBILITY

submitted by **BORA GERÇEKER** in partial fulfillment of the requirements for the degree of **Master of Science in Mechanical Engineering Department, Middle East Technical University** by,

Prof. Dr. Canan Özgen   _____
Dean, Graduate School of **Natural and Applied Sciences**

Prof. Dr. Süha Oral   _____
Head of Department, **Mechanical Engineering**

Prof. Dr. Abdullah Ulaş   _____
Supervisor, **Mechanical Engineering Dept., METU**

Examining Committee Members:

Prof. Dr. Suat Kadıoğlu   _____
Mechanical Engineering Dept., METU

Prof. Dr. Abdullah Ulaş   _____
Mechanical Engineering Dept., METU

Prof. Dr. Levend Parnas   _____
Mechanical Engineering Dept., METU

Asst. Prof. Gökhan Özgen   _____
Mechanical Engineering Dept., METU

M. Sc. Eng. Bülent Acar   _____
Lead Engineer, ROKETSAN

Date: _____

I hereby declare that all information in this document has been obtained and presented in accordance with academic rules and ethical conduct. I also declare that, as required by these rules and conduct, I have fully cited and referenced all material and results that are not original to this work.

Name, Last name: Bora GERÇEKER

Signature   :

ABSTRACT

DROP TEST SIMULATION OF A MUNITION WITH FOAMS AND PARAMETRIC STUDY ON FOAM GEOMETRY AND MATERIAL

Gerçeker, Bora

M.S., Department of Mechanical Engineering

Supervisor: Prof. Dr. Abdullah ULAŞ

Co-Supervisor: Prof. Dr. K. Levend PARNAS

September 2012, 162 pages

Unintentional drop of munitions could be encountered during the storage, transportation, and loading processes. In such an impact, malfunctioning of crucial components of munitions is the worst scenario that may be encountered and level of loads should not reach to critical levels. From two possible methods, experimental one is not frequently applied owing to high cost of money and time. On the contrary, particularly in last couple of years, interest is shifted to numerical simulations such as finite element method.

In this thesis, foam materials will be investigated as energy absorbers to reduce the effect of loads during the impact. However, modeling the behavior of foam materials by FE codes is a challenging task. In other words, more than a few material parameters which are not commonly specified in literature are sufficient to represent the behavior of foams in an appropriate way. For this reason, material characteristics of the selected two foam materials, expanded polypropylene and

polyethylene, have been obtained in this study. Characterization of EPP and PE is followed by the selection of the appropriate material models in LS-DYNA which is a nonlinear explicit finite element code.

Drop tests of munitions on which initially specified foam materials are integrated were done to identify the load levels. Validation of drop tests which are explained in detail in this thesis has been accomplished by LS-DYNA. Final section of the thesis is related to optimization of the foam geometry which will provide reducing load levels to allowable limits. After optimization studies, three alternative geometries which succeed in to reduce loads to allowable load levels were reached. Finally, one of three alternatives is selected considering cost and manufacturing difficulties.

Keywords: Munition, expanded polypropylene, polyethylene, material characterization, foam material models, hexagonal geometry, geometrical optimization

ÖZ

KÖPÜK MALZEME ENTEGRE EDİLMİŞ MÜHİMMAT DÜŞÜRME TESTLERİ SİMÜLASYONLARI VE KÖPÜK MALZEMELERİN BOYUTSAL OPTİMİZASYONU

Gerçeker, Bora

Yüksek Lisans, Makina Mühendisliği Bölümü

Tez Yöneticisi: Prof. Dr. Abdullah Ulaş

Ortak Tez Yöneticisi: Prof. Dr. K.Levend Parnas

Eylül 2012, 162 sayfa

Mühimmatlar, depolama, taşıma, istifleme vb gibi durumlarda istenmeyen düşürme senaryoları ile karşılaşabilmektedir. Böyle bir senaryoda mühimmat üzerinde kritik komponentlerin fonksiyonelliklerini yitirmemeleri gerekmektedir ve bunun icin askeri standartlarda belirlenen kritik yük seviyelerinin geçilmemesi gerekmektedir.

Bunun sağlanabilmesi için kullanılan metodlardan biri yüksek maliyet ve zaman problemlerini doğuran deneysel metodlardır. Son yıllarda ise deneysel metodlar yerine numerik metodlara bir eğilim gorülmektedir ve sonlu elemanlar metoduna sıkça başvurulmaktadır.

Köpük malzemelerin enerji emebilme yetenekleri sayesinde düşürme anında ortaya çıkan yük seviyeleri azaltılabilmektedir. Ancak sonlu elemanlar kodları ile köpük malzemelerin davranışlarının sergilenmesi oldukça zordur. Bunun temel nedeni de

köpük malzemelere ait malzeme parametrelerinin literatürde sıkça yer almamasıdır. Bu yüzden seçilen iki köpük malzemeye ait parametreler malzeme karakterizasyon testleri ile belirlenmiştir. Bir sonraki aşamada ise bu malzemelere uygun malzeme modelleri kullanılan nümerik kod olan LS-DYNA içinden seçilmiştir.

Daha sonra mühimmatların düşürme testleri ile ortaya çıkan yük mertebeleri belirlenmiştir. Bu testlerin nümerik ortamda simulasyonları ise bir sonraki adımdır ve bu aşamada benzer mertebelere ulaşıldığı görülmüştür. Yapılan çalışmaların son bölümlerinde ise test ve analizlerde görülen yüksek yük seviyelerini kabul edilebilir limitlere çekebilmek için nümerik ortamda köpük malzemelerin boyutları üzerinde parametrik bir çalışma gerçekleştirilmiştir. Yapılan parametrik çalısma sonunda mühimmat üzerindeki yük seviyelerini kabul edilebilir seviyelere çeken üç adet alternatif geometri belirlenmiştir. Son olarak da bu üç alternatiften üretimsel zorluklar ve maliyet unsurlari da göz önüne alınarak en uygun olanı seçilmiştir.

Anahtar Kelimeler: Muhimmat, genişletilmiş polipropelin, polietilen, malzeme karakterizasyonu, köpük malzeme modelleri, altıgen geometri, boyutsal optimizasyon

TO MY FAMILY

ACKNOWLEDGMENTS

TABLE OF CONTENTS

LIST OF TABLES

TABLES

LIST OF FIGURES

FIGURES

LIST OF SYMBOLS

a : Acceleration

g : Gravity

m: Mass

V : Velocity

h: Drop height

k: Stiffness

c: Damping coefficient

$u(t)$: Displacement as a function time

$f(t)$: Force as a function of time

h^*: Vertical displacement between Connector 1 and the ground at the time of maximum crush

V_0 : Initial velocity

ρ: Density

σ: Stress

ε: Strain

$\dot{\varepsilon}$: Strain rate

ε_D: Dynamic relaxation modulus

$\dot{x}$: 1st derivative of displacement with respect to time

$\ddot{x}$: 2nd derivative of displacement with respect to time

E: Young Modulus

A: Area

L: Length of beam element

w_{max} : Maximum natural frequency

$\Delta t_{critical}$: Critical time step

c_{beam} : Speed of sound for beam

c_{2D} : Speed of sound for a 2D element

c_{3D} : Speed of sound for a 3D element

$p1$: Distance of accelerometer-1 from the nose of missile

$p2$: Distance of accelerometer-2 from the nose of missile

$p2$: Distance of accelerometer-3 from the nose of missile

LIST OF ABBREVIATIONS

FE: Finite Element

EPP: Expanded Polypropylene

PE: Polyethylene

PU: Polyurethane

Material Model 1: *MAT_FU_CHANG_FOAM

Material Model 2: *MAT_MODIFIED_CRUSHABLE_FOAM

Contact Model 1: *CONTACT_TIED_NODES_TO_SURFACE

Contact Model 2: *CONTACT_AUTOMATIC_SURFACE_TO_SURFACE

ESD: Energy spectral density method

FAA: Federal Aviation Administration

ATD: Anthropomorphic Test Dummy

MIL-STD: Military Standard

COG: Center of Gravity

CHAPTER 1

INTRODUCTION

1.1   GENERAL

An unexpected drop scenario causing loads that cannot be disregarded is the worst case for a munition while it is transported, stored or stacked.   What is not acceptable after such an impact is malfunctioning of the components on munitions which are mainly electronic.   Due to the shock-induced vibrations measured by accelerometers on munitions, one can easily claim that such devices may not keep their structural integrity. However, as long as allowable limits of loads are not exceeded, loads on munitions are said to be acceptable.   It is somehow possible to reduce the load levels on munitions. As it is most commonly seen in military projects, energy absorbing materials, foams, have a big mission for this purpose.

There is no better way than drop tests to be able to detect the allowable range of loads on components. Thanks to the drop tests, it is possible to observe whether critical components are damaged or not. In military applications such tests are often applied. Automobile and white good companies also conduct these tests to be aware of the consequences of unintended drop cases.   Besides the pros of conducting such tests, cons of the same procedure should not also be underestimated. Necessity of excessive amount of money and time are mutual pitfalls that cannot be pushed something into the background in drop tests.

Owing to great expense of money and time of experimental studies, finite element simulations take to the stage. Within the Millennium and following years, it has become a routine process to simulate even very complex models that were nearly impossible previously. Nowadays, companies have to lower their budgets for

carrying out experimental studies; instead arising capabilities of computers force them to expand their budgets for technologic innovations. For the avoidance of misunderstanding, it should be stated that performing drop analysis by FE codes aims not to put an end to the tests entirely, but to reduce the number of tests. A nonlinear dynamic explicit finite element code, LS-DYNA, is a valuable tool for performing such types of analysis. Two main reasons can be asserted to explain why LS-DYNA is the best choice. The former is its pre-eminent position in similar codes when contact capabilities are taken into account. The latter, LS-DYNA offers a wide selection of foam modeling alternatives (20 distinct foam models are available) which is rare compared to similar codes.

As it is stated earlier, high levels of g which is expressed as ten times of gravity should be reduced to tolerable degrees. Foam materials whose dissipation of energy capability and withstanding large compressible strains fit for this goal. However, not only absorption capabilities and good resistance to strain but also low weights make them use widely. By integrating appropriate dense and shaped foam materials to the munitions for tests, key components can be now safe and no longer in danger of malfunctioning. Whereas, when FE modeling of foams is the case, big troubles are encountered owing to absence of physical and mechanic parameters. For this reason, characterization of foam materials which is a very expensive process is inevitable. Expanded Polypropylene (EPP) and Polyethylene (PE) are commonly used foam types thanks to their unique features that will be enlightened later. In the light of this procedure, desired material properties of EPP and PE at different densities and strain rates are attained. (Young moduli, stress-strain curves, yield stresses etc.). Reaction force versus time graphs are also attained by this process and they will be used for validation of material testing later.

Validation of numerical results with experimental results is an indispensable task for analyst to start over further analysis. Thus, it needs to be paid strict attention to the process of validation. Goal of validation process is to solve the model numerically and compare its results with the tests. Similar path of curves for

acceleration, strain and energy is expected. Furthermore, peak values of both test and analysis curves should be close to each other.

To be able to have a good correlation between test and analysis, one should pay attention to data filtering. Accelerations recorded on munitions need to be filtered due to high frequency content. Particularly, it is necessary to filter the data if the energy of the signal is low at high frequencies. This brings us to the concept of energy spectral density method (ESD) which will be explained in detail in following chapters. Above mentioned concepts are related to post-processing which will designate whether test-analysis correlation is sufficient or not.

Optimization process of foam geometry is last, but not least part of this thesis. An initial geometry for foam parts is established thanks to similar studies utilized throughout time. Initial geometry is of course needed to be optimized to be able to obtain desired values in terms of acceleration. Parametric study on foam dimensions, material type and density will be done in this thesis. Optimization process is based on the trial and error method. Apart from shape optimization, cost as well as time-consumed are taken into consideration to select the ultimate model. In the light of these developments, optimized-shaped foam geometry is integrated to the munitions and subjected to final drop tests. To finalize the study, validation of the tests is again carried out.

1.2 OBJECTIVES OF THE THESIS

The fundamental task of the thesis is to lower the effects of impact on munitions in terms of g level so that critical components on munitions can go on functioning properly. Integration of foams as energy absorbers into the system helps critical components not to lose their functionality.

Finite element modeling of a drop scenario is always a challenging process due to the fact that excessive deformations and nonlinear behaviors come to the stage. A very common usage of foam materials in drop cases makes this kind of analysis even harder. Absence of mechanical properties of foam materials is the main problem. For this reason material characterization tests of the foam materials should be performed.

Later, appropriate material models in LS-DYNA should be selected by using the results of material characterization tests. This is followed by drop tests of munitions with initial shaped foam designs. After validation of the simulations of drop cases are performed, a parametric study should be done in order to select the best alternative. After this selection, final tests should be conducted in order to verify the model.

A flowchart of the thesis study is given in Figure 1-1.
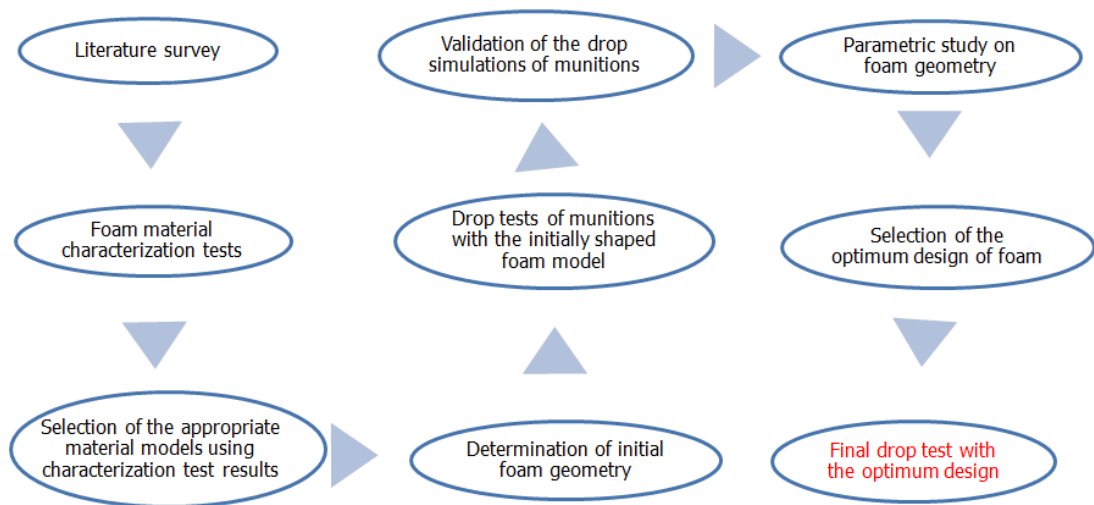
Figure 1-1 Flowchart of the thesis study

1.3   OUTLINE OF THE THESIS

In the very beginning of this chapter, a brief introduction in which the aim of the thesis, as well as the description of the problem is made. Furthermore, the methods to be able to solve this problem are shortly summarized. The finite element code is also named in the beginning of this chapter within the capabilities of solving this kind of scenarios. In the second part of this chapter objectives of the thesis are told and the solution process is represented within the flowchart.

Chapter 2 is a section where a very big portion of the literature survey is given. Importance of the drop tests are tried to be explained by exemplifying the researches done on this topic. An introduction to foams is also done in Chapter 2 by giving the characteristic behaviors of foams. Their usage as energy absorbing

materials is also presented by literature studies. Material characterization method of this kind of materials is explained by defining the test set-ups used in these tests.

Chapter 3 is totally dedicated to the experimental approach. Two fundamental tests are conducted during this study and details of these tests and test set-ups are given in this part of the thesis. At the very beginning part of this chapter, material characterization tests are introduced. Quasi-static tests and drop tower test set-ups are given in detail. Second part of this chapter is related to the drop tests of munitions. Details of the drop test apparatus and accelerometers are also specified here. Finally, initial foam geometry selection is also given in this chapter with its reasons.

Chapter 4 is totally related to numerical approach. This chapter starts with the information about distinct FE codes used in this area. Pros and cons of these codes are summarized at the beginning of this chapter. Later, the fundamental reasons of the selection of the FE code, LS-DYNA, are given. This is followed by the introduction of theoretical information of the FE code. Selected material models used in numerical modeling are also given here. Later, a general procedure for finite element modeling is given in detail. Selection of the appropriate material model from the code is also explained in this chapter. Finally, simulation of the drop tests of munitions is explained. Definitions, assumptions and boundary conditions used in these models are illustrated at the very late part of the chapter.

Chapter 5 explains the experimental results of the tests conducted during this study. Not only material characterization results of selected foam materials, EPP and PE, but drop tests of munitions for the usage of numerical modeling are also pictured in this section.

Chapter 6 where numerical results are given contains the results of material model selection. Moreover, validation of the drop simulations of munitions as well as parametric studies on foam geometry is given with all their details in Chapter 6. Comparison of numerical results with experimental results is also taken place in this chapter.

Chapter 7 is the part of the thesis where final test results are shown. This chapter contains the information about the final drop test results within optimized foam design to prove the success of the study.

Chapter 8 finishes the study with a conclusion.

CHAPTER 2

BACKGROUND AND LITERATURE SURVEY

In this chapter, foam material characteristics and a deep literature survey of drop tests of various products are presented. In addition, foam characterization test set-up information, foam manufacturing techniques will also be given in detail. Yet, similar tests are going to be conducted within the scope of the thesis.

Some of the previous works explained in this chapter are not directly related to the thesis work whereas; it is thought to be significant to understand the logic behind. Due to the fact that results of drop tests of munitions are accepted as confidential information, they are seldom published. However, there are a bunch of papers related to drop cases including both experimental and numerical studies.

2.1 FOAMS

2.1.1 Introduction to Foams

Structural foams, also called cellular solids, are universally used in a wide range of applications owing to their ability of energy absorption combined with low weight and ease of production. Low price is also one of their special motivations of being picked by companies. When ratio of the usage of foams is considered, automotive industry gathers the big portion of the pie. Passive safety issues in car crashes make use of foams in such applications essential. Other than automotive protection, foam materials are always an option in defense industry projects thanks to their unique characteristics which are mentioned above.

Foams can possess rather distinct characteristics which are consequences of the selection of the numerous factors such as type and mechanical properties of the constitutive material, density (porosity), foaming method and micro-structure [1]. One can design specific kind of foam, whose characteristics are depending on the selection of appropriate types of these factors. However, in order to reach desired properties, repeated material characterization process resulting in loss of a big amount of money should be applied. In this process, supplier is asked for some material properties to be used in numerical methods.

Foams can be found as open cell, closed cell and sometimes both. In the thesis of Al-Tinawi Dalia [2] cell structures of foams were explicitly summarized. In order to classify foam as open-cell in which free flow fluctuation is allowed, their cells are needed to be connected through open faces. On the contrary, if blowing gas is captured in closed area, this type of foam is called closed-cell. The fundamental difference of closed-cell foams than open-celled ones is that cells are joined from one to another by their faces. In Figure 2-1 microstructures of foam is revealed. At the very left of Figure 2-1 2D honeycomb foam is shown, while the middle and right one represent the 3D foams with open cell and closed cell, respectively.
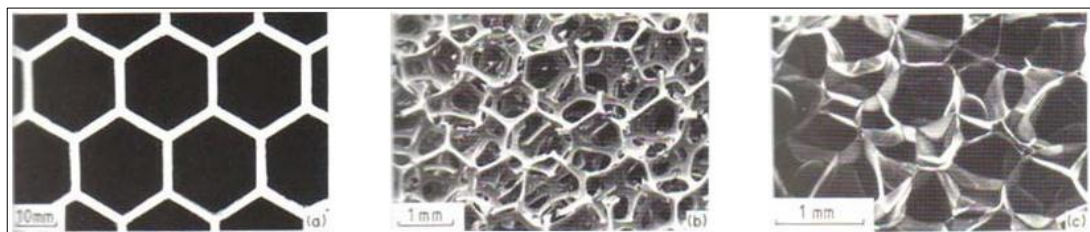
Figure 2-1 Microstructure of 2D distinct types of foams [2]

2.1.2 Manufacturing Process of Foams

Producing of foams can be divided into three main regions which are pre-foaming, ripening and molding. Firstly, raw materials need to be prepared for expansion purposes. In the beginning of the process, bead particles are steamed resulting in the penetration of pentane gas into the bead to expand. According to the desired density of the foam, various parameters can be adjusted in this step.   This beginning phase is named pre-foaming, followed by ripening process.

Following pre-foaming, storage of beads in ventilated silos for a period of half a day to two days is necessary. Depending on the material grade and density desired, time for capturing of beads in the storage can alter. Special attention needs to be given to this phase owing to the fact that once the material is pre-foamed, no back process is allowed. In case of a long periodic storage, beads will no longer fuse to the mold resulting in the loss of material.

In final section, pre-foamed beads are filled to sealed mold. Following heating of the mold with high-pressure steam, beads undergo a final expansion in order to be fused together in the shape of the mold. Moreover, cooling is sufficient for stabilization during the process. Molding cycles may change depending on the density desired and the level of fusion required. Besides, as seen in Figure 2-2 volume of the block wanted or other requests of the clients affect the number of cycles [4].

Figure 2-2 Molding process [4]

2.1.3 Characteristics of Foams

The very first thing needs to be known about foams is that foams usually offer high strength in compression. Their excellent energy dissipation capabilities make use of foamed materials very common. Other than that, relatively lower costs and allowing great design flexibility are prominent features of them. High-energy efficiency that

can be achieved by foams is possible to be explained in the following way: Typical foam materials show a long flat plateau zone when stress-strain curve is considered and stress is limited in this region. Without doubt, this zone is not typically seen in other materials than foams. The following figure revealing the zones in compression of typical foam is obtained in almost every study related to foams.
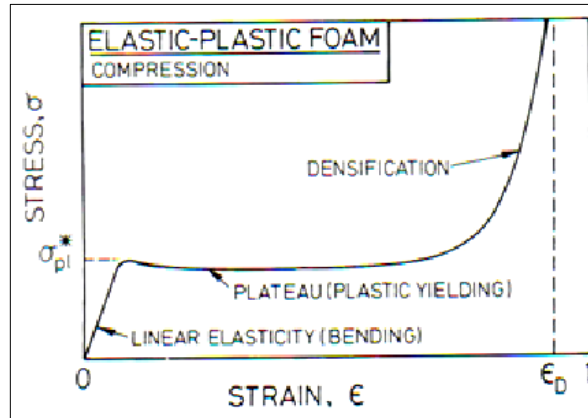
Figure 2-3 Three definite regions typically monitored on foams [2]

As shown in Figure 2-3, the first zone in which small strains are seen is followed by plastic yielding. With a slope equal to Young Modulus, it is possible to name the first zone as linear elastic. For open-cell foams, cell wall bending controls the first zone, while face stretching is the case for closed-cell foams.

Increase of the load causes the collapse of cells by elastic buckling, plastic yielding or brittle crushing depending on the mechanical properties of the cell walls. Collapse lasts at more or less invariable load, giving a stress plateau, till opposing walls in the cells get together and touch. Finally densification regime is seen causing the stress to increase sharply.

In the paper of Quellet [3], strain rate dependency of foams is investigated. In the most of the polymeric foams if strain rate is increased, elastic modulus and plateau stress levels are increased while densification strain is decreased. This is easily seen in Figure 2-4.
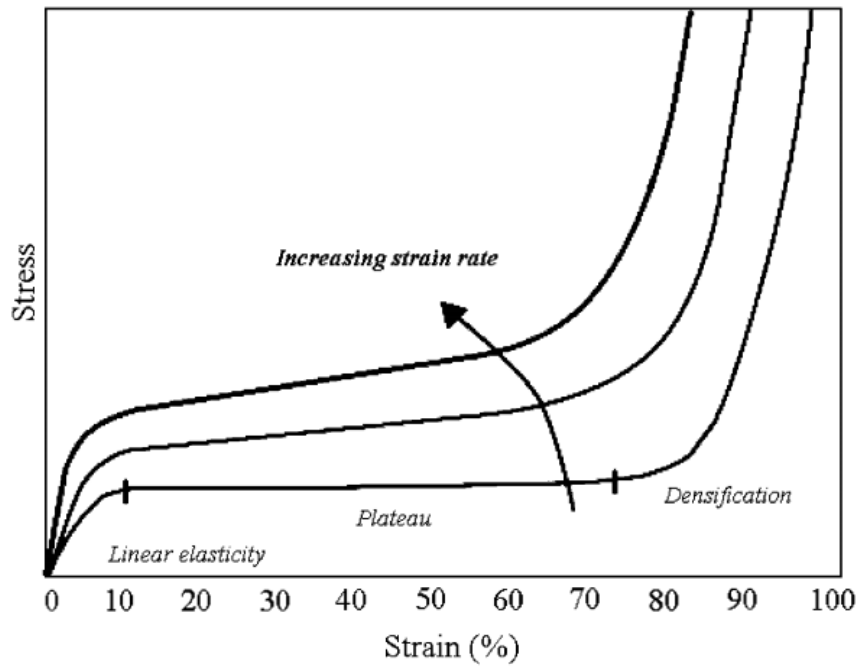
Figure 2-4 Strain rate effects on polymeric foams [3]

2.2   EXPERIMENTAL AND NUMERICAL METHODS

Experimental approach is a very common but costly method applied in drop cases. Although numerical methods are replacing with the experimental ones in last ten years, experimental tests are still an indispensable for validation processes. Furthermore, numerical tools still need the test data as input which proves the claim that experimental process is vital. In the context of the thesis, experimental methods will be used not only for the drop tests of munitions, but also material characterization of foams will also be done by experimental approach.

On the other hand, numerical methods are being used very often in many applications. This is achieved by enhancement of the capabilities of the computers. High cost of the experimental methods is the fundamental reason of the tendency to numerical methods. Apart from the cost efficiency, most of the time numerical simulations necessitate less effort than experimental ones.

Literature studies related to the common usage of foam materials in various drop test and analysis scenarios with or without foam materials, drop test set-ups,

11

material characterization of foam materials will be exemplified in the rest of this chapter.

2.2.1 Foams as Energy Absorbers

Foam materials are accepted as effective energy absorbers and used very commonly in a wide range of applications. In the study [5], car body stiffness and crash performance are tried to be improved by local reinforcements of foam materials. Bulk polyurethane foams are already in use in automotive industry, e.g. seat cushions. This material is used at distinct areas of a body in white (BIW) of a car as shown in Figure 2-5. The reason behind the selection of the areas is not mentioned in the paper. However, experience is the key factor determining the areas of reinforcements.
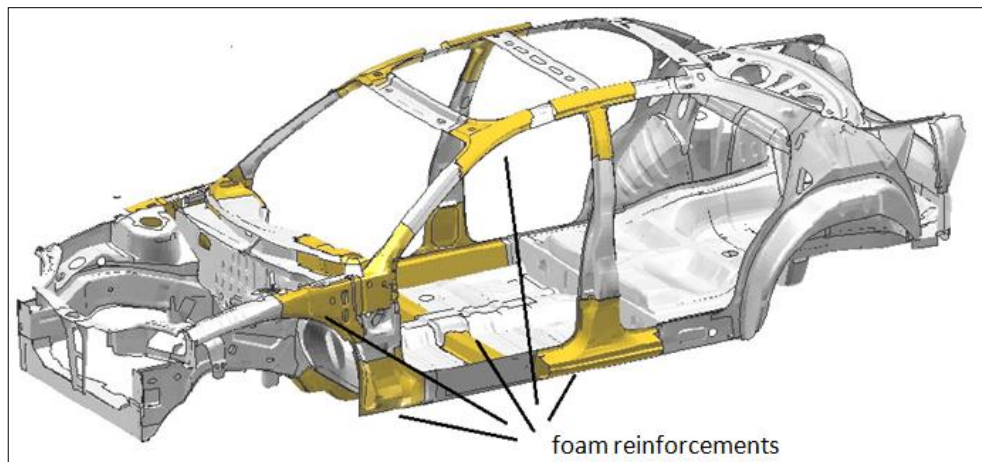
Figure 2-5 Areas of foam reinforcements [5]

Numerical modeling of the car is done by using explicit finite element code LS-DYNA. For the representation of the *Betafoam*, a crushable material model that is also used in this thesis is selected. In order to monitor the gains of the foam reinforcements in a crash scenario Figure 2-6 is shown. As seen in Figure 2-6, the base model without foam reinforcements has some serious deformations on the selected areas. By means of the energy absorbing capabilities of the foam materials, a better scenario after the crash is reached by foamed car.
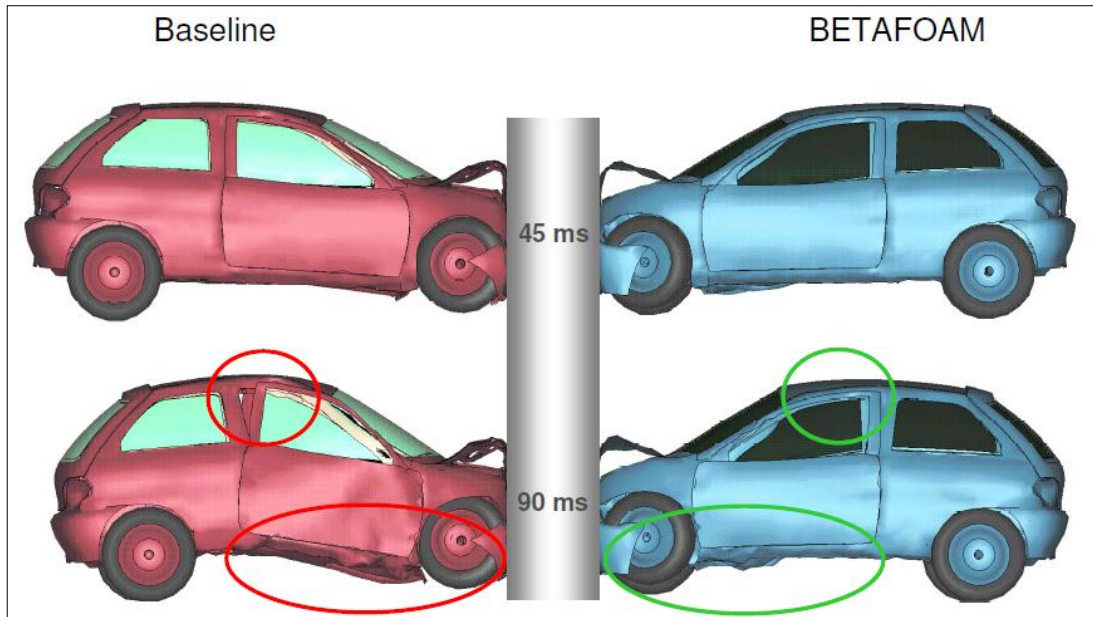
Figure 2-6 Baseline and foamed car deformation in frontal crash [5]

Campbell [6] also used polyurethane foam materials in automotive seating applications. With densities ranging from 27– to 48-kg/m^3 five different polyurethane foams are characterized and three tests on each material performed to provide the consistency. In the numerical modeling part of the foam cushion, it is stated that not a high degree of accuracy is necessary as a starting point. According to the results of the initial model, a more detailed modeling can be performed.
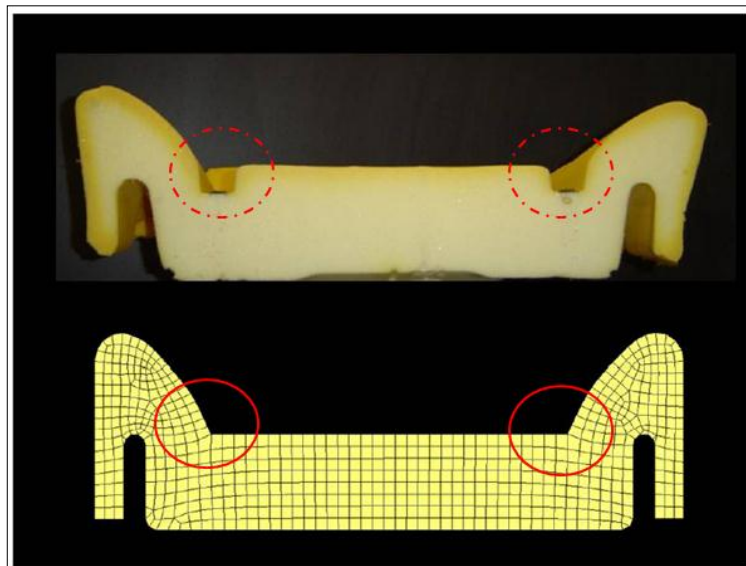
Figure 2-7 Finite element seat mesh [6]

In Figure 2-7, real foam cushion and its finite element representation is shown. It is also stated that elimination of the sharp edges of polyurethane foam provides a significant amount of computational time. LS-DYNA is the numerical tool used for numerical modeling and reversible foam material model is selected from material library for the representation of seat foam cushion.

Reid and his friends developed a new barrier system to withstand the severity of high-energy vehicular impacts [7]. As seen in Figure 2-8, new barrier system is attached to concrete walls. The main goal of these systems is to reduce the vehicle and impact accelerations especially in high-speed racing accidents. It is stated in the conclusion section of paper that new designs are reduced the levels of impact as expected.

For the numerical simulations of these scenarios LS-DYNA is used. In this paper, detailed information about the simulations is not given. However, some valuable information about the difficulties during simulations is specified. Moreover, suggestions are also done to overcome.

It is stated in the paper that simulations are often aborted due to the contact penetrations. That is why it is suggested that changing contact penalty scale factors can help to get rid of this problem. In addition, refining the mesh size or lowering the overall time step may also be practical to get rid of instabilities.

Figure 2-8 Test vehicle and impact condition [7]

14

Following two references have more common points than previous studies in terms of the context of the thesis. These papers consist both foam modeling and drop cases together. In the reference [8], numerical simulation of a drop test of a cooker including packaging foam is performed as it is seen in Figure 2-9. What is significant for performing such a simulation can be explained in a way that less hardware tests have to be conducted. In the same paper it is underlined that LS-DYNA is a solid tool when large deformation and lots of interactions are in case. Furthermore, total number of elements (shell, solid, beam etc.), material modeling strategies both for metallic and foam parts as well as assumptions made are given in detail. Principal strain values at certain regions, energy balance graphs, displacements nearby the impacted edges are pictured too.
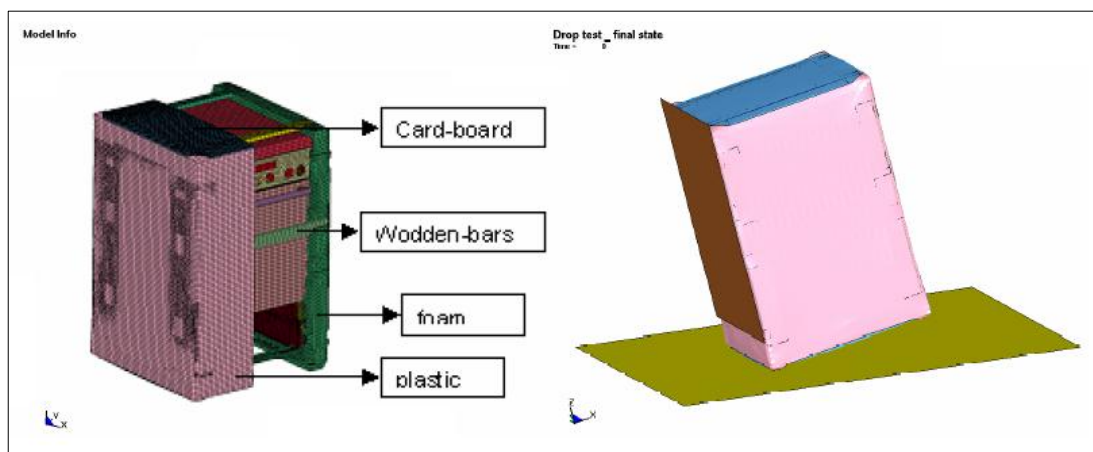
Figure 2-9 FE Model and drop test of cooker [8]

A more appealing part of the study is the paragraph related to foams. The crucial point of the study in terms of foam modeling is the emphasis of necessity of the reliable dynamic material input data to provide user a good agreement with experimental tests. To do so, it is also mentioned that foam specimens with different densities are tested at various strain rates, following by validation of material modeling. Additionally, to compare numerical and experimental results, Figure 2-10 is revealed. Here, stress concentration in numerical model and damaged section of the structure in experimental scenario seem to be similar to each other.
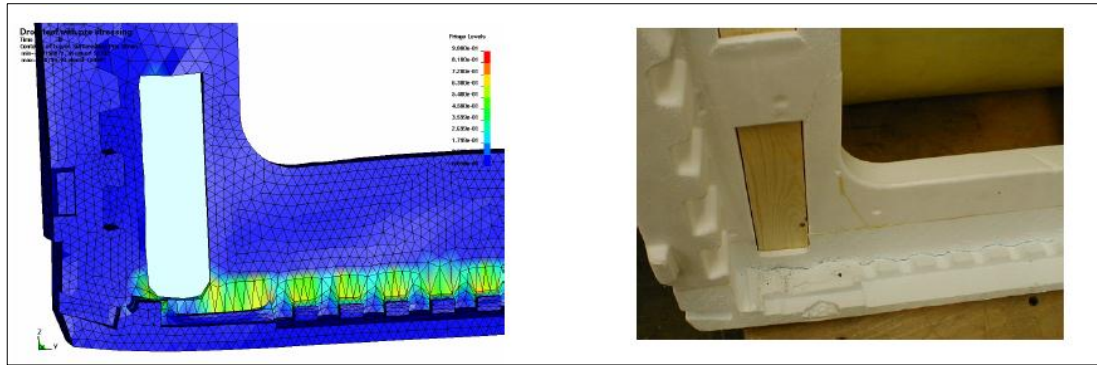
Figure 2-10 Principal strains simulation vs. experiment [8]

In the study dealing with comparison of two different polyethylene foam cushion designs for packaging [9], tempting lines are placed in the section of foam characterization.
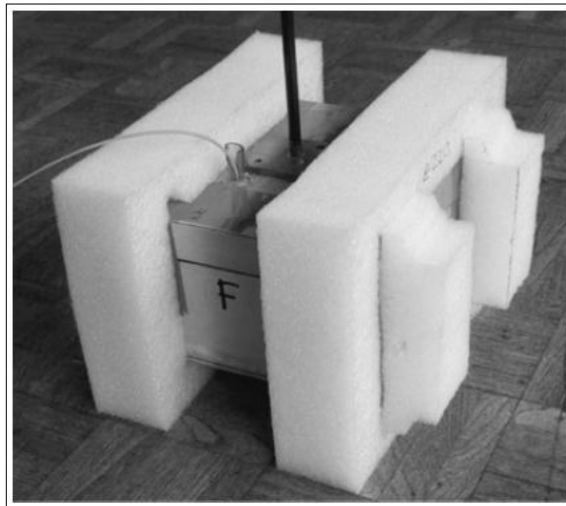
Figure 2-11 Product surrounded by foam materials [9]

It is stated in this title that during repeating impacts which are five times at three minutes intervals, initial thickness of the foam as seen in Figure 2-11 is reduced a bit, however in general, the foam is recovered its dimensions well. This may be accepted as tolerable, however in case of an increase of number of repetition, e.g. ten times in the same interval, may affect the behavior of foam. This information is should be kept in mind. Because, material characterization study of PE and EPP will also be done within the context of thesis.
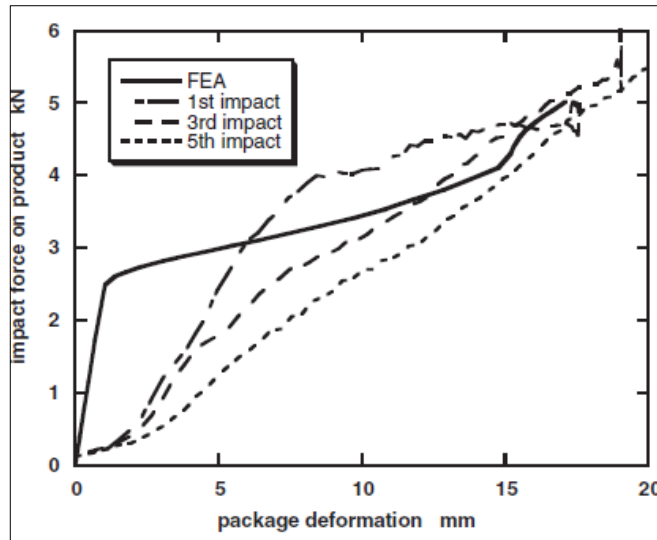
Figure 2-12 First, third and fifth impact of foam design, compared with FEA [9]

According to Figure 2-12, it is clear that increase in the number of tests changed the behavior of the foam. However, the difference between the 1st and 3rd impact can be tolerable when it is compared to the 1st and the 5th impact. It can be concluded from this study that more than three tests for a specimen can cause to problematic results.

In the same study, finite element modeling of the foam material is done by the code ABAQUS. A crushable material model is selected for the representation of this material. This material model necessitates a Poisson ratio value for uniaxial compression data and it is stated in the paper that zero Poisson ratio is given for this value. In the discussion section of the study, it is mentioned that the irreversible foam material model used in the code does not capture the exact behavior of the foam. This is because of the underestimation of the slope of the predicted impact force versus deflection curve. This is clearly seen in Figure 2-12.

2.2.2   Drop Tests

Drop test for a product is accepted as an essential process for years. Such a case can sometimes be carried out for a fundamental component of a system or a whole system within most of its components can also be dropped into the ground to be able to monitor their interaction. Dummy models representing real segments are attached to system not only for financial concerns of critical components, but also

17

usages of dummies speed up the process. Above pointed out dummies are mounted on the original position of real component with its exact mass.

A challenging point to execute such a test is the arrangement of the drop height of the test. Especially for rather complex systems obtaining interactions in consequences of having a lot of components, drop tower mechanisms are developed. In the article of Karen E. Jackson and Edwin L. Fasanella [10], published in 2008, vertical drop test of an ATR42 aircraft is conducted at Dynamic Drop Test Facility at the FAA Technical Center. As it is depicted in Figure 2-13, ATR 42 aircraft is raised to a drop height of 14 feet (= ~ 4 m) and released onto a concrete surface.

Figure 2-13 Pre-test photograph of the ATR42 aircraft at 14 feet [10]

Accelerometers are instrumented to collect the test data using data acquisition systems. Locations of accelerometers are determined regarding desired output. In Figure 2-14 a post-test photograph of the scenario is shown.

Figure 2-14 A post-test photograph of exterior-interior view of aircraft [10]

In another study [11], performed in 2000, a vertical drop test of a B737 fuselage section is conducted at FAA Technical Center. The target is to evaluate the response of the overhead stowage bins in a narrow-body transport fuselage section when subjected to severe impact condition.

Similar to Karen's study, dummies are positioned at their original locations. Again, accelerometers are positioned and data acquisition systems are used.
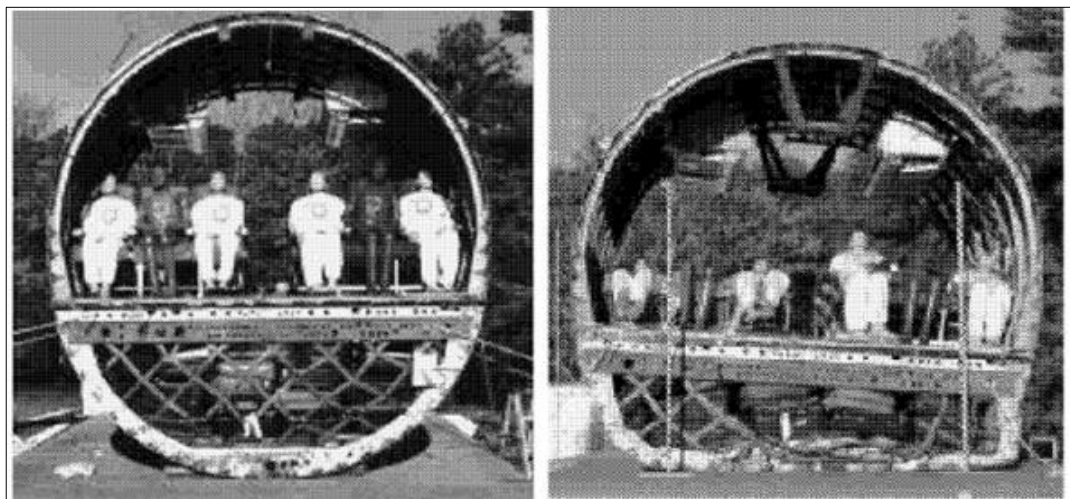
Figure 2-15 Pre and post-test photograph of B737 fuselage section [11]

In the same article, post-photograph of the test is also depicted. After drop case, asymmetric position of displacement is easily seen in Figure 2-15.

At an experimental study [12] which is developed at NASA Langley Research Center, crash protection is aimed. To encounter structural and flight loads requirements, a composite fuselage section is dropped onto a rigid surface from a 10 feet drop height. Apart from previous two studies, energy absorbing structures are integrated to the system. Foam materials are used as absorbers to dissipate kinetic energy that will occur during the impact. Polyurethanes and crushable foam blocks are utilized in experimental set-up.

As shown in Figure 2-16, fuselage section, seats and dummy occupants are instrumented. A 10 feet drop height is positioned for the representation of 25 feet per second vertical velocity.
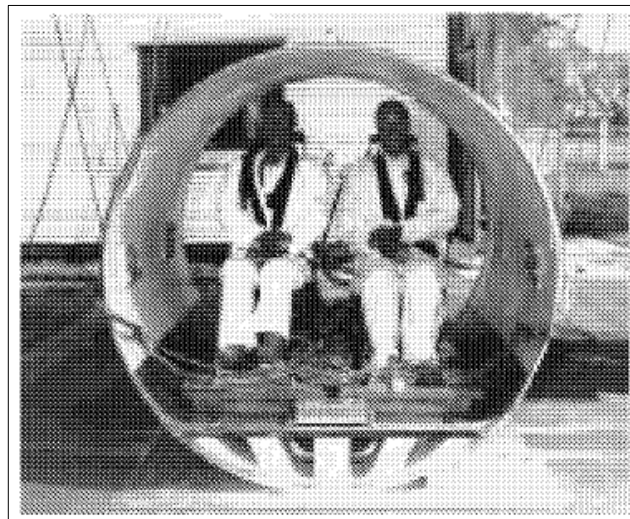
Figure 2-16 Composite fuselage section prior to test [12]

In the same study, finite element modeling of the scenario is also developed. Dytran is the name of the finite element code used during studies. Similar to LS-DYNA and ABAQUS, this finite element code is also capable of simulating drop scenarios. Furthermore, blast, penetration or impact problems are other areas of application of this code.

For the representation of the foams, crushable foam material model is preferred in this code. For foam material, Poisson ratio is given zero in this paper as it is seen in other papers too. Finite element representation of the scenario is depicted in Figure 2-17.

(a) Front view – full model   (b) One-half cut of the model
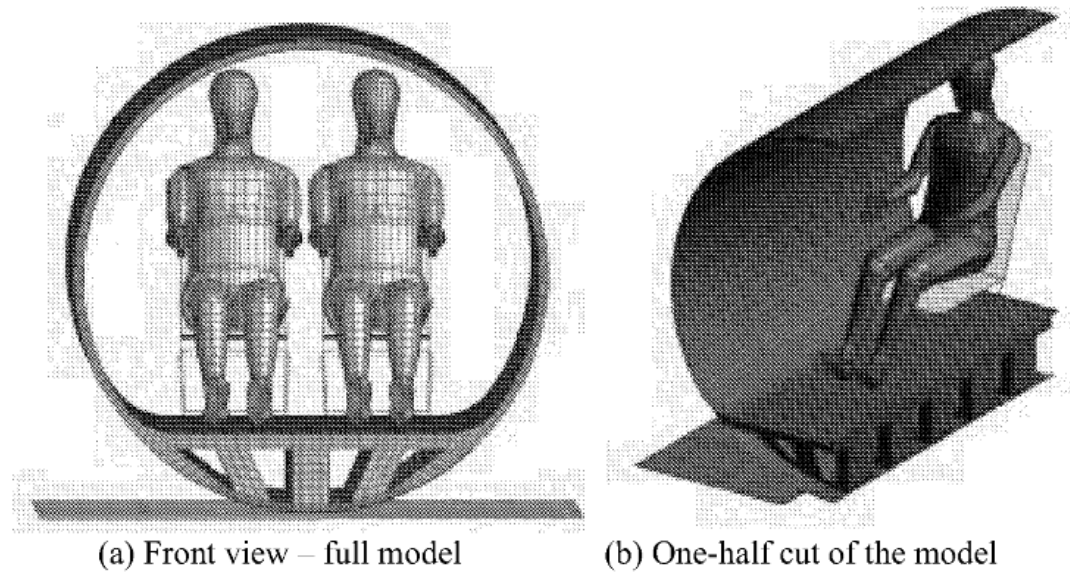
Figure 2-17 Finite element model [12]

In the final section of the paper desired acceleration records are also given. As it is depicted in Figure 2-18, shape of the curves, duration and the maximum acceleration value of the curves are quite similar.
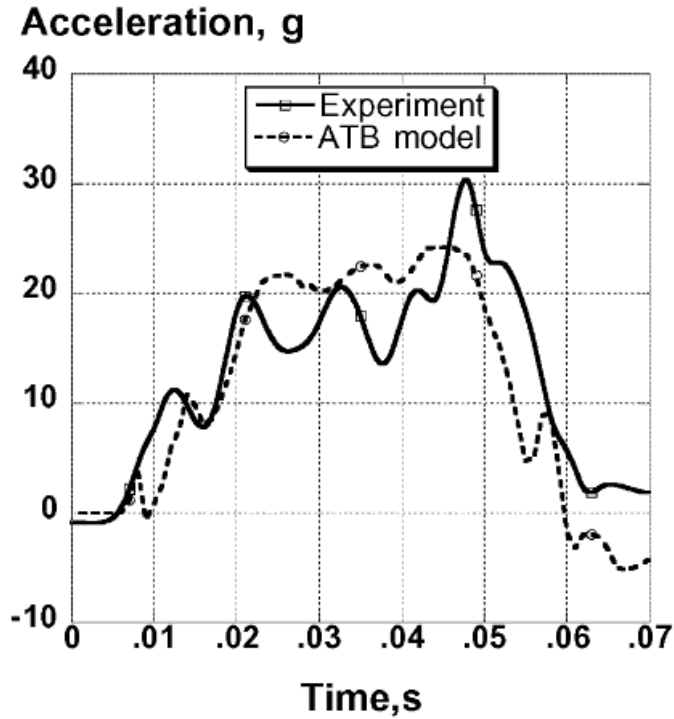
Figure 2-18 Acceleration vs. time responses of both models [12]

In a thesis study done in 2006 [13], a refrigerator drop test is validated by numerical methods. A nonlinear dynamic problem code, Dytran, is used for comparison of numerical results with experimental ones. The aim of the thesis is explained in a way that it is advantageous to use numerical codes instead of conducting tests in terms of money and time. Moreover, polystyrene material is also used for packaging material to reduce the effect of the impact. According to Figure 2-19, energy absorbing material has completed its mission and dissipated some of the energy occurred. However, the refrigerator is still damaged and some other innovations are seemed to be sufficient.
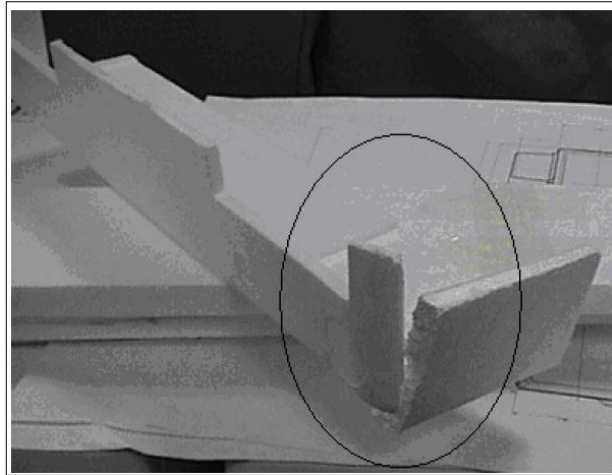
Figure 2-19 Damaged Polystyrene material [13]

In the final section of the study some suggestions are also given for further studies. It is suggested that it is better to increase the number and types of elements used in simulations. Different contact algorithms can be developed to be able represent the scenario in a better way. Moreover, by using a more complex finite element model it is possible to obtain better results.

In another study done by Wang and his friends [14], a packaging material is used for a TV-set and the system is dropped onto the ground. Finite element modeling of the TV-set and packaging material are depicted in Figure 2-20. In this finite element model, television is surrounded by foam material. It is stated in the paper that at the expected high stress region, a very detailed mesh is developed. The main goal of this paper is to compare the system response for different casing designs.

However, modeling technique of foam material is more appealing part of the paper. For this reason, more attention is given in this section. Expanded Styropor is the name of the material used in this paper with 20 kg/m3. Crucial expression in this paper is that behavior of foam material is very sensitive to the strain rate changes. In the conclusion part of the paper it is mentioned that computer aided simulation can help reduce the number of physical tests required and thus shorter time for the product-to-market results. [14]
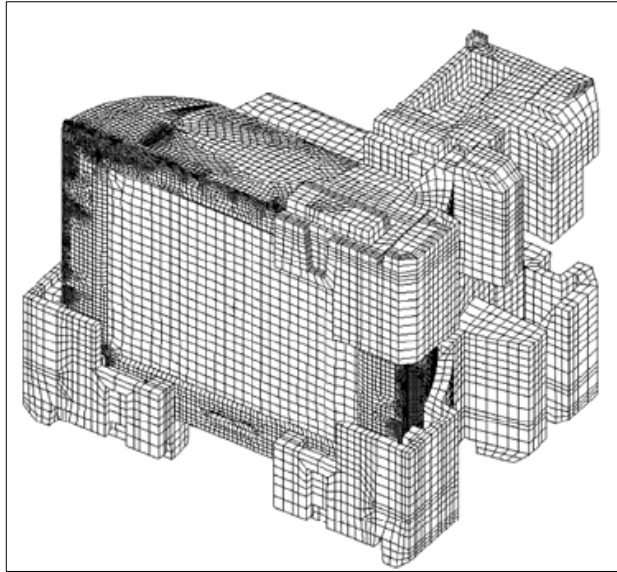
Figure 2-20 Finite element model of TV set with packaging material [14]

Finally, some key factors for efficient modeling are given in the same paper. The most important one of these is related to the one with contact definition. It is suggested that an extra attention should be paid to the contact of two materials with quite distinct properties.

Posch W. and Sageder A. represented a paper [15] related to the drop scenario of a dishwasher. The main goal of the drop scenario can be explained in a way that dishwasher should withstand a 0.5 meter drop at an angle of inclination of 10 degrees onto a concrete floor. In this study tub of the dishwasher are thought to be made of polyurethane compound instead of stainless steel. Moreover, a numerical study is also conducted for further developments. In order to simulate the nonlinear dynamic response of the structures, finite element code Dytran is used. Thanks to the results of these simulations, development time and costs could be significantly reduced.

Strain rate dependency of polymeric foams is also emphasized in this paper and with the cooperation of universities necessary material data at high strain rates are reached. At the very end of the paper it is mentioned that study was concluded within the success and necessary material properties are available for future studies without important financial expenditure.
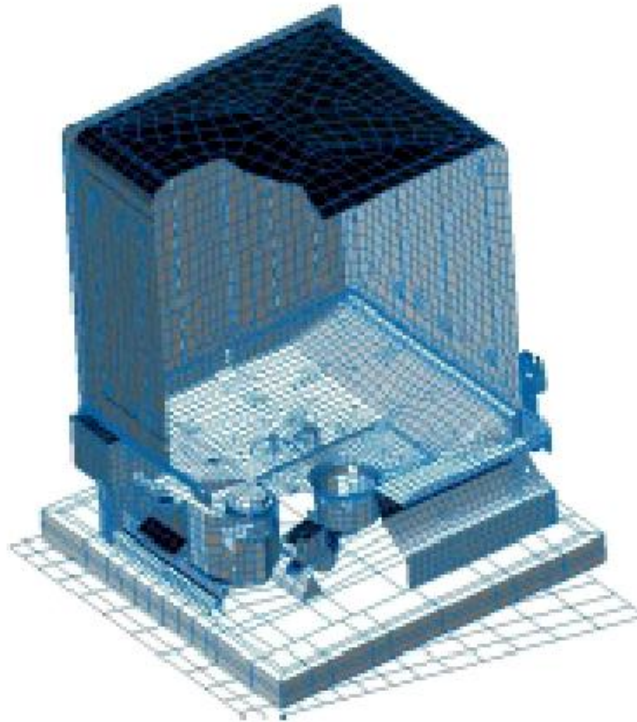
Figure 2-21 Cross section of the dishwasher [15]

Wang H.L. represented his study [16] related to simulation and verification of the drop test of 3C products in 8th International LS-DYNA Users Conference. In Figure 2-22, acceleration-time histories of test and analysis are depicted with the FE model of the phone. According to Figure 2-22, peak value in analysis curve is higher than experimental one. However, the trend of these two curves is similar to each other.
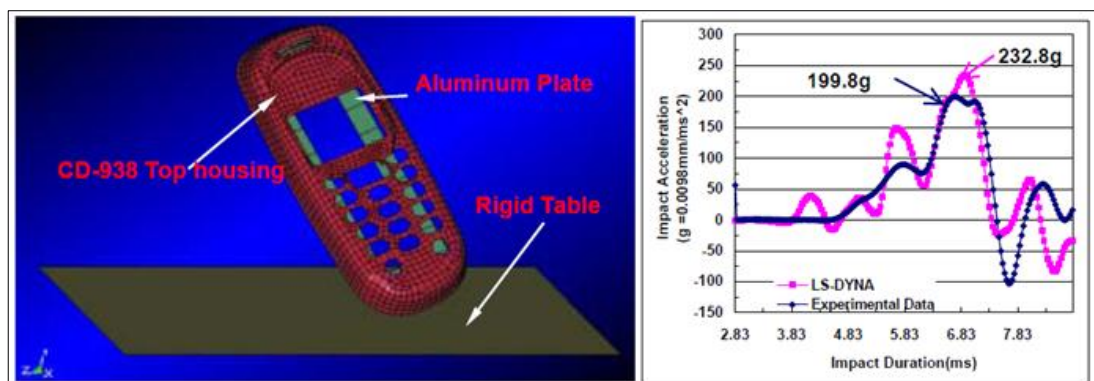
Figure 2-22 FE Modeling of a phone and comparison of results [16]

Schwer and Kennedy published a paper [17] in which three different steel billet drop tests are investigated as it is seen in Figure 2-23. End drop, side drop and tip over drop scenarios are developed in order to monitor acceleration levels. Accelerometers, from A1 to A5, are instrumented at distinct locations of the model to record the data.
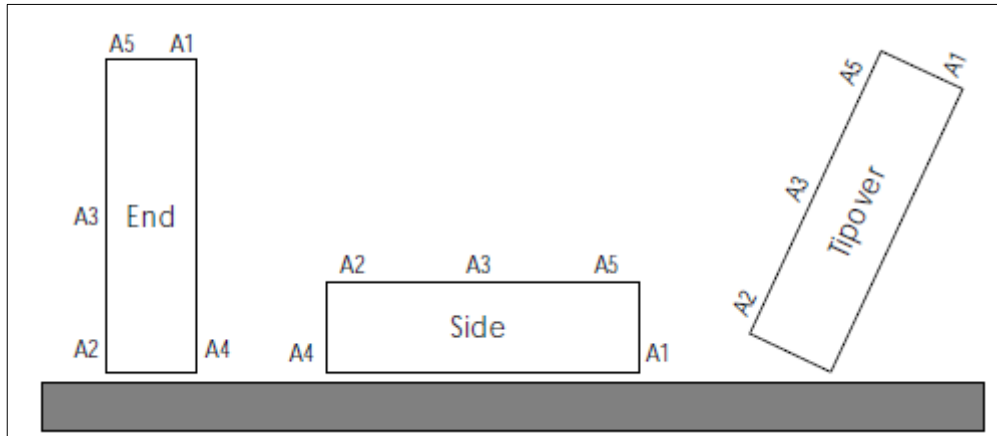
Figure 2-23 Accelerometer locations on steel billets [17]

As it can be inferred from these three scenarios, different accelerometers will be focused. It is also given in the same study that extremely noisy results need to be filtered. For this reason, higher frequency vibrations induced in the steel billet should be removed. Figure 2-24 shows that peak value of a raw data is not realistic at all. Because, peak value in unfiltered data is almost reduced to half of this value.
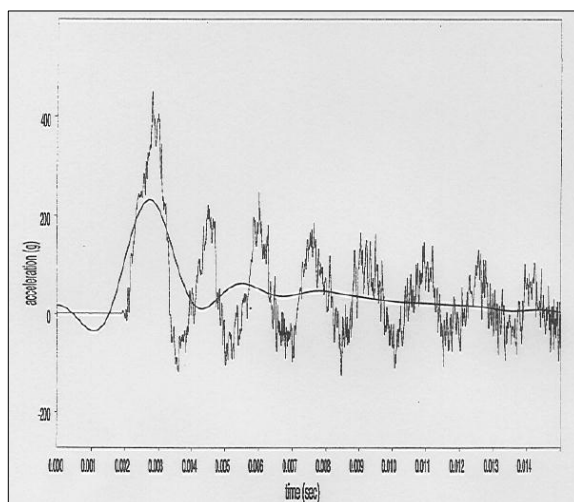
Figure 2-24 Recorded acceleration data and filtered version [17]

In reference [18], LCD television is packaged with foam material and dropped onto wooden surface. This is the typical application area where foam materials are used for energy absorption. Main idea of the use of the foam material which is Expanded Polyethylene is to reduce the level of impact. LS-DYNA is preferred as finite element code thanks to its good capability of representing foam materials. In Figure 2-25, actual and finite element model of LCD television is depicted.
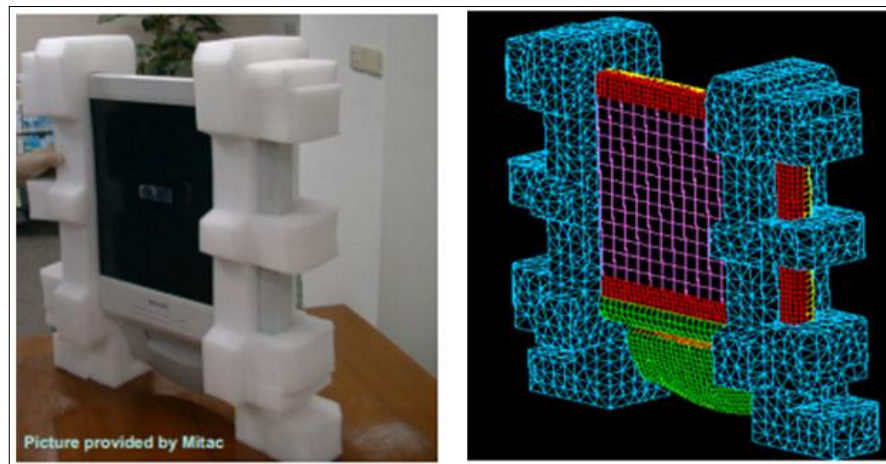
Figure 2-25 Actual LCD and FEM of LCD [18]

It is depicted in Figure 2-25 that a very similar scenario to the drop test is developed with finite element model. However, in the FEM model of LCD, it is shown that tetragonal elements are used for foam parts. On the contrary, for LCD part hexagonal elements are preferred. This is because of the fact that area of interest is the LCD part of the set. In Figure 2-26 accelerometer locations are depicted.
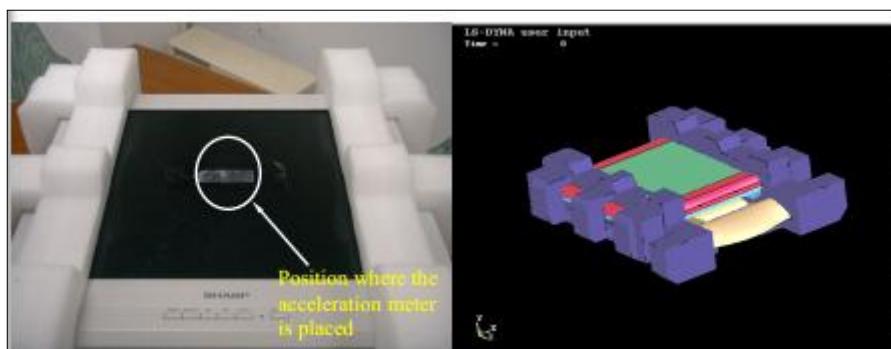
Figure 2-26 Accelerometer locations [18]

According to Figure 2-27, it can be said that a good agreement between the test and simulation is reached. This is because of the similar trend of both curves. Moreover, peak values of acceleration and times show similarities too.
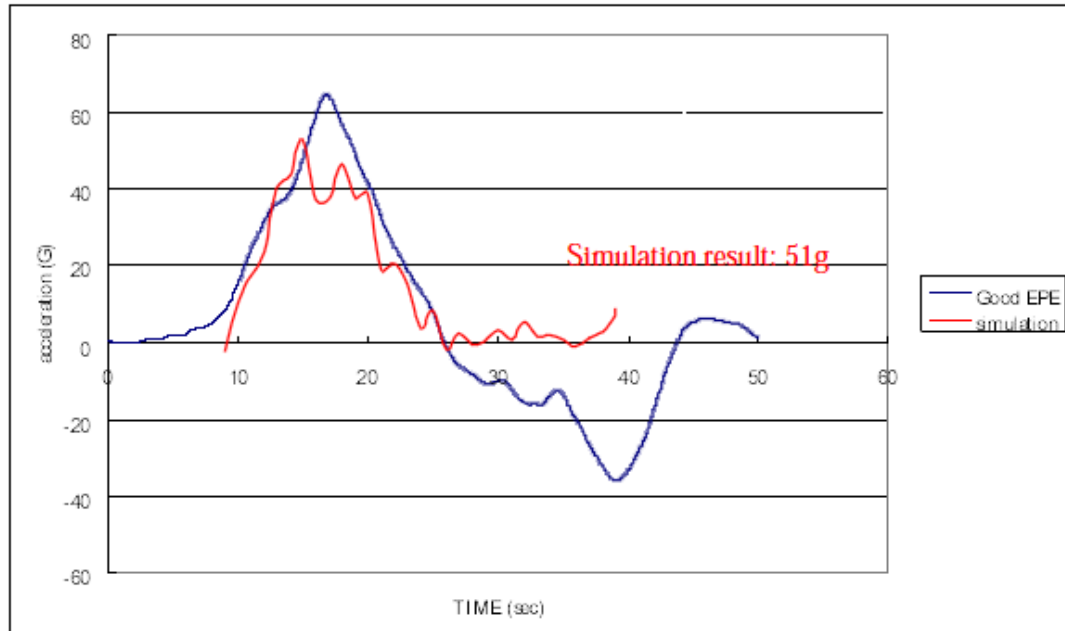
Figure 2-27 Acceleration comparison of test and simulation [18]

In a study [19], Low and his friends presented a paper related to the impact analysis of the top-drop of a Hi-Fi set with buffer onto the concrete wall. PAM-CRASH is the finite element code used in this study. By using this commercial code, drop analysis can be conducted similar to ABAQUS, LS-DYNA and DYTRAN. In this analysis, top drop is thought to be the worst scenario and the system is released from 0.8 meter height onto a rigid wall. Results of simulations are then compared to the experimental ones.

In the final part of the paper it is mentioned that outputs for some tiny substructures are expected. However, this leads to extremely small elements which cause to longer run times. This is because of the fact that drop simulation is controlled with the minimum element size. As a suitable solution global-and-local method which is not commonly used is suggested. In this method, coupling global simulation (whole model level drop simulation) and local analysis (only substructures) are performed.

28
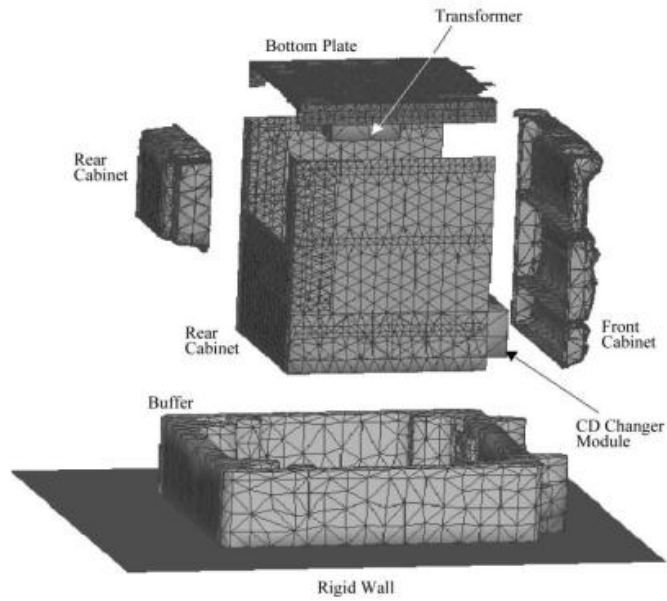
Figure 2-28 FE model of Hi-Fi audio set [19]

Another point mentioned in this paper is that reliability of the material database is significant, especially for nonlinear dynamic problems.

Minnicino M. developed a finite element model [20] to replicate all of the experimental works of Excalibur munition. In this study, munition is dropped onto ground from 36 inches. For sake of the analysis, this scenario is turned into an initial velocity problem as it is depicted in Figure 2-29.
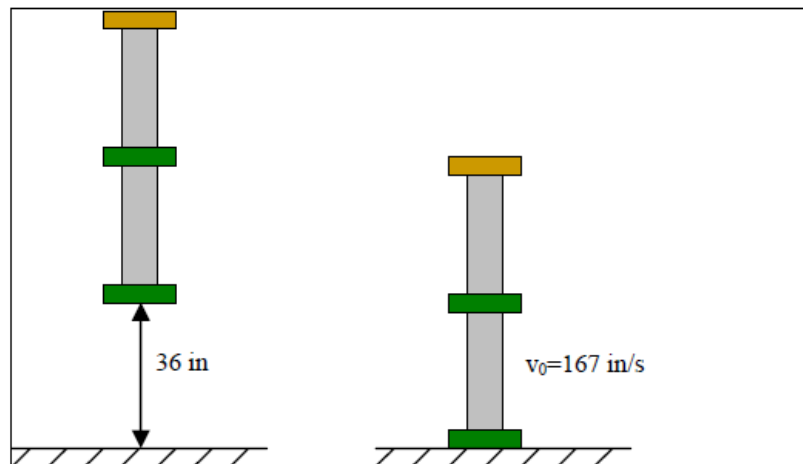
Figure 2-29 Initial velocity problem set-up [20]

The very first thing to be known about finite element modeling of a drop scenario is that no gravity is given as input. This is fair enough because of the fact that initial velocity of the scenario is calculated considering the height of the drop and gravity. However, it should be known that effect of the gravity is not included in the rebound behavior of the munition. As mentioned in the reference [20] , this is acceptable for the impact event. Bounce back behavior of the munition is not the area of interest in drop scenarios.

A foam support system is also developed to protect the munition from effects of the shock. In Figure 2-30, it is clear that distinct regions of the munition are surrounded by various foams. Finite element code, LS-DYNA, is used to simulate the scenario.
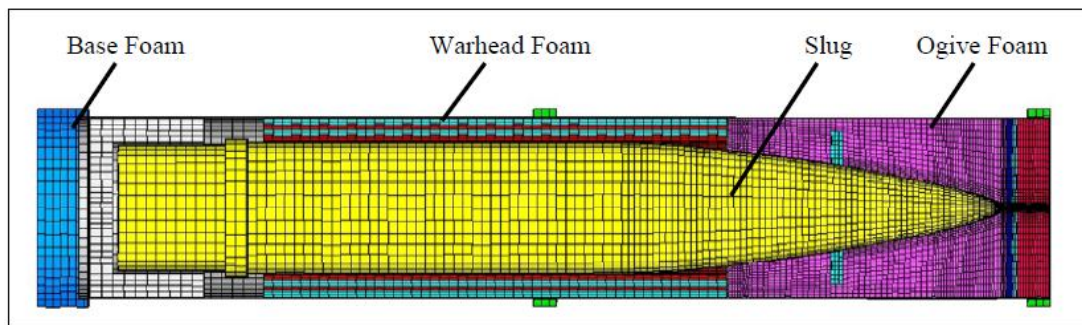
Figure 2-30 Foam supports to protect system [20]

Hexahedral elements are preferred for foam modeling as expected. Use of brick elements for foam parts is commonly seen in drop analysis. This is because of the fact that excessive distortion of foam materials causes run-time errors and use of brick elements reduces the possibility of run-time errors. Nevertheless, run-time errors can still be encountered even if perfectly hexahedral elements are used. It is stated in the paper that interior contacts are implemented to the finite element model to prevent foams from large deformations. Main advantage of this type of contact is that additional contact surfaces are created within each element. Another method to get rid of highly localized elements is permitting element erosion. In this method, highly distorted elements are deleted from finite element model within its energy and mass. This is provided by giving erosion parameters to the foam materials. This is not a usual method seen in foam modeling whereas; it is stated in

the paper that this is a reasonable approximation for light and relatively slow moving materials. In Figure 2-31, element deletion process of foam material is depicted. Highly distorted elements seen in Figure 2-31b are eroded and new contact surfaces are generated as seen in Figure 2-31c.
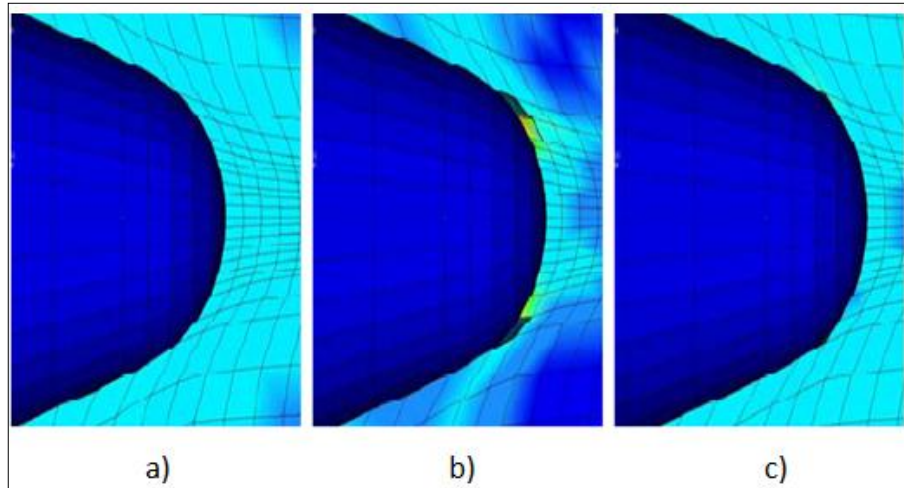
Figure 2-31 Element erosion of foam material [20]

In the same paper it is stated that during the characterization process of foams, Poisson ratio could not be determined owing to the porosity of the foam. Instead, pretty low values are used to monitor the effects of Poisson ratio. Later in the paper, it is mentioned that Poisson ratio has a little effect on foam response.

Some other assumption in the paper is that Excalibur munition is modeled with rigid material. The major advantage of this assumption is that lower run times are expected on contrary to deformable modeling. In addition to this, rigid modeling is found reasonable owing to the fact that strain energy stored by deformation of Excalibur munition is rather negligible when compared to the energy stored by foam.

However, it is mentioned in the final section of the study that lack of foam material properties caused some troubles in terms of the reliability of the results.

2.2.3 Data Filtering

Due to high frequencies typically seen in acceleration-time histories, acceleration data must be filtered using a filter method. Peak acceleration and rise time of the data are directly related to filter frequency, thus importance of filtering should not be underestimated.

In crash tests and drop tests of various components SAE J211/1 Standard is applied for filtering of the acceleration data. The general algorithm that can be used to generate low-pass Butterworth digital filter is given in SAE J211/1. SAE has defined a set of Channel Frequency Classes (CFC) for impacts of vehicles. Main CFC's are 60, 180, 600 and 1000. Nevertheless, standards are general and not applied to all cases. The CFC60 filter is using cutoff frequency of 100 Hz. at 3 db. The cutoff frequency at 3 db is usually about 1.67 times of the number appears in the CFC filter name [38]. By using CFC60 filer, spikes in the acceleration graph can be captured well. Furthermore, acceleration responses are filtered by CFC180 filter too. Then, this data is used as a basis for integrating to find velocities and displacements. Some of the higher frequencies may come from the structures that accelerometers are attached to. Generally the filter class that should be used can be very dependent to some extent on the particular application. For example, an impact that occurred in a very short duration (1-2 milliseconds) is totally different than a longer one (100 milliseconds). The same cut-off frequency should not be used for such a scenario However, in the applications of car crash CFC60 and CFC 180 filter are good enough for getting rid of spikes in the curves [39].

There may be encountered some oscillations in the acceleration histories of the FE code. There is an idea [40] on calculating the nodal accelerations on the FE codes. It is mentioned that it is advisable to calculate nodal accelerations by differentiating the nodal velocities rather than reading the accelerations directly. The differentiated velocity should give a smooth acceleration, because the velocity is integrated over time of acceleration seen at the node. Also, because the mass is taken concentrated at the nodes, this causes the acceleration to oscillate. The discretized mesh only approximates the state gradients (force, velocity, acceleration stress) over the model, so some smoothing is required with respect to nodes. As the time

step is very small differentiating the velocity is a good way to get reasonable results.

Apart from the applications in the automotive industry, there are not strict recommendations on filtering issues. In this thesis, Energy Spectral Density Method (ESD) is used to filter acceleration-time responses of 50 cm parallel drop tests. The theory of the ESD method is given in APPENDIX B. The main idea of the ESD Method is that the ESD plot of a signal is displayed as a 2D plot of amplitude versus frequency. The unit of the amplitude is "units^2-sec/Hz." [41]. In other words, variation of the energy of a signal is shown on a frequency bandwidth. By checking ESD, it is also possible to find out whether the energy of a signal is seen at high frequencies or not. It is necessary to filter the data if the energy of a signal is low at high frequencies. In this method, acceleration-time response of a shock wave is transformed into Energy Spectral Density-Frequency bandwidth.

2.2.4   Drop Test Set-ups

Within the increasing usage of low density foams in a wide range of applications in recent years, characterization of them started to become a routine process. Two fundamental test set-ups are commonly being used for such experiments. Firstly the quasi-static compression test method is the choice at lower strain rates. As it is seen in Figure 2-32, foam blocks are compressed by two rigid blocks. Moreover, desired strain rates are reached by changing the test velocity. In quasi-static tests, load cells are utilized to measure force levels up to 300 kN.

Figure 2-32 Quasi-static compression test device

In the study of Kellas [21], a quasi-static test device is introduced so that one can understand better how it works. Quasi-static compression device configuration is given in Figure 2-33. It should be known that in quasi-static test capability of energy absorption is relatively higher. Thus, drop mass has still a velocity when maximum crush is attained.
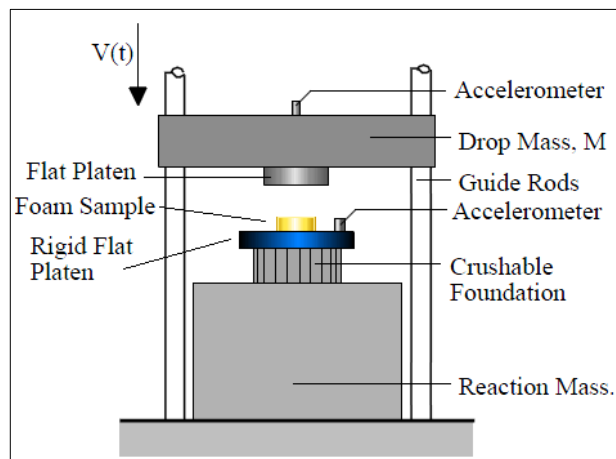
Figure 2-33 Quasi-static compression device configuration [21]

Alike higher strain rated tests, a crushable foundation whose both stiffness and strength are several times greater than the stiffness and strength of the test

sample is accommodated into the mechanism. In this case, foundation remains intact up to the total crash of the test sample. Starting from this point on, sample is totally crashed, crushable foundation dissipates the kinetic energy.

In order to obtain the stress-strain response, two configurations of accelerometers are possible to use. In the first method, a single accelerometer which is mounted on the drop mass is utilized. Within this configuration the crush load is easily determined in a way that measured deceleration multiplied by the magnitude of the drop mass. Double integration of the deceleration curve gives crush displacement while impact velocity is reached by a single integration of the drop head. In case of a deformation of crushable foundation, a second accelerometer is needed to be placed on the rigid platen. This time, double integration of the relative acceleration between the drop mass and rigid platen is necessary in order to improve the accuracy of the crush displacement. However, if a low mass sample within a high impact-velocity is the case, accelerometer should be selected carefully. Yet, in an aforementioned case, accelerometer cannot measure the values in the range of one-g (free-fall). Such a problem can be remedied by an additionally high sensitive (low g) accelerometer placed on the drop mass. Nonetheless, this extra scenario is not valid if acceleration of the drop mass is much greater than gravity.

Figure 2-34 Drop tower test mechanism and reservoir of foam in test apparatus

Secondly, drop tower test set-up which is depicted in Figure 2-34 is the case when high strain rated behaviors of foam blocks are needed to be obtained. By changing the mass of the impactor and height of the impactor, desired impact velocities are reached. Maximum speed of the impactor which is allowed to be is 24 m/s for drop tower tests.

Kellas [21] explained the drop test apparatus and its method for higher strain rate tests too. Higher loading speeds can be achieved easily within the mechanism showed in Figure 2-35.
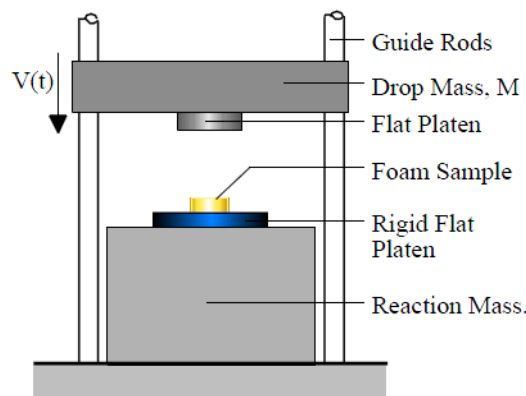
Figure 2-35 Variable strain rate configuration of drop test set-up [21]

A load cell accommodates on the flat platen records the force time history, while accelerometer placed on the drop mass records the acceleration time responses. Optical sensors help measuring crush displacements. Moreover, string potentiometers can also be used for displacement measurements. These instruments could cause troubles owing to inertial or flexibility issues in case of high acceleration cases. In this configuration, impact velocity is limited by the amount of energy that can be absorbed by the crushable sample. Hence, strain-rate changes during the crush event and depends on the crush velocity. For this reason this relatively cheap method cannot be used for quasi-static tests.

2.2.5 Material Characterization of Foams

Characterization of foams is a costly process where material properties are reached for different densities and strain rates. However, within the increasing usage of numerical tools resulted in an increase of the need of the experimental results of

such tests. As a result, nowadays foam materials are being characterized much more than it ever is.

Zhang and his friends presented a paper [22] related to modeling of polymeric foam materials. In their study, an experimental program is developed and different test modules are applied to foam samples to obtain material properties of them. In this study a 50 x 50 x 50 mm foam samples are utilized to obtain stress-strain curves of them under uni-axial compression tests.
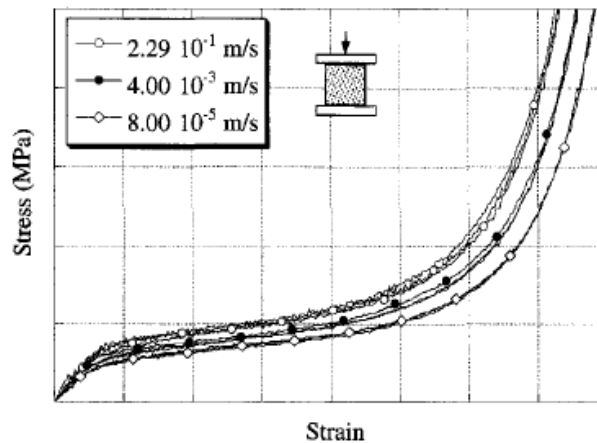
Figure 2-36 Stress-strain response of a polyurethane foam [22]

In Figure 2-36, stress strain response of a foam material under uni-axial compression condition is depicted. As seen in Figure 2-36, quasi-static compression tests are applied to obtain material parameters.
In a study done by Avalle M. [23], mechanical properties of three polymeric foams are evaluated in both static and impact loading conditions.
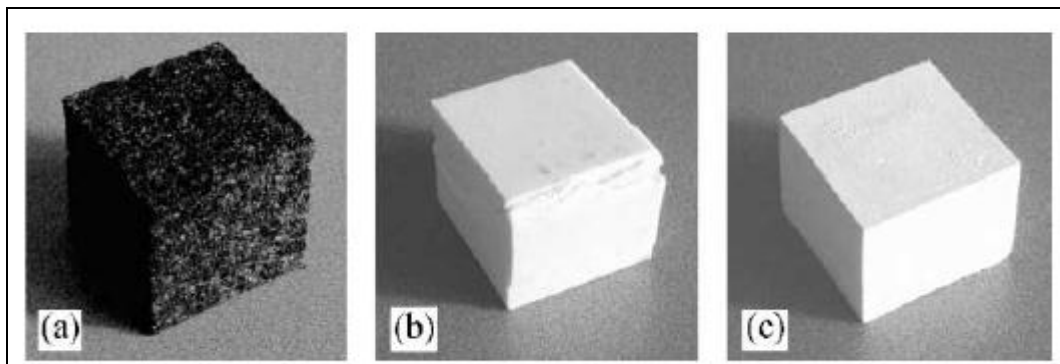
Figure 2-37 Three different types of polymeric foams [23]

In Figure 2-37, three distinct types of foams which are expanded polypropylene (EPP), polyurethane (PU) and polystyrene (PS), respectively are depicted. 50x50x50 mm specimens are selected as dimensions and each tests repeated three times under the same nominal condition. In the same paper, it is also mentioned that quasi-static tests are conducted on an electronically controlled universal testing machine, while the choice is drop dart machine for dynamic tests. It is emphasized that quasi-static compression test procedure is consistent with the standard [35]. In the conclusion section of the paper it is emphasized that EPP material is strongly sensitive to strain-rate changes.

In a study [24] conducted by University of Waterloo, automotive seat foams are characterized at high strain rates. Five distinct types of polymeric foams which are used in automotive industry are measured under both quasi-static conditions and at high strain rates.
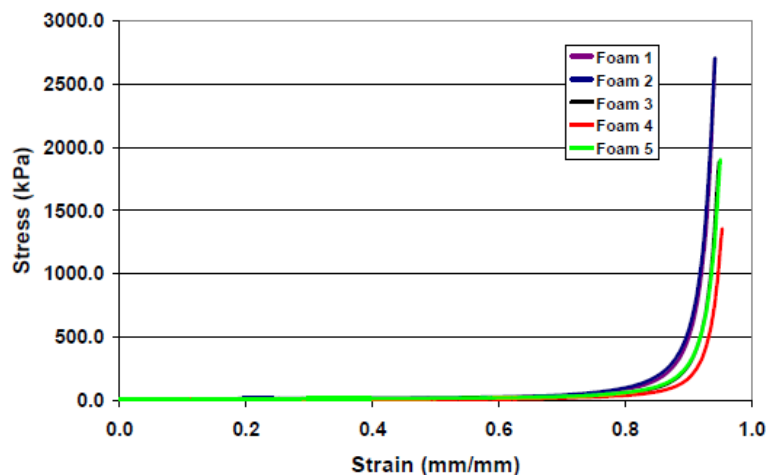
Figure 2-38 Quasi-static stress-strain test data of five foams [24]

Typical quasi-static responses of foam materials under compression are depicted in Figure 2-38. Almost 95 % of the specimens are crashed as it is seen in Figure 2-38. The same study also mentions about the number of the tests per foam specimen. According to the paper, three tests on each sample are performed to guarantee that consistent results are attained. It is also possible to understand from the title of the article that some dynamic tests are also conducted. In order to compare both

quasi-static and high strain-rated results, Figure 2-39 is given. It is also stated in the paper that automotive foams have zero Poisson ratios.
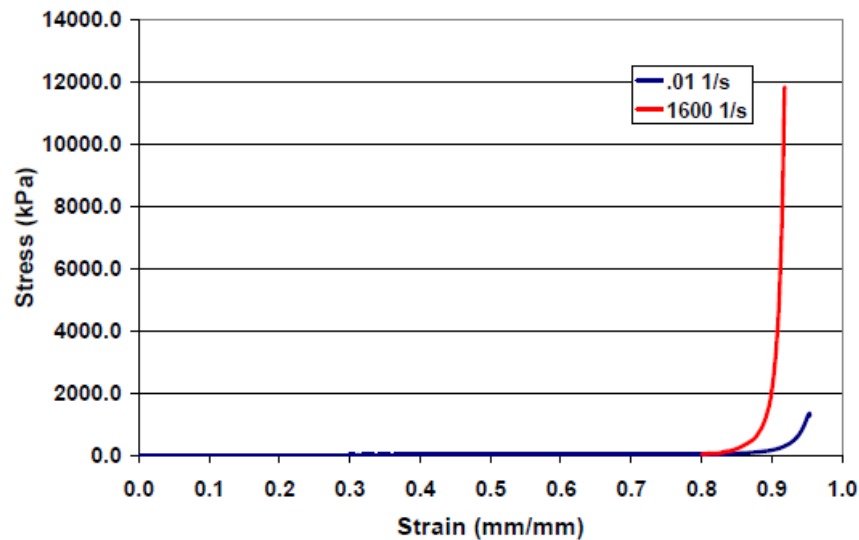
Figure 2-39 Comparison of quasi-static and high rate stress-strain data [24]

In a study [25] two different types of polymer foams are mechanically characterized. The former is called *IMPAXX* and generally used for crash protection. The latter foam is named *Johnson Controls* inc. (JC) and this material is used for the interior sections of the cars such as seat cushions. For the compression tests of energy absorbing foam, three distinct densities are determined. JC foams are compressed for four distinct densities. Each specimen is tested for five different strain rates varying from 10- to 10^{-3} s^{-1}. It is also mentioned in the paper that compression tests are conducted on an MTS 810 Elastomer Test System with a 25 kN load cell. In order to acquire the stress strain curve, following method is utilized: Applied load is divided by the original specimen area (engineering stress) and the specimen displacement is divided by the original specimen height (engineering strain) [25].

In the conclusion and discussion section of the paper, it is stated that deformation of foams almost never will be fully axial. Even in car crashes, distinct deformation regimes are encountered. To be able to describe the foam material perfectly, tests with other conditions should also be done.

2.2.6   Finite Element Modeling of Foams

In reference [26], finite element modeling of the energy absorbing barriers for high speed impact is presented. According to the paper, polystyrene foam is the most suitable foam type due to the extensive static and dynamic testing on various foams. Modeling of polystyrene foam is performed using LS-DYNA which has several foam material models. An irreversible material model is selected for the representation. The reason behind this choice is stated in the paper that this material model is easily obtainable from dynamic crash test data.

A simple foam compression model is developed in order to mimic the test data as shown in Figure 2-40. A drawback of this scenario can be said in a way that foams used in the tests are glued to each other instead of forming one piece. This kind of a technique may not cause to troubles in axial loadings, however it can be problematic if the loading is not fully axial. The major conclusion of this study is that polystyrene foams can be effectively modeled using appropriate material model in LS-DYNA.
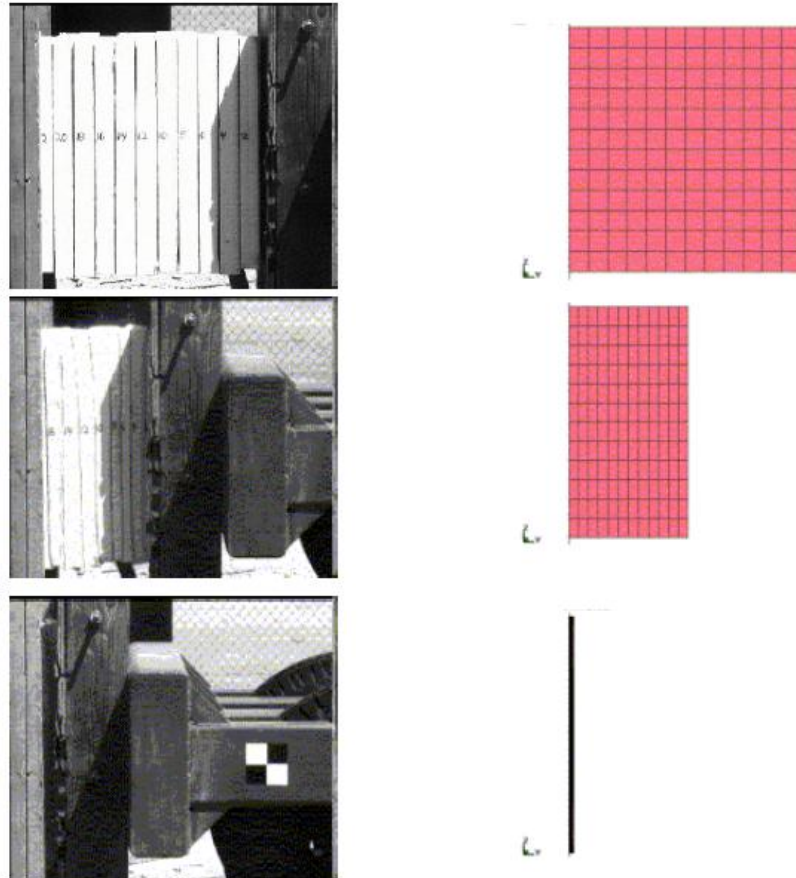
Figure 2-40 Sequential comparison of test and simulation [26]

In 2006, Slik, Vogel and Chawda presented a paper [27] related to material model validation of energy absorbing foam. It is stated in the paper that trustworthy material models play a big role for the success of the simulations. Test and simulation results are close enough to each other. The foam represented in the paper is styrenic foam and commercialized under the name IPMAXX. LS-DYNA is the numerical code used in this paper.
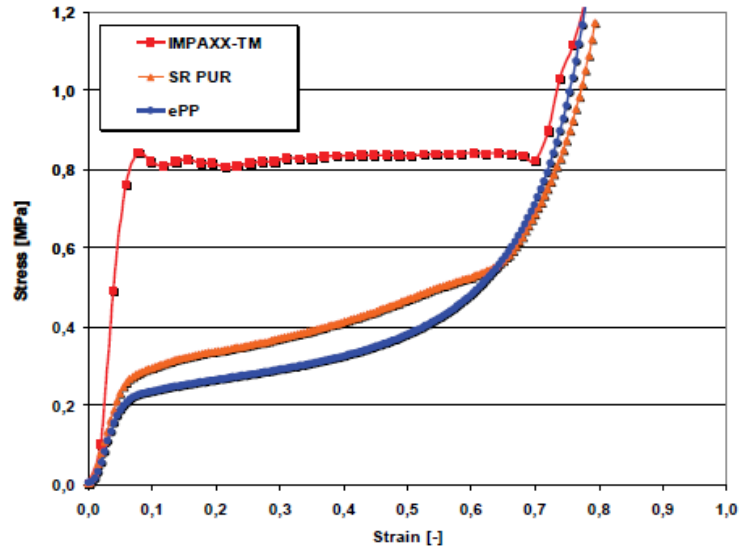
Figure 2-41 Comparison of IPMAXX with EPP and PUR [27]

According to Figure 2-41, selected foam material, *IPMAXX*, is the most effective type of all three models. This comment is based on the idea that an ideal energy absorber is expected to show a square wave response. For the representation of this foam material both crushable and reversible material models were investigated. It is stated in the final section of the paper that both irreversible and reversible foam material models showed a good correlation and both of them can be used for *IPMAXX* foam. Although this material is an effective model, it showed a pretty distinct behavior than PE and PU. For this reason it is not a candidate for the material used in the thesis.

In the reference [28], comparison of distinct material models in LS-DYNA is given for the representation of polypropylene foam material. A brief description of three constitutive material models is done and some tricks for these materials are given. Here a short summary of these three material models will be done. First material model is developed for low density foams. Typical application areas are seating foams and skins on the outer surface of impact dummies. A downside of this model is lack of rate dependency. Second material model is mainly similar to the first one, whereas rate effects are also seen in this model. Third material model is constructed for honeycomb structures and anisotropic foams. This material model allows for input of compressive stress-strain curves in three major coordinates of

the material. Two out of these three material models can be accepted as candidates for representing the foams used in this thesis.

Müllerschön used a visco-elastic material model for the representation of a high density Poly-Ethylen named *LUPOLEN* [29]. LS-DYNA is used for simulations of this material. *LUPOLEN* is a strain-rate dependent material and a reversible material up to a relatively high level of deformation strains. Furthermore, in order to model non-linear elastic behavior in combination with rate dependent properties a visco-elastic material model is sufficient. That is the principal idea of using a visco-elastic material model. In the conclusion section of the study, it is stated that capability of the selected material model in LS-DYNA to fit experimental curves with distinct strain rates is relatively poor. For this reason this material model is not suitable enough to be able to use in this thesis.

Hassan and his friends developed a study [30] in which three different explicit finite element method packages (RADIOSS, FCRASH and LS-DYNA) are used. It is stated in the paper that success of the study relies extensively on foam material models. That is why five classes of foam types are given in detail. Their fundamental features and available material models in aforementioned codes are also area of interest of this study. Appealing part of this study is that one of the five distinct foams is the same material which is used in this thesis. Hence, focus is shifted to this material (EPP). However, a short description of all five distinct foams will be given here. *Soft polyurethanes* are usually applied in automotive industry. Seat cushions and dummy parts are the main application areas thanks to the reversibility of this foam type. Another example which is used in automotive industry is named *energy absorbing polyurethanes.* This material is similar to soft polyurethane in a lot of way whereas, rebounding characteristics of these foams make the difference. *Expanded particle foam* is the main area of interest of this study. Different crash strengths can be obtained for given density. Moreover, this foam is generally a polypropylene and its density can be changed from 20- to 200-g\l. Some applications of this type of foam, as it is used in this thesis, require strain rate effects. This type of foam material is easy to model in LS-DYNA owing to the fact

that it only necessitates uni-axial compression test data. Thanks to the guidance of this paper, it is now easier to model this kind of foam in the thesis.

Croop and Lobo presented a paper [31] in which foam material characteristics and some material models in LS-DYNA are offered to use. It is mentioned in this paper that *Expanded Polypropylene* is possible to be represented by a specific type of material model. The most valuable information in this paper is that it suggests a material model which is strain dependent for a specific type of foam. Similar usage can also be applied for the foam materials in the thesis.

In the reference [32], it is figured out that the foam material (*BX-250)* used as a projectile is a very similar to a class of automotive foam. However, our interest is shifted to the reversible material model which is a strong candidate for usage of EPP and PE. It is stated in the paper that for the representation of *BX-250* there is an appropriate reversible material model in LS-DYNA. Moreover, this material model allows for multiple stress-strain curves as input for rate dependency. What is learned from this paper is that it is possible to modify stress-strain curves in such a way that material model is asked for.

Mines gives information about distinct material models for distinct finite element codes in his paper [33]. LS-DYNA and ABAQUS are two nonlinear finite element codes for simulating experimental tests to understand the behaviors of foam materials. In his paper he mentioned that ABAQUS necessitates large number of material test data which are compression, tension, shear and hydrostatic. On the contrary, LS-DYNA can simply be used only with uni-axial compression data. The same paper also talks about two main material models for foams in LS-DYNA. It is also declared in the paper that reversible material model can also be used for crushable foams. This is the key sentence of this study and this method will also be used in this thesis.

Ozturk and Anlas presented a paper [34] related to FE simulaton of multiple compressive loading and unloading of Expanded Polystyrene (EPS) foam which is used in packaging applications. In this paper, results of ABAQUS and LS-DYNA compared. The finite element model of the scenario is depicted in Figure 2-42. Foam dimensions are determined to be 50x50x50 mm. Universal test machine is

used for the compression of the foam material. Average density of EPS specimens is 19.8 kg/m^3.
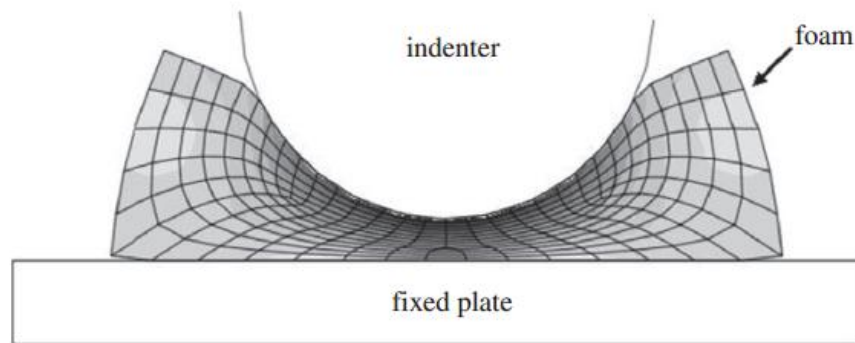
Figure 2-42 Deformation of foam during hemi-sphere indentation [34]

In the finite element modeling part of the study, material models used in two different codes are specified. According to paper, a crushable foam material model is selected for ABAQUS simulations. On the other hand, a reversible material model is selected for LS-DYNA simulations.

In the conclusion part of the paper, it is stated that in both codes stress-strain curves are predicted well for single loadings. However, when the case is multiple loading ABAQUS is overestimated the values. On the other hand, by adjusting two distinct parameters in LS-DYNA satisfactory results are reached.

CHAPTER 3

EXPERIMENTAL APPROACH

Chapter 3 is a section in which experimental approach is explained in detail. Two fundamental tests which are material characterization tests of polymeric foams and drop tests of munitions were conducted throughout this study. The former tests were chosen to acquire specific mechanic properties of two distinct foams which are Expanded Polypropylene (EPP) and Polyethylene (PE). The latter is necessary in order to start parametric studies in which optimum design of foam cushions will be developed.

3.1   MATERIAL CHARACTERIZATION OF FOAMS

In order to obtain material properties of Expanded Polypropylene (EPP) and Polyethylene (PE), material characterization tests are conducted. Young Modulus, compressive stress-strain data, force vs. time data are the main areas of interest by these tests. EPP and PE foam materials at three distinct densities are characterized for various strain rates. Depending on the strain rates two distinct material test set-ups which are drop tower test machine and quasi-static test machine are used.

As clearly named in the introduction paragraph, Expanded Polypropylene EPP and PE were selected as the energy absorbing materials and these materials are subjected to drop tower and quasi-static test which were conducted at İZTEK Laboratory in İzmir. Foam specimens shown in Figure 3-1, were selected for characterization at three distinct densities and seven different strain rates.
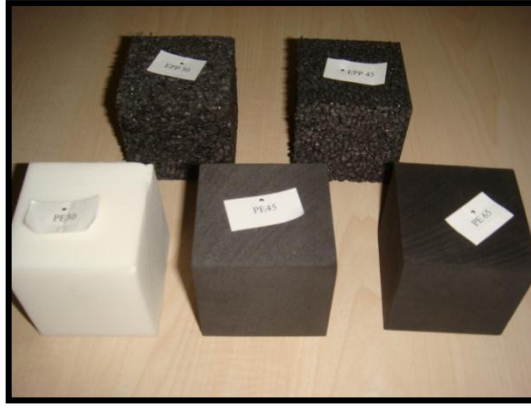
Figure 3-1 50x50x50 mm foam specimens

Densities : 20 kg/m^3, 30 kg/m^3, 45 kg/m^3 for EPP and 30 kg/m^3, 45 kg/m^3, 65 kg/m^3 for PE.

The foam dimensions are chosen to be 50 mm x 50 mm x 50 mm considering the standards [35] related to material characterization. During the tests of EPP and PE, quasi-static set-up was used for four distinct strain rate values which are $10^{-4}s^{-1}$,10^{-3} s^{-1}, 10^{-2} s^{-1}, 0.16 s^{-1}. Moreover, every single test was repeated three times for each specimen at above mentioned strain rates values to find out the significance of response variability. Young Modulus values of different types of foams were also gathered at lower strain rated quasi-static tests which is $10^{-4}s^{-1}$.

Behaviors of EPP and PE foams at 20 s^{-1}, 50 s^{-1} and 100 s^{-1} strain rates were obtained by drop tower test mechanism. By doing so, stress-strain relations, force-time diagrams, as well as energy-time changes were obtained. Repetition of the drop tower tests were similar to quasi-static tests, that is each specimen was compressed three consecutive times at different strain rates.

3.1.1 Quasi-static Tests

Numerous tests were conducted in order to get mechanical properties of foams under quasi-static and dynamic compression loading. `Shimadzu AG-X 300 $kN$ testing machine` was utilized for quasi-static compression tests in which maximum 8 mm/sec velocity is allowed for the actuator. In quasi-static compression tests, actuator moves at a constant velocity which defines strain rates. For a desired

strain rate value, e.g. 0.1 s^{-1}, actuator compressed to the 50x50x50 mm specimen at a velocity of $5\ mm/s$.

$$50\ mm * 0.1\ s^{-1} = 5\ mm/s$$

Reference [35] is taken into consideration for performing quasi-static compression tests.

3.1.2   Drop Tower Tests

Fractovis Plus is the name of the machine which is used for high strain-rated tests. In dynamic tests, piezoelectric load cells with a maximum 22.4 kN load were used to measure the force, while displacement and velocity is gathered by the integration of the acceleration with respect to time. Absorbed energy was calculated using Equation (3-1) in which $F(t)$ represents the time dependent force and v_0 is the expression for initial velocity.

$$E = V_0 \int F(t)dt \qquad\qquad (3\text{-}1)$$

3.2   DROP TEST OF MUNITION

At the beginning of this chapter material characterization tests are introduced. This part of the chapter covers the preparation of 50 cm parallel drop tests of foam integrated munitions on which high loads are not allowed to be. An unintentional drop of munitions may cause to malfunctioning of critical components that take part in the system. However, load levels that will appear on munitions in case of a drop scenario are limited by reference [40]. After munitions exposed to such loads, it is expected to be on the safe side which means that critical levels of loads are not reached.

During the tests a prototype of a missile which has no functionality, a composite launching tube and two foam cushions with an initial geometry were used to establish the mechanism. Besides, steel screws which are trying to hold the missile and the launching tube together prevent the missile to slide in the launching tube.

Two foam cushions made of Expanded-Polypropylene which is placed at both ends the launching tube are supposed to absorb the energy caused by impact. There is a shrink fit contact between foam cushions and the tube so that no separation can be seen between two materials.

The drop test apparatus can be seen in Figure 3-2 where drop height can be controlled. Quick-release mechanism produces a signal to release the munitions for free fall from desired drop height. Munitions are dropped onto a rigid-like grounds or sometimes ply-wood ground. Both concrete and wood grounds were used throughout the experimental process. Figure 3-2 is given just for the representation of the drop mechanism. That is why munition is not taken place in this figure.

High-speed camera permits us to observe the behavior of the foams in millisecond levels. Data collection system is an indispensable tool for acceleration signals which is recorded to post-process.
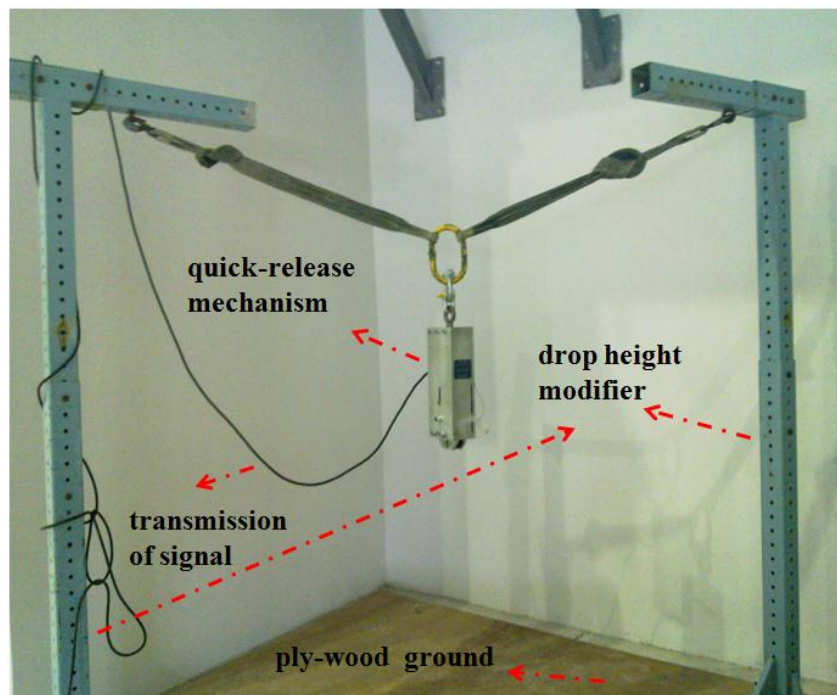
Figure 3-2 Drop test apparatus

Another significant process prior to tests is to position accelerometers (*PCB 356B21)* which are able to collect signals in three axes. Considering the

requirements, accelerometers are positioned on missile as depicted in Figure 3-3. Accelerometer II is located at the center of gravity of the missile and p1, p2 and p3 represents the distance from the nose of the missile.
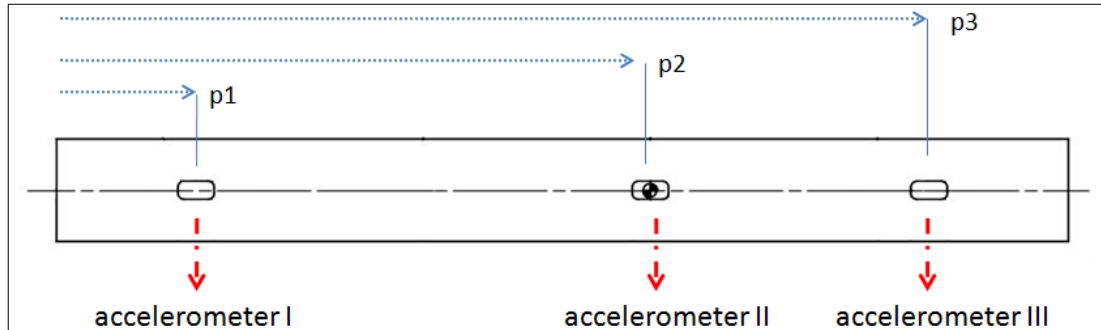
Figure 3-3 Schematic view of positioning of accelerometers

In the paper [36], it is mentioned that selection of the accelerometer is particularly significant for mechanical shock measurements. It can be concluded that selection of the appropriate accelerometer depends on the physics of the event. In addition, data obtained by drop tests is directly affected by the type of the accelerometers. For this reason, selection of the accelerometer should be done carefully.

In another study [37], accelerometer types are investigated. *IEPE Piezoelectric Accelerometer* is a typical one used in drop tests. The main advantage of this type of accelerometer is that it is used in a wide dynamic range. In the same paper, its frequency range is given as 0.5 Hz. to 50000 Hz. The same type of accelerometer is used in the drop tests of munitions too. Low cost and ease of use are two main reasons of this selection. However, it is also suggested to use *MEMS accelerometers* in shock events. The main advantage of this type of accelerometer is that thanks to having a stiffer structure than piezoelectric accelerometer, the first natural frequency is higher.

Prior to experimental program, selection of the initial geometry of foam cushions will be detailed in the following section.

3.2.1 Determination of the Initial Foam Geometry

Drop test trial of munitions is not the very beginning of experimental agenda. Before conducting tests, distinct missiles which are exposed to familiar loads on a drop case are surveyed. No more than a few studies are reached owing to the fact that they are not distributed for public and so contain classified information.

According to Figure 3-4, octagonal designs are preferred for foam caps. No rectangular type of shapes is chosen for energy absorbers. Main reason is that sharp edges may cause to stress concentration. Moreover, a rectangular shape design has a bigger volume than other type of shapes which is not desirable because of the increase of mass.
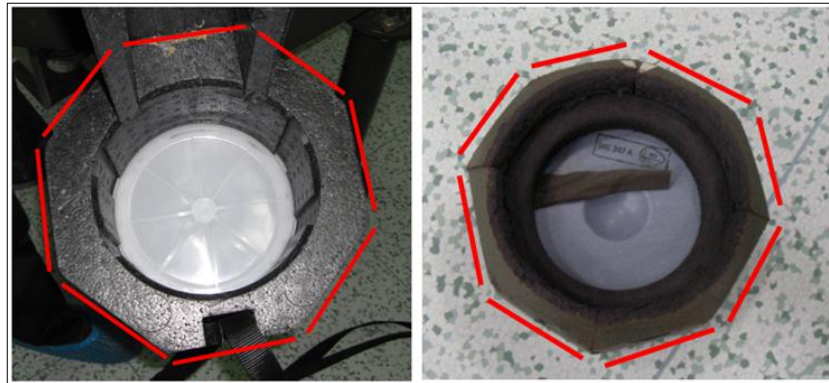
Figure 3-4 Octagonal shaped foam cap designs

A French made missile, *Eryx* uses a design seen in Figure 3-5. French company also preferred an octagonal design for cushions, whereas they are possibly transported by a container which is not seen in our transportation procedure. Similar to the designs depicted in Figure 3-4, neither rectangular nor cylindrical designs are preferred by French company. Apart from reasons causing not to use of rectangular designs, there are some other drawbacks of cylindrical designs.
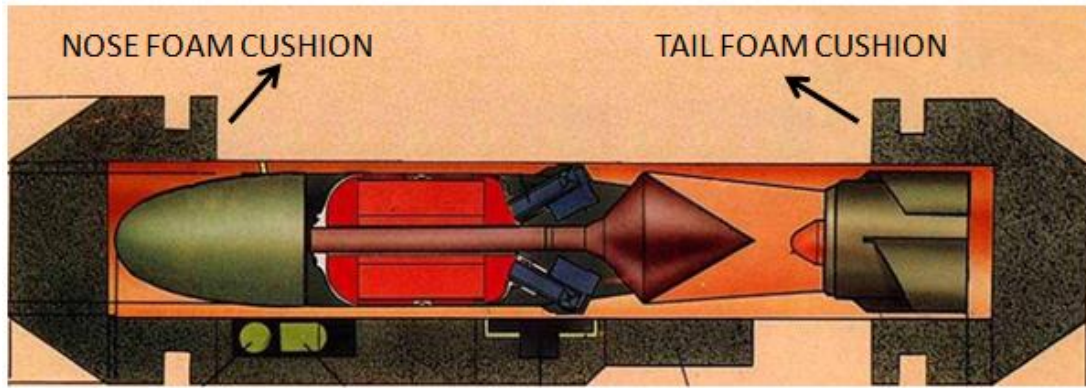
Figure 3-5 A foam cap design that Eryx (French made missile) used

An effortless predictable setback of a cylindrical design is the danger of roll-over of the system after impact. In addition, storage and piling of missiles would be problematic and cannot be underestimated if cylindrical designs were preferred.

Cylindrical and rectangular design ideas can be elected owing to the drawbacks of these designs. It is thought that jeopardy of roll-over of the missile will not vanish in case of an octagonal design. That is why in this thesis, foam shape is determined to be hexagonal.

Considering the pitfalls of other shapes, as seen in Figure 3-6, hexagonal shaped foam shock absorbers were manufactured.

Figure 3-6 Hexagonal shaped foams as initial designs

CHAPTER 4

NUMERICAL APPROACH

A sharp increase of the capabilities of the computers in recent years changed the strategies of the companies on product development. Furthermore, high cost of the experimental process also shifted the interest from experimental methods to numerical ones. For this reason, this tendency is still increasing and numerical codes are being used at almost every process of the products.

There are a bunch of numerical methods that are used so often in this kind of applications. However, ANSYS (code 1), ABAQUS (code 2) and LS-DYNA (code 3) are the three major codes whose capabilities are higher when compared to others. For this reason, almost all these kind of analyses are being conducted by these three codes in the market. Of three codes, code 1 is the one which has the worst user friendly interface. This is apparently a reason why Code 2 and code 3 are preferred more often among three of them. However, this is not the main reason of this selection. Contact capabilities and material model variety of code 2 and code 3 are the fundamental reason. Both these two codes have a solid performance in terms of contact capabilities. Furthermore, these two codes are very successful when representation of the behavior of foam materials is the case. Although both code 2 and code 3 are the two available tools for the drop simulation of munitions, code 3 necessitates less experimental data for foams. At this point, this minor difference became the major factor for this selection.

Starting from the selection of suitable material models by using results of characterization tests, drop tests were validated by finite element code, LS-DYNA. After that, a parametric study is conducted to optimize the geometry of the foam. In this section of the study, nonlinear dynamic code will be introduced. After,

selected foam material models in this code will be summarized and a very late part of the chapter belongs to the general procedure for finite element development process.

4.1.1 Finite Element Code (LS-DYNA)

LS-DYNA, as a nonlinear finite element program capable of simulating complex real world problems, is more than suitable considering the duration of event and strain rates involved. Highly nonlinear and transient dynamic finite element analyses are the principal areas of interest of the code which is firstly used in 1976 as a name of DYNA3D. The very first application of the code is related to the stress analysis of structures subjected to a variety of impact. Mature contact treatments, low memory requirements, wide range of material models and inexpensive time-step calculations can be counted as pros of the code.

The fundamental difference between explicit codes and static, structural dynamic codes is based on the solution method they used. Unlike a static model which is solved for a small number of load steps, a dynamic model must be solved for each time step. The time step for an explicit dynamic code depends on the time required for a sound wave to move across the smallest element, which can be 1 microsecond or shorter. Thus, a dynamic model that is run for only 0.1 seconds in real time will be solved 100.000 times.

LS-DYNA is an explicit code using central difference method. Stability requires that the time step size be less than the highest frequency in the system.

Starting from here, conservation equations that LS-DYNA used are given. Boundary and initial conditions and solution methods are explained.

Consider a body shown in Figure 4-1. We are interested in time-dependent deformation in which a point in b initially at $X_\alpha(\alpha = 1,2,3)$ in a fixed rectangular Cartesian coordinate system moves to a point $x_i(\alpha = 1,2,3)$ in the same coordinate system. Since a Lagrangian formulation is considered, the deformation can be expressed in terms of the convected coordinates X_α, and time t

$$x_i = x_i\,(X_\alpha, t) \qquad\qquad (4\text{-}1)$$

At time = 0, initial conditions

$$x_i(X_\alpha, 0) = X_\alpha \tag{4-2}$$

$$\dot{x}_i(X_\alpha, 0) = V_i(X_\alpha) \tag{4-3}$$

Where V_i defines the initial velocities [48].

4.1.1.1 Governing Equations

We seek a solution to the momentum equation

$$\sigma_{ij,j} + \rho f_i = \rho \ddot{x}_i \tag{4-4}$$

satisfying the traction boundary conditions

$$\sigma_{ij} n_i = t_i(t) \tag{4-5}$$

on boundary ∂b_1, displacement boundary conditions

$$\dot{x}_\iota(X_\alpha, t) = D_i(t) \tag{4-6}$$

on boundary ∂b_2, the contact discontinuity

$$(\sigma_{ij}^{+} - \sigma_{ij}^{-})\, n_i = 0 \tag{4-7}$$

along an interior boundary ∂b_3 when $x_i^{+} = x_i^{-}$. Here σ_{ij} is the Cauchy stress, ρ is the current density f is the body force density, $\ddot{x}$ is acceleration, the comma denotes covariant differentiation, and n_j is a unit outward normal to a boundary element of $\partial \tilde{b}$.
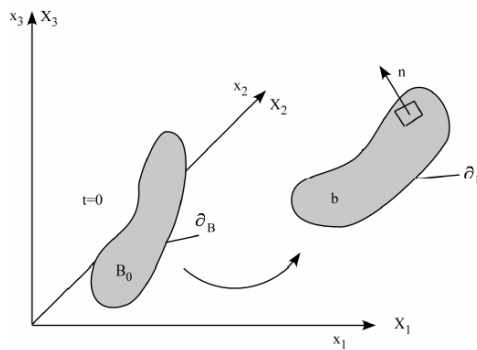
Figure 4-1 Notation [48]

Mass conservation is trivially stated

$$\rho V = \rho_0 \qquad (4\text{-}8)$$

where V is relative volume, i.e., the determinant of the deformation gradient matrix, F_{ij},

$$F_{ij} = \frac{\partial x_i}{\partial X_j} \qquad (4\text{-}9)$$

and ρ_0 is the reference density. The energy equation

$$\dot{E} = V s_{ij} \dot{\varepsilon}_{ij} - (p + q)\dot{V} \qquad (4\text{-}10)$$

is integrated in time and is used for equation of state evaluations and a global energy balance. In Equation (4.10) s_{ij} and p represent the deviatoric stress and pressure,

$$s_{ij} = \sigma_{ij} + (p + q)\delta_{ij} \qquad (4\text{-}11)$$

$$p = -\frac{1}{3}\dot{\sigma}_{ij}\delta_{ij} - q = -\frac{1}{3}\,\sigma_{kk} - q \qquad (4\text{-}12)$$

respectively, q is the bulk viscosity, δ_{ij} is the Kronecker delta ($\delta_{ij} = 1 \; if \; i = j$; otherwise $\delta_{ij} = 0$) and $\dot{\sigma}_{ij}$ is the strain rate tensor. The strain rates and bulk viscosity are discussed later [48].

We can write:

$$\int_v \left(\rho \ddot{x}_i - \sigma_{ij,j} - \rho f\right) \delta x_i dv + \int_{\partial b_1} \left(\sigma_{ij} n_j - t_i\right) \delta x_i ds$$
$$+ \int_{\partial b_3} \left(\sigma_{ij}^+ - \sigma_{ij}^-\right) n_j \,\delta x_i ds = 0 \qquad (4\text{-}13)$$

where δx_i satisfies all boundary conditions on ∂b_2, and the integrations are over the current geometry. Application of divergence theorem gives

$$\int_v \left(\sigma_{ij}\delta x_i\right)_{,j} dv = \int_{\partial b_1} \sigma_{ij} n_j \,\delta x_i ds + \int_{\partial b_3} \left(\sigma_{ij}^+ - \sigma_{ij}^-\right) n_j \,\delta x_i ds \qquad (4\text{-}14)$$

57

And nothing that

$$\left(\sigma_{ij} \delta x_i \right)_{,j} \sigma_{ij,j} \delta x_i = \sigma_{ij} \delta x_{i,j} \qquad (4\text{-}15)$$

Leads to the weak form of the equilibrium equations:

$$\delta \pi = \int_v \rho \ddot{x}_i \, \delta x_i dv + \int_v \sigma_{i,j} \, \delta x_i dv - \int_v \rho f_i \, \delta x_i dv - \int_{\partial b_1} t_i \, \delta x_i ds = 0 \qquad (4\text{-}16)$$

a statement of the principal of virtual work [48].

We superimpose a mesh of finite elements interconnected at nodal points on a reference configuration and track particles through time, i.e.,

$$\dot{x}_\iota (X_\alpha, t) = x_i (X_\alpha (\xi \eta \zeta), t) = \sum_{j=1}^{k} \phi_j \, (\xi \eta \zeta) x_i^j (t) \qquad (4\text{-}17)$$

Where ϕ_j is shape (interpolation functions) of the parametric coordinates $(\xi \eta \zeta)$, k is the number of nodal points defining the element, and x_i^j is the nodal coordinate of the jth node in the ith direction [48].

Summing over the n elements we may approximate the $\delta \pi$ with

$$\delta \pi = \sum_{m=1}^{n} \delta \pi_m = 0 \qquad (4\text{-}18)$$

and write

$$\sum_{m=1}^{n} \left\{ \int_{v_m} \rho \ddot{x}_i \, \phi_i^m dv + \int_{v_m} \sigma_{ij}^m \, \phi_{i,j}^m dv - \int_{v_m} \rho f_i \, \phi_i^m dv - \int_{\partial b_1} t_i \, \phi_i^m ds \right\} = 0 \qquad (4\text{-}19)$$

where

$$\phi_i^m = (\phi_1, \phi_2, \dots \phi_k)_i^m \qquad (4\text{-}20)$$

In matrix notation Equation (4.16) becomes

$$\sum_{m=1}^{n} \left\{ \int_{v_m} \rho \, N^t N \alpha \, dv + \int_{v_m} B^t \, \sigma \, dv - \int_{v_m} \rho \, N^t b \, dv - \int_{\partial b_1} N^t t \, ds \right\}^m = 0 \qquad (4\text{-}21)$$

where N is interpolation matrix, σ is the stress vector

$$\sigma^t = (\sigma_{xx}, \sigma_{yy}, \sigma_{zz}, \sigma_{xy}, \sigma_{yz}, \sigma_{zx}) \qquad (4\text{-}22)$$

B is the strain-displacement matrix, α is nodal acceleration vector

$$\begin{pmatrix} \ddot{x}_1 \\ \ddot{x}_2 \\ \ddot{x}_3 \end{pmatrix} = N \begin{pmatrix} a_{x_1} \\ a_{y_1} \\ \vdots \\ a_{y_k} \\ a_{z_k} \end{pmatrix} = N\alpha \qquad (4\text{-}23)$$

b is the body force load vector, and t is applied traction loads

$$b = \begin{pmatrix} f_x \\ f_y \\ f_z \end{pmatrix}, t = \begin{pmatrix} t_x \\ t_y \\ t_z \end{pmatrix} \qquad (4\text{-}24)$$

4.1.1.2 1-D Equation of Motion
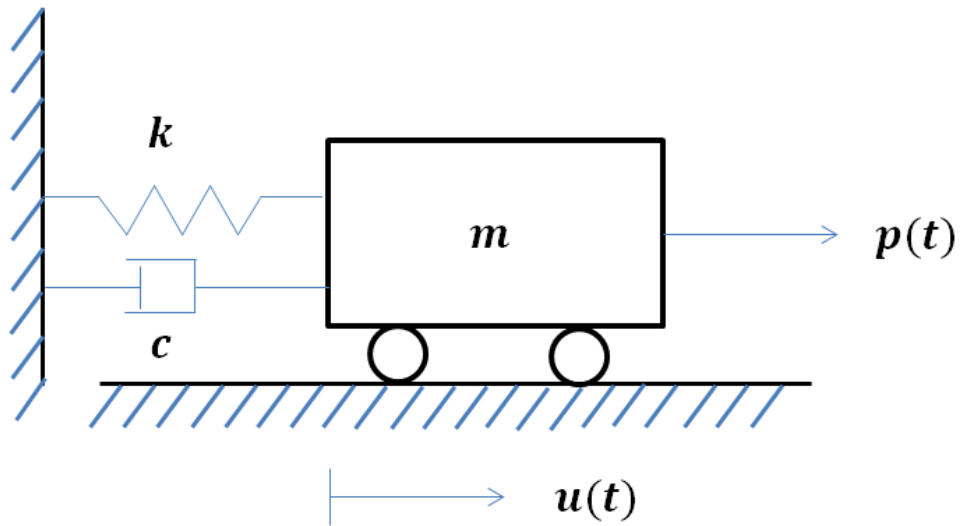
Figure 4-2 Single degree of freedom system [42]

Free body diagram of the mass is shown in Figure 4-3.
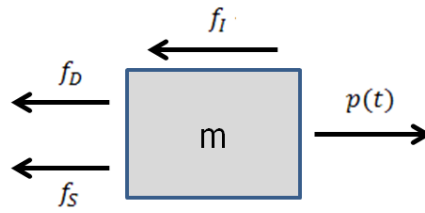
Figure 4-3 Free body diagram of mass [42]

Equilibrium of forces (D'Alembert's principle) can be written as follows:

$$f_I + f_D + f_S = p(t) \qquad (4\text{-}25)$$

The terms in Equation (4-25) are written as follows:

$$f_I = m\ddot{u} \qquad (4\text{-}26)$$

$$f_D = c\dot{u} \qquad (4\text{-}27)$$

$$f_S = ku \qquad (4\text{-}28)$$

where

f_I = inertia force

f_D = viscous damping

f_S = linear elasticity

k = stiffness

u = displacement

$\dot{u} = \dfrac{du}{dt}$ = velocity

$\ddot{u} = \dfrac{d^2u}{dt^2}$ = acceleration

For the linear elastic case, ordinary linear differential equation can be written as follows:

$$m\ddot{u} + c\dot{u} + ku = f(t) \qquad (4\text{-}29)$$

Analytical solutions of linear ordinary differential equations are available. For a harmonic loading case solutions can be given as follows:

60

$$p(t) = P_0 \sin \overline{w}t \tag{4-30}$$

$$w = \sqrt{\frac{k}{m}} \tag{4-31}$$

$$f = \frac{w}{2\pi} \tag{4-32}$$

$$\xi = \frac{c}{c_{crit}} = \frac{c}{2m} \tag{4-33}$$

$$w_b = w\sqrt{1 - \xi^2} \tag{4-34}$$

$$\beta = \frac{\overline{w}}{w} \tag{4-35}$$

where

$p(t)$ = harmonic loading

w = circular frequency

f = natural frequency

ξ = damping ratio

ξ = damped vibration frequency

β = applied load frequency

$$u(t) = u_0 \cos(wt) + \frac{\dot{u}_0}{w}\sin(wt) + \frac{p_0}{k}\frac{1}{1-\beta^2}\left(\sin(\overline{w}t) - \beta \sin(wt)\right) \tag{4-36}$$

where

u_0 = initial displacement,

$\dot{u}_0$ = initial velocity,

$\frac{p_0}{k}$ = static displacement,

$\frac{1}{1-\beta^2}$ = dynamic magnification factor.

For the physically and geometrically nonlinear case, ordinary nonlinear differential equation can be written as follows:

$$m\ddot{u} + c\dot{u} + f_S(u) = f(t) \tag{4-37}$$

61

On contrary to linear elastic case, only numerical solutions are possible for nonlinear problems. This type of systems (especially for systems with many DOF) are generally treated by direct intregration methods.

It should be kept in mind that events that only have short duration are generally solved by explicit methods, while problems that occur during a longer time range may be treated by implicit methods.

4.1.1.3 Time Integration

General expression is:

$$\dot{\boldsymbol{u}} - \boldsymbol{f}\big(t, \boldsymbol{u}(t)\big) = 0 \; and \; \dot{\boldsymbol{u}} \sim \frac{\boldsymbol{u}(t_{n+1}) - \boldsymbol{u}(t_n)}{\Delta t} \tag{4-38}$$

The system of equations is evaluated at the old time step for explicit schemes. For example; using explicit Euler method Equation (4-38) can be written as follows:

$$\frac{\boldsymbol{u}(t_{n+1}) - \boldsymbol{u}(t_n)}{\Delta t} - \boldsymbol{f}\big(t_n, \boldsymbol{u}(t_n)\big) = 0 \tag{4-39}$$

Equation (4-35) can be directly solved for $u(t_{n+1})$ using explicit Euler method.

On contrast to explicit schemes, the system of equations is evaluated at the new time step for implicit schemes. For example; using implicit Euler method Equation (4-38) can be written as follows:

$$\frac{\boldsymbol{u}(t_{n+1}) - \boldsymbol{u}(t_n)}{\Delta t} - \boldsymbol{f}\big(t_{n+1}, \boldsymbol{u}(t_{n+1})\big) = 0 \tag{4-40}$$

Equation (4-40) has to be iteratively used implicit Euler method.

4.1.1.4 Comparison of Explicit and Implicit Time Step

In general, the implicit time step will be larger than explicit time step. Moreover, implicit time step may need to be reduced if the physics of the problem requires a small time step. In addition to this, if contact surfaces are being used or there are material or geometric nonlinearities, implicit time step can be reduced. Most of the CPU is involved in matrix inversion. Therefore, the accuracy of each DOF is

maximized and complex element formulations are used in preference to increasing the mesh density. A 3-D mesh refinement by factor S increases the CPU cost by S^7 for an implicit solution. It is likely to be cheaper when the model size is small and nonlinearity is limited for an implicit analysis. Furthermore, a large step can be used for implicit analysis.

In explicit time integration method, all the computational time is in the element processing. The update of nodal accelerations is trivial. Element accuracy is maximized relative to the time to the process each one. The CPU cost is proportional to the number of elements and the time required to process element. A 3-D mesh refinement by factor S increases the CPU cost by S^4 for an explicit solution. It is likely to be cheaper when the model is large and the problem involves significant material, geometric or contact nonlinearities. The physics of the problem require a short time step for explicit solutions.

The summary of the comparison is given in Table 4.1.

Table 4.1 Comparison of explicit and implicit time integration methods

	Explicit	**Implicit**
matrix inversion	no	yes
the time step size	small	can be large
limitation of the time step	stability	accuracy
cost per time	small	large
what dominates the costs	element processing	matrix inversion (time integration)
cost increase for doubling the mesh density (solid elements)	x16	x128
element formulation	simple	complex

Advantages and disadvantages of both time integration methods can be listed.

For implicit time integration method:

- the method is unconditionally stable

- can be used for static simulations

- relative inexpensive for long durations

- requires often large amount of memory

- can have problems with strong nonlinear models

For explicit time integration method:

- computationally fast

- robust, even for strong nonlinear problems

- conditionally stable

- expensive to conduct long durations

Main application areas of implicit time integration method are low rate dynamic analyses, static simulations, eigenvalue analyses, spring-back, gravity loading, preload etc. For explicit time integration method, application areas are high rate dynamic analyses, car crash, impact/penetration problems, explosives etc.

4.1.1.5   Explicit Time Integration

Central difference sheme will be given in this part of the thesis. Approximation of velocity and acceleration is illustrated in Figure 4-4.
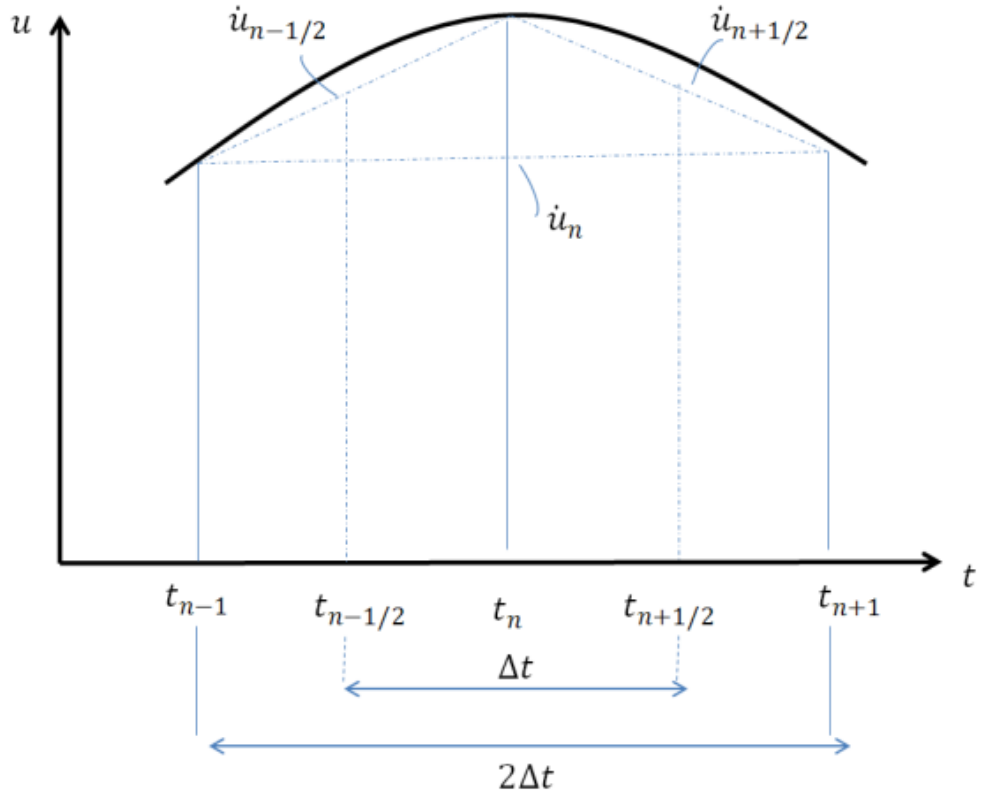
Figure 4-4 Approximation of velocity and acceleration [42]

$$\dot{u}_n = \frac{1}{2\Delta t}(u_{n+1} - u_{n-1}) \tag{4-41}$$

$$\ddot{u}_n = \frac{1}{\Delta t}\left(\dot{u}_{n+\frac{1}{2}} - \dot{u}_{n-\frac{1}{2}}\right) = \frac{1}{\Delta t}\left(\frac{u_{n+1} - u_n}{\Delta t} - \frac{u_n - u_{n-1}}{\Delta t}\right)$$
$$= \frac{1}{\Delta t^2}(u_{n+1} - 2u_n + u_{n-1}) \tag{4-42}$$

General equation of motion of the 1D system in Figure 4-2 at the current time step can be written as follows:

$$\boldsymbol{M}\ \ddot{u}_n + \boldsymbol{C}\ \dot{u}_n + \boldsymbol{K}u_n = \boldsymbol{P}_n(t) \tag{4-43}$$

Equation (4-43) can be solved by central difference method. Using approximations for velocities and accelerations Equation (4-43) can be written in terms of Equation (4-41) and Equation (4-42):

$$\left(M + \frac{1}{2}\Delta t\, C\right) u_{n+1} = (\Delta t^2) P_n - [(\Delta t^2)K - 2M]u_n - \left(M - \frac{\Delta t}{2} C\right) u_{n-1} \quad (4\text{-}44)$$

For lumped mass and damping, the matrices M and C are diagonal:

$$M = \begin{bmatrix} m_1 & \cdots & 0 \\ \vdots & \ddots & \vdots \\ 0 & \cdots & m_i \end{bmatrix} \quad C = \begin{bmatrix} c_1 & \cdots & 0 \\ \vdots & \ddots & \vdots \\ 0 & \cdots & c_i \end{bmatrix} \quad (4\text{-}45)$$

where i= the number of nodes in spatial discretization

Inversion of the diagonal matrices M and C is trivial. Hence, inversion of mass and damping matrix is trivial.

$$M^{-1} = \begin{bmatrix} \frac{1}{m_1} & \cdots & 0 \\ \vdots & \ddots & \vdots \\ 0 & \cdots & \frac{1}{m_i} \end{bmatrix} \quad C^{-1} = \begin{bmatrix} \frac{1}{c_1} & \cdots & 0 \\ \vdots & \ddots & \vdots \\ 0 & \cdots & \frac{1}{c_i} \end{bmatrix} \quad (4\text{-}46)$$
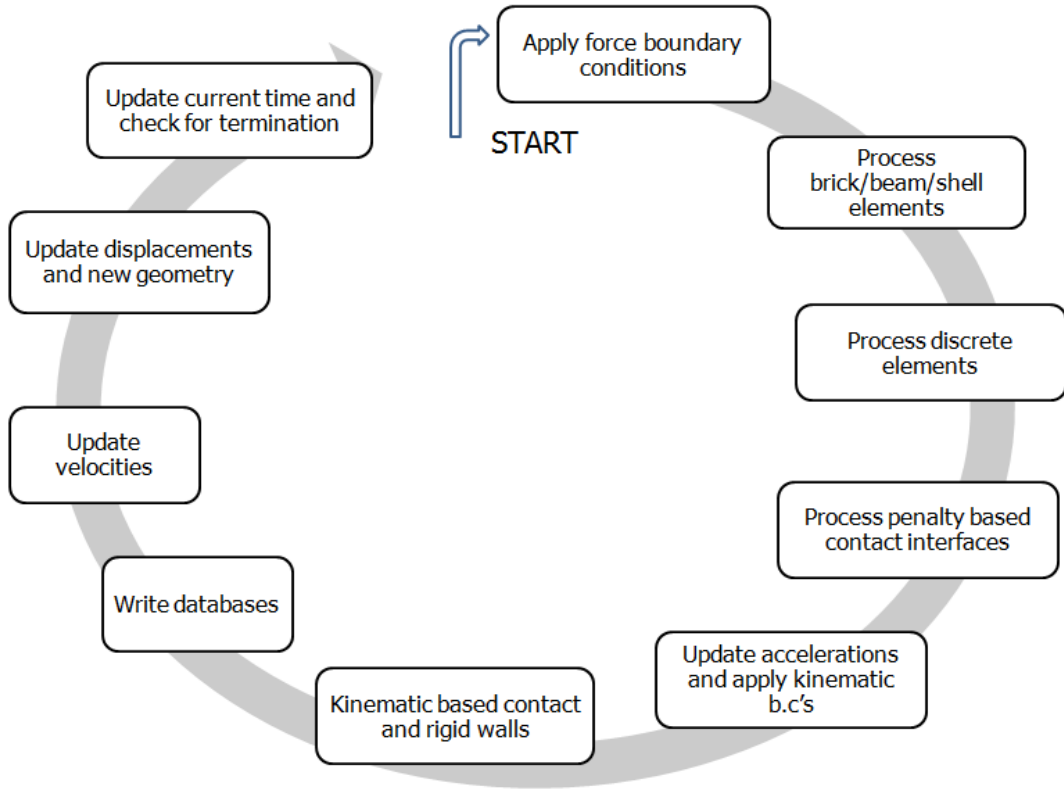
Figure 4-5 Integration loop repeated in every time step [42]

4.1.1.6 Critical time step

$$u = \emptyset_1 x_1 + \emptyset_2 x_2 + \emptyset_3 x_3 + \cdots + \emptyset_i x_i = \emptyset_x \qquad (4\text{-}47)$$

$$\underline{\emptyset^T M \emptyset}\, \ddot{x} + \underline{\emptyset^T C \emptyset}\, \dot{x} + \underline{\emptyset^T K \emptyset}\, x = \emptyset^T P \qquad (4\text{-}48)$$

$$I\ddot{x} + 2\xi_k w_k \ddot{x} + w_k{}^2 x = Y_k \qquad (4\text{-}49)$$

where

$\emptyset$ = modal matrix with M-orthogonalized eigenvectors stored in columns

x = generalized displacements

Y = generalized forces

Hence, i uncoupled equations of motion in terms of generalized displacements are gained.

$$\ddot{x} + 2\xi_k w_k \dot{x} + w_k{}^2 x = Y_k \qquad (4\text{-}50)$$

$$\dot{x}_n = \frac{(x_{n+1} - x_{n-1})}{2\Delta t} \text{ and } \ddot{x}_n = \frac{(x_{n+1} - 2x_n + x_{n-1})}{\Delta t^2} \qquad (4\text{-}51)$$

Here, central difference method is used within Equation (4-51) and equation of motion can be written for damped and undamped system as follows:

$$\Delta t_{critical,undamped} \leq \frac{2}{w_{max}} \qquad (4\text{-}52)$$

$$\Delta t_{critical,damped} \leq \frac{2}{w_{max}} \left[\sqrt{1 - \xi^2} - \xi \right] \qquad (4\text{-}53)$$

It can be inferred from the above equations that time step in explicit analysis is bounded by the largest natural frequency of the structure [42]. Furthermore, explicit time integration is more stable for lower time steps. Calculation of critical time step

Critical time step for a beam element is can be calculated by using above equations as follows:
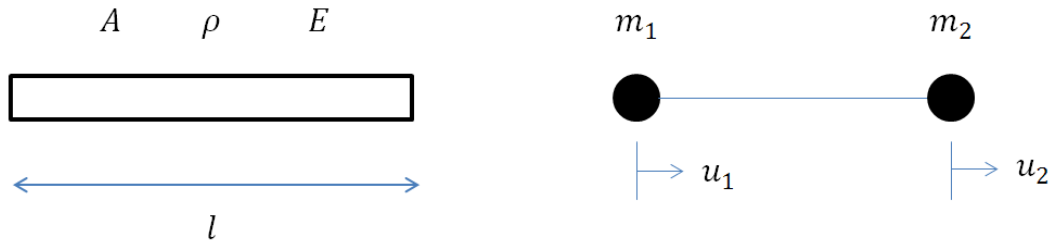
Figure 4-6 Standard beam element with two nodes [42]

Stiffness and lumped mass matrix can be written as follows for the element shown in Figure 4-6:

$$\text{mass lumping: } m_1 = m_2 = \frac{1}{2}\rho A l \qquad (4\text{-}54)$$

$$\text{mass matrix: } M = \frac{1}{2}\rho Al \begin{bmatrix} 1 & 0 \\ 0 & 1 \end{bmatrix} \tag{4-55}$$

$$\text{stiffness matrix: } K = \frac{EA}{l} \begin{bmatrix} 1 & -1 \\ -1 & 1 \end{bmatrix} \tag{4-56}$$

By using Equation (4-54), (4-55) and (4-56) natural frequencies of the system can be found as follows:

$$w = det \left\{ \frac{EA}{l} \begin{bmatrix} 1 & -1 \\ -1 & 1 \end{bmatrix} - w^2 \frac{1}{2}\rho Al \begin{bmatrix} 1 & 0 \\ 0 & 1 \end{bmatrix} \right\} = 0 \tag{4-57}$$

$$w_{max} = \frac{2}{l}\sqrt{\frac{E}{\rho}} = 2\frac{c_{beam}}{l} \tag{4-58}$$

Speed of sound can be written as follows:

$$c_{beam} = \sqrt{\frac{E}{\rho}} \tag{4-59}$$

$\Delta t_{critical}$ can be written as follows:

$$\Delta t_{critical} = \frac{l}{c} \quad (Courant - Friedrichs - Lewy - criterion) \tag{4-60}$$

It can be noticed in Equation (4-60) that if element size decreases or stiffness increases, $\Delta t_{critical}$ decreases. Also, increase in density causes to an increase in $\Delta t_{critical}$.

For a 2D and 3D element speed of sound can be written as follows:

$$c_{2D} = \sqrt{\frac{E}{(1-v^2)\rho}} \tag{4-61}$$

$$c_{3D} = \sqrt{\frac{E(1-v)}{(1+v)(1-2v)\rho}} \tag{4-62}$$

Time step is defined as the time step for an explicit dynamic code depends on the time required for a sound wave to move across the smallest element [12]. Owing to the changes of the shape of the elements, time step is recalculated after each step. The code cannot be forced to use a time step bigger than critical one. However, it is possible to lower the time step for stability. LS-DYNA uses a value of 0.9 times critical time step as default, whereas it should be lowered for some certain applications such as shock analysis. Reduction of time step will not affect the results of the simulations, its effects will be seen on run time.

4.1.2 Selected Foam Material Models

LS-DYNA is known as its wide range of material models which is based on distinct assumptions and unique application areas. Material model selection is a tough process in such a way that appropriate material model is one of the main factors affecting the success of the results. For this reason, it requires special attention for this selection. Used numerical code has a wide material library for foam materials. However, not all of these models are available for the representation of Expanded Polypropylene and Polyethylene. For example, some of these material models (*MAT_GENERAL_VISCOELASTIC and *MAT_PLASTICITY_POLYMER) are used for shell elements and this type of modeling is rare for energy absorbing foams. Absence of rate dependency is another drawback of some material models (*MAT_CRUSHABLE_FOAM and *MAT_LOW_DENSITY_FOAM) and these models do not allow the input of stress strain curves into the model. This is the reason of the elimination of these models for the representation of foam behaviors. Other than all these material models, some other alternatives (*MAT_HONEYCOMB and *MAT_VISCOUS_FOAM) are eliminated for their special usage.

Two polymeric foams, Expanded Polypropylene and Polyethylene, will be represented by two distinct material models which are Material Model 1, *MAT_FU_CHANG_FOAM (MFCF) [43] and Material Model 2, *MAT_MODIFIED_ CRUSHABLE_FOAM (MMCF) [43], respectively. Thanks to a wide range of use of foams in different application areas, some of the parameters of these material models can be found from literature. However, their rate dependency forces analyst to obtain stress-strain curves at different strain rates. Material characterization of

these two materials, EPP and PE, will be given in detail in the following chapters. Above mentioned two material models will be discussed in this section of the study.

4.1.2.1 Material Model 1 (MFCF)

The very first thing that is needed to be known about Material Model 1 is that Poisson ratio is set to zero. For this reason, it is accepted as one dimensional material law. Rate effects can be easily modeled for low and medium density foams. Shining point of this material model is that it allows user to input experimental results of uni-axial compression tests directly.

Crucial point in this material model is that LS-DYNA interpolates linearly between the strain rates to calculate stress-strain values for the applied strain rate in case only uni-axial compression load curves with different strain rates are defined. No extrapolation is made for strain rates above the highest strain rates. As shown in Figure 4-7, LS-DYNA simply takes the stress-strain values of the highest strain rate, assuming that the stress is constant above the highest strain rate [44].
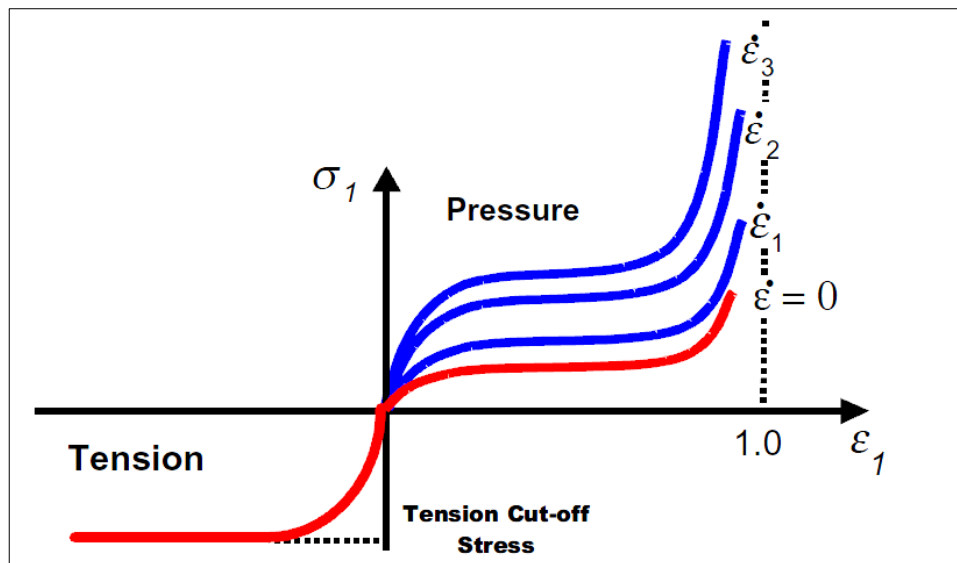
Figure 4-7 LS-DYNA interpolates linearly between the strain rates [44]

High recovery of this material makes it a perfect choice for representing the behavior of Expanded Polyethylene. Here are some critical comments on Material Model 1 which is better to be known:

- No use of engineering stress-strain curve is expected. Instead, this material model is always used with true-stress-strain curves.

- It only allows user to input loading curves. Unloading curves may not be introduced as input. Minimum strain rate load curve is used for unloading curve resulting in stiffer behaviors than usual

Finally, following data is needed to set-up the card:

i. Young`s modulus

ii. Density

iii. True-stress strain curve as a function of strain rate

4.1.2.2   Material Model 2 (MMCF)

In contrast to Material Model 1, Material Model 2 is generally not used for the representation of recoverable materials. They may not be seemed as a logical candidate for Polyethylene material which is reversible at first sight. However, this material model can be used for simulating the behavior of Polyethylene too. A big portion of the dissipated energy is provided by the loading behavior of the foam when compared to the unloading one. That is why unloading of foam can be slipped into background and Polyethylene can be represented by Material Model 2 within this assumption.

This model is fairly simple to calibrate, requiring simply output of the rate dependent stress-strain data. When the case is axial crush of foam this model is said to be effective. This material model allows input of a user-defined curve representing the yield stress versus volumetric strain. It is important to note that volumetric strain is defined as 1 minus the relative volume, which is the ratio of the current volume to the initial volume. Thus, as crushing initiates, the volumetric strain is low and increases as crushing progress [45].

4.2   FINITE ELEMENT DEVELOPMENT PROCESS

Here, a guide for a general procedure for finite element modeling development process will be given. The process starts within the simplifications of the CAD

model. Yet, in most analysis the initial geometry of the system should be inverted to a simplified model due to getting rid of complex components. Finite element mesh development is the next stage which is followed by element types and material selections. After defining contact algorithms, boundary conditions will be applied. Solving the model by the code requires the interpretation of the results. Aforementioned process is explained in a detailed way as follows:

4.2.1   Transition From CAD to FE Model Development

Evolution of a FE model is generally a hard task and extra attention needs to be taken during this phase. Initially, it should be decided whether it is necessary to model a system in detail or not. Experience has a big role at this point because of the fact that an analyst with experience may have easily forecast the pros and cons of modeling techniques. Most of the time, systems which are very intricate by nature and there is no possibility to analyze such systems within this complexity owing to the labor and time cost they may cause to.

It can be inferred from above paragraph that assumptions and engineering judgments come to the stage. To sum up, analyst can and should develop a FE model by simplifications and correct approaches. In the study of Vezina M. and Firoozrai A. [46], a 7 meter plastic boat is dropped into the water.
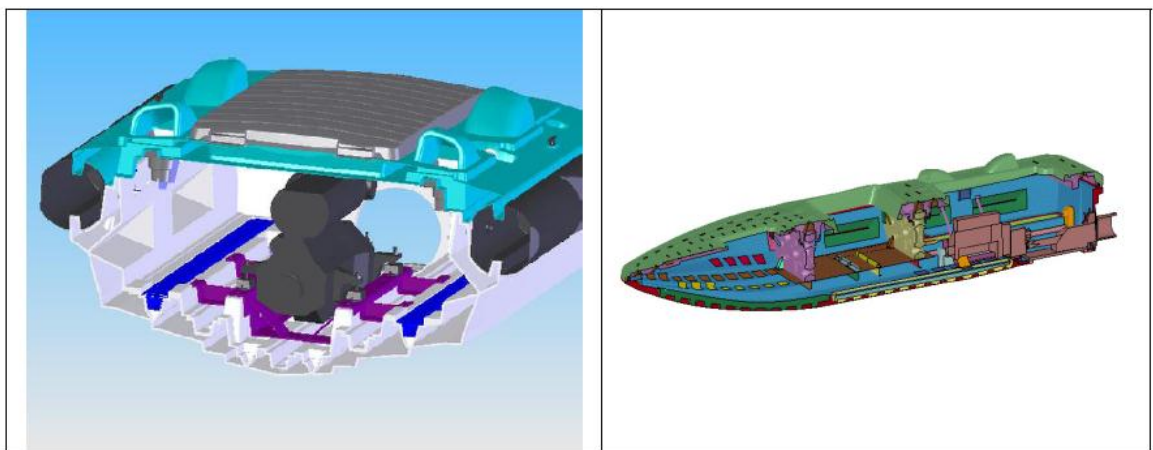

Figure 4-8 Cross-section of boat (a) original CAD (b) simplified CAD model [46]

As seen in Figure 4-8, CAD model of the boat has transformed into a simpler model by some modifications. For instance; seats, air bag mechanism and hatches are

directly removed from model. Furthermore, all the thicknesses of plates assumed to be same. What is more, components that take part in the propulsion system of the boat are not taken into consideration and thought as rigid.

Another reason that forces analyst to make assumptions is absence of material properties of some components. More detail related to material effects will be given in the following sections.

4.2.2 Finite Element Discretization

Typical way of meshing is to give a mesh seed along a curve or line, or along two edges of a surface, or three edges of a solid using the preprocessors. Meshing of a CAD model is prepared by pre-processors which are developed for this reason. Pre-processors actually provide users to prepare finite element model entirely by their interface. However, text editors which allow users flexibility to design keywords are in use recently. Once, FE discretization is performed by pre-processors, node numbers and coordinates, element numbers and types, material types and properties are written in keyword files which can be edited later.

Meshing of a model (coarseness or fineness) is one of the key roles which can directly affect the results of simulations. Besides, types, numbers and orders of elements are straightforwardly correlated to results as well as run time. Types of analysis also affect the mesh discretization in a way that in static analysis finer mesh is expected to be developed. Whereas, dynamic analysis does not require a very fine mesh structure as static analysis do. Dynamic models must be solved in each time step, while static models are solved for a small number of load steps.

Explicit dynamic codes work at a very low time steps, which can be 1 microsecond or even shorter. Time step is defined as the time required for a sound wave to move across the smallest element.
Initial mesh structure can sometimes be not fine enough for the first runs. In such a scenario, extra refinement could be applied to the regions which are point of interest in later runs. Another critical point that is needed to be mentioned is that in explicit scenarios e.g. drop analysis, quality of elements is more important than

quantity. That is why better aspect ratios and hexagonal elements are desired for explicit scenarios [12].

4.2.3   Types of Elements and Formulations

As it is mentioned in above paragraphs, types of element selection can change the output values. Different kind of analysis can force analyst to use distinct type of elements as it is in static analysis. For example; necessity of the usage of radius at sharp edges and corners may force one to use tetrahedral or pentagonal elements at these regions in a static analysis whose point of interest is stress concentration. Other than types of analysis, material models used for analysis can also dictate the element type to be used. For example, some material models in LS-DYNA can only be used with shell elements, while some others require solid elements.

Solid elements (hexagonal, pentagonal and tetrahedral), shell elements (triangular, quadrilateral) beams, springs are fundamental elements generally applied in dynamic FE codes. Quadrilateral elements for shells and hexagonal elements for solids should need to be applied most the time owing to the fact that tetragonal, pentagonal and triangular elements may behave more stiff than it should be. When the order is the case, higher order of elements should be avoided, instead large number but simpler elements should be preferred. It is also advisable using three elements through thickness, if it is significant to simulate bending in solid elements. For shell elements, this is not necessary thanks to all integration point through the center of the element while solid elements have one. Besides, hourglass energy problems which will be later explained can also be avoided by changing the formulation of elements in LS-DYNA [12] .

4.2.4   Material Models

Selection of material models can be though depending on the material used. As it is mentioned before, some material models allow only to be used with shells whereas, others solids or beams. Analyst should consider this limitation when selecting the material model. Most the metallic materials may be accurately represented by bilinear elastic-plastic model. Behavior of this material model can be summarized as follows: Material is assumed to be elastic up to the yield point followed by perfectly

plastic behavior. A failure criterion is not an option for some of material models while others can reach a more realistic behavior by using failure value. However, some materials are too complex to be represented by bilinear curves. Stress-strain curves are integrated to the systems by using tables.

Owing to the fact that foams are lately used very often in various applications, code developers released a bunch of foam material models to the market. Although most metallic materials are rate independent, foams are not. Strain rate dependence of this kind of materials makes their usage very troublesome. In order to simulate such foams in an appropriate way, initially material testing is necessary. By integrating mechanical properties of foams to the material model, it is possible to make these models robust and efficient. However, it is not often expedient to obtain mechanical properties of foams owing to the fact that experimentation of them is difficult and time-consuming [12].

4.2.5   Contact Algorithm

Sophisticated contact algorithms are seen on nonlinear dynamic FE codes. Other than surface to surface contact model, node to surface algorithm is also commonly used. Master and slave definitions are needed to be carefully done especially if discretization of both surfaces is quite different than each other. As a common sense, coarser side is selected as master surface. If contact is defined between distinct types of materials, it is better to have closer element lengths of both master and slave surfaces. In case of drop scenarios where excessive material deformations are possible to seen, distinct surfaces can interact to each other. Automatic contact algorithm is the one which has widespread usage. No definition of master and slave surfaces is compulsory for automatic contact algorithms because of the fact that all the surfaces in the model are checked by code whether or not they touch each other. However, this option has a vital drawback which is causing excessive increase in the run time. For this reason, apart from automatic contact algorithms, special contact algorithms are also developed e.g. edge to edge contact. LS-DYNA is accepted as an outstanding FE code thanks to the capability and capacity of contact algorithms.

Owing to the good energy absorbing capability of foams, they are exposed to excessive distortion resulting in contact loses at some points. Especially, when crushing is occurred at off-axis dominant situations, foam materials may lose their stability causing excitation of simulations with errors. This problem can sometimes be solved by refining mesh. When foam materials are considered, other than refinement of mesh, a special contact algorithm, named "Interior contact", is available. By defining interior contact algorithm, extra contact surfaces for each foam element are developed.

In case of penetration of a slave node to master surface, generation of a contact force which tries to push the node back. LS-DYNA uses a penalty based method to calculate this force in a way that stiffness of material times penetration distance gives contact force on node. Friction parameters between lots of materials are available in handbooks or sometimes can be obtained by experiments [12].

4.2.6   Energy Considerations

Energy checks can be applied if analyst is not sure whether simulation represents the real case or not. Law of conservation of energy should not be violated by simulation which means total energy of the system ought to be same unless external effects are applied. For example, in a drop scenario if the model's structural rebound height is much larger than measured, insufficient energy was dissipated by the model. FE codes can examine the various forms of energy separately.

In drop analysis, most crucial check belongs to hourglass energy modes. Hourglass energy modes are non-physical, zero-energy modes of deformation that produce zero strain and no stress [47]. As it is mentioned before, excessive distortions of elements may cause non-physical energy issues. Even though overall volume of an element may remain reasonable, one corner can be inverted (e.g., an edge going to zero length and beyond), causing a negative volume. Extreme energy increase can be prevented by defining extra definitions. Otherwise, reliability of analysis will be questionable. Non-physical hourglass energy of a part that takes part in the

system should be low enough (<10% as a rule-of-thumb) for the reliability of the analysis.
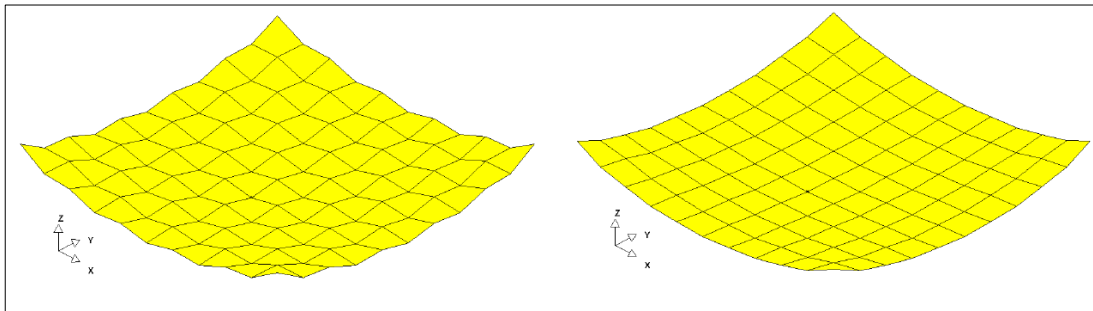
Figure 4-9 Hourglassing of a shell plate [47]

Effect of hourglass control on a shell plate is explicitly seen in Figure 4-9. Unless HG modes are controlled, elements on the shell plate are highly distorted (on the left). However, HG modes of the shell plate can be inhibited by various algorithms (on the right). Because of the nature of the foam materials, such a phenomenon is so often encountered. Excessive deformation capabilities of these materials may occasionally be caused to hourglassing problems unless sufficient algorithms are used.

Figure 4-10 Hourglasing of foam materials

In Figure 4-10, hourglassing of the foam materials which is causing excitation of simulations with errors are depicted. In order to prevent these unrealistic behaviors, correct definitions are needed to be done. Apart from hourglassing

checks, total, kinetic and internal energy changes by time should also be confirmed to be true.

4.2.7 Post Processing

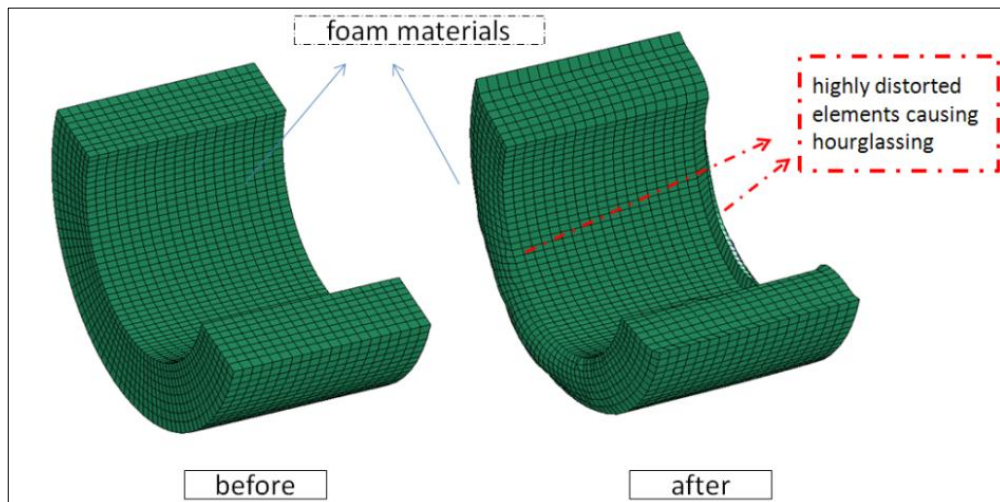Prior to analysis, which outputs are points of interest is known by analyst. In case of a drop scenario, probably acceleration is in the center of attention and is mainly supposed to be measured at the center of gravity. However, in simulations, analyst can figure out the acceleration value at any point on the FE model and generally it depends on the experimental tests' areas of interest.

Change of velocity by time is another output in which a drop scenario analyst will focus on. According to a procedure applied on drop analysis, initial impact velocity is determined by considering the conservation of energy.

4.3 SIMULATION OF MATERIAL CHARACTERIZATION TESTS

Numerical models which are used for the representation of Expanded Polypropylene and Polyethylene should be validated by using material characterization test results conducted at IZTEK in Izmir Institute of Technology. Selected material models in LS-DYNA should represent the behaviors of EPP and PE in an appropriate way. The most appropriate two material models for representation of EPP and PE out of approximately twenty models were selected considering the previous studies. Expanded Polypropylene, as well as Polyethylene is a material which are very sensitive to strain rate changes. Being rate dependent of these foams narrowed the alternatives to be selected from LS-DYNA material library. This is because of the fact that most of the alternatives from the material library do not allow rate dependence.

Both EPP and PE are kind of reversible foams which may be explained in a way that they come back to their original position after compressed. This ratio is almost 95-100 % for EPP foam, while it is relatively lower for Polyethylene. At this point, it should be mentioned that reversibility of polymeric foams are directly related to the number of compression they have been exposed to. However, foam materials do not generally lose their functionality until they have been compressed so often.

There are a few studies related to validation of material characterization tests. In one of them, Sambamoorthy B. and Halder T. [49] used a 15 mph speed-steel impactor consisted by solid elements, foam specimen which is Polyurethane and a rigid plate on which foam is supported.
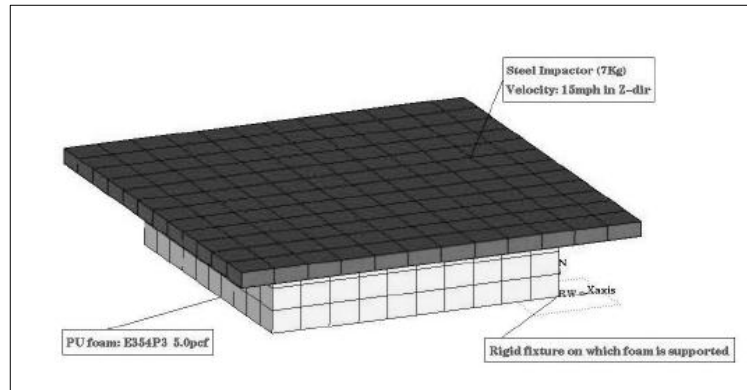
Figure 4-11 Finite element Model of the test set-up [49]

In Figure 4-11, elastic material models are used for foam specimen. This is not commonly used in this type of simulations. Another study conducted by Reid J.D. and Bielenberg R.W. [50] also preferred a solid conductor to compress foam specimen to get mechanical properties of them. In Figure 4-12, solid elements are used for rigid structure. However, this is not suggested owing to the fact that using unnecessary elements causes longer run times which is not desirable.

Figure 4-12 Simplified Model of the test [50]

4.4   SIMULATION OF DROP TEST OF MUNITION

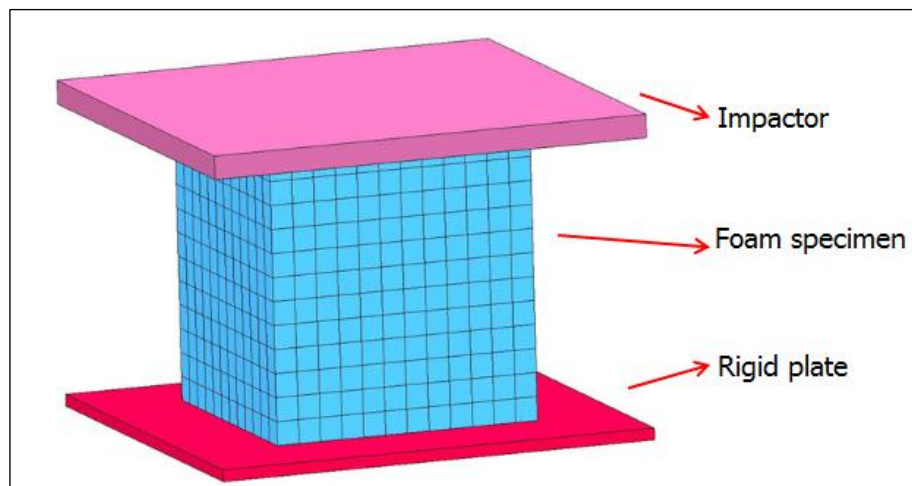In this thesis, a nonlinear dynamic explicit finite element code, LS-DYNA, was utilized to simulate experimental process. In order to accomplish the goal of the thesis which is minimizing load levels up to allowable limits, validation of the tests is an issue for analyst to be overcome. This chapter covers validation process of experimental works by using LS-DYNA.

4.4.1   Definitions and Assumptions

Validation process begins with FE development of the CAD model that is used in drop tests. CAD models may commonly have detailed sections that are not indispensable for FE model. Instead, a classical FE model requests various reductions and removals of the CAD geometry to have a simpler model within some assumptions that may have little effects on results of simulations.

Prior to the getting into details, drop configuration of the munitions should be given in order to identify the scenario. Figure 4-13 reveals the schematic view of components that were used in experimental process and they can be listed as follows:

- Missile
- Composite launching tube
- Connector
- Expanded Polypropylene foam cushions (nose and tail)
- Drop apparatus which releases the mechanism for free fall
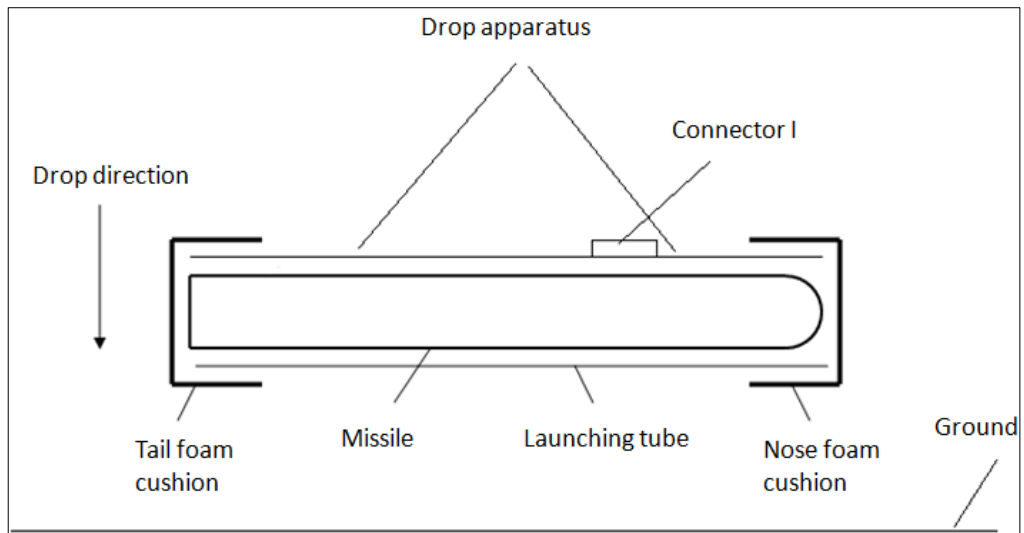
Figure 4-13 Schematic view of the components of the system

It is also better to mention again that missile used in the drop test is a functionless dummy model whose center of gravity and mass are correlated with real time missile. Dummy model of the missile which is composed of 1 mm thick Belytschko-Tsay (default) shell elements was developed as simple as possible as depicted in Figure 4-14, while it is too complicated for real case missile.

Figure 4-14 Both CAD model and FE model of missile

Dummy missile accommodating in the launching tube was modeled as rigid material within the assumption of no effect on results. An essential detail about the dummy missile is the arrangement of center of gra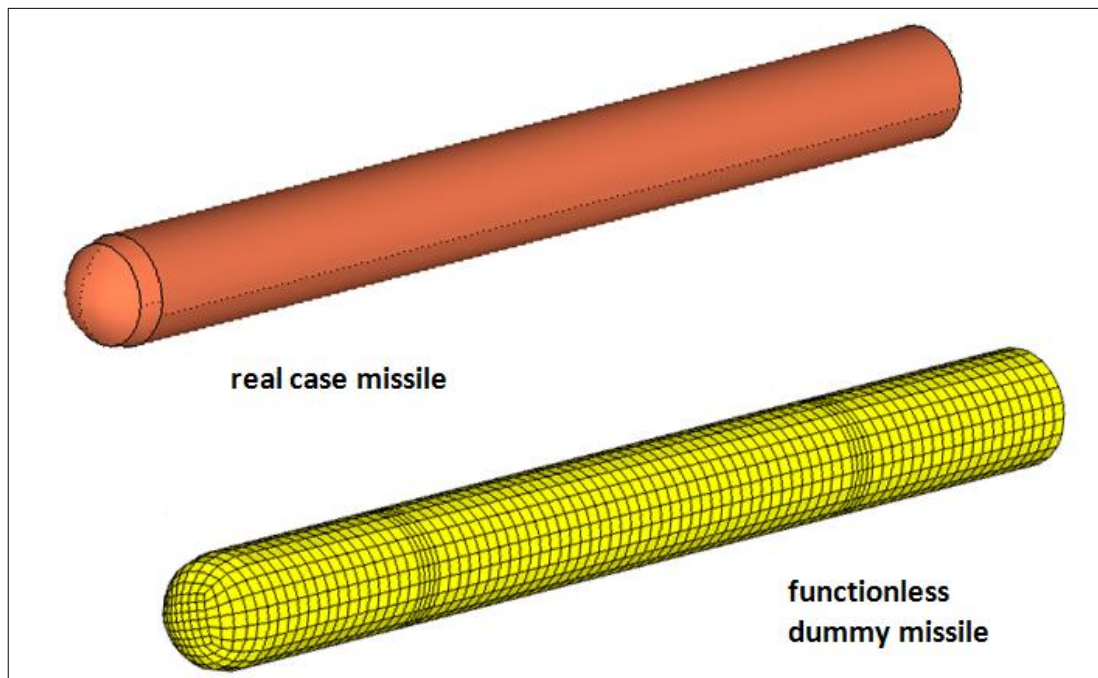vity, inertial properties as well as mass of the missile. All the assignments mentioned above was achieved by *PART_INERTIA card. They have been arranged in a way that dummy missile is ballasted to possess the same mass and inertial properties as real case missile. Besides, aluminum material properties was given to the missile using *MAT_RIGID [51] material model in LS-DYNA. In addition to the apparent benefits of rigid body assumption which is improving computational efficiency, it is rather logical too because of the fact that no energy storage is expected from missile compared to the foams. Material properties assigned to the missile are given in Table 4.2.

Table 4.2 Material properties of aluminum missile

Material type	Density [kg/m^3]	Young modulus [GPa]	Poisson ratio
Aluminum	2810	72	0,33

Dummy missile contains approximately 2161 nodes. Types and numbers of elements are given in Table 4.3 just for information even if they are not significant for rigid materials.

Table 4.3 Types and numbers of elements of missile

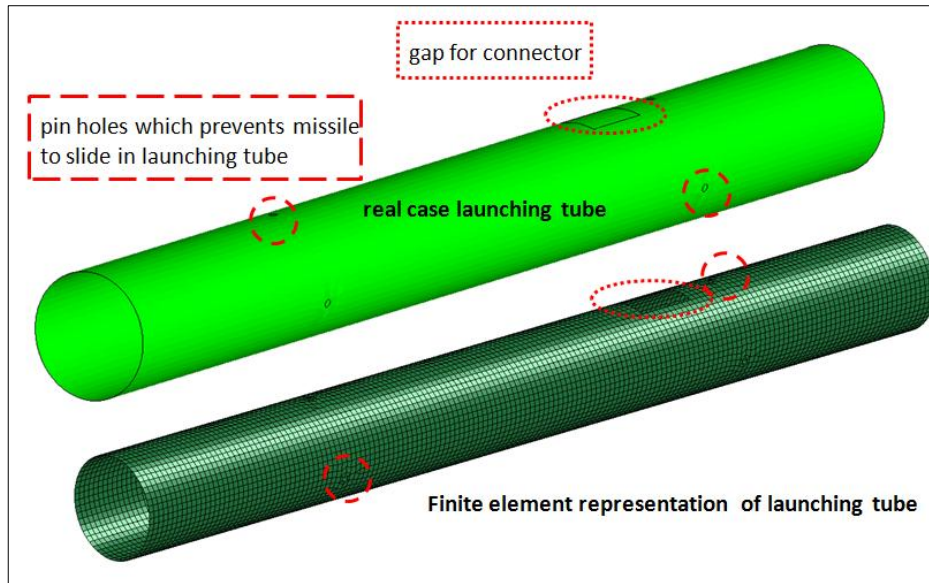| element type		numbers of elements	Total
shell	quadrilateral/triangular	2148/0	2148

83

Figure 4-15 CAD and FE modeling of the launching tube with the pinholes

As seen in Figure 4-15, composite launching tube is another segment of the system where missile is accommodated. Similar to the missile, Belytschko-Tsay (default) shell elements were used for launching tube whose thickness is mostly uniform and assigned by *SECTION_SHELL card. Pretty low thickness/length ratio of the launching tube supported us to prefer this type of elements. Besides, no rigid body assumption was made for composite launching tube.

Composite material properties which are obtained by experimental tests were assigned to *MAT_ENHANCED_COMPOSITE_DAMAGE material model. In the section where results are given, energy dissipated by composite tube will be compared to the energy absorbed by foams. Material properties assigned to composite tube are given Table 4.4. Here, the parameters with superscript star are directly taken from the reference [52] owing to the fact that similar composite material is used. Rest of the parameters is provided by the Material Division of ROKETSAN A.Ş.

Table 4.4 Material properties of composite tube

Density (g/cm^3)	1,57
Longitudinal modulus, E_1 (GPa)	153,6
Transverse modulus*, E_2 (GPa)	11
In-plane shear modulus, G_{12} (GPa)	6,5
Poisson's ratio, v_{12} (GPa)	0,308
Longitudinal tensile strength, X_T (MPa)	2110
Longitudinal compressive strength*, X_C (MPa)	900
Transverse tensile strength*, Y_T (MPa)	27
Transverse compressive strength*, Y_C (MPa)	200
In-plane shear strength, S_{12} (MPa)	80
Orientation, $\alpha(°)$	45

Other than composite modeling of the launching tube, elastic modeling is also examined. Aim of this type of modeling is to check whether distinct modeling techniques have notable effect on the energy absorption or not. Comparison of the results of these two modeling technique is discussed in Chapter 6.

Shell tube was composed of 8888 nodes and in Table 4.5, total number and types of elements were also given.

Table 4.5 Types and number of elements of launching tube

Element type		Numbers of elements	Total
shell	quadrilateral/triangular	8797/16	8813

No other than default type of formulation (Belytschko-Tsay) was tried for shell elements owing to the fact that area of interest was mainly shifted to foam materials. Besides, not much change will be seen on foam behavior in case of a change of the formulation of launching tube. Thanks to this approach, average element lengths were chosen to be approximately 10 mm and 20 mm for tube and missile, respectively.

Apart from aluminum missile and composite launching tube, system has another component whose effect on results is negligible, named Connector. Different than the missile and tube, connector was modeled with solid elements by using default element formulation. As it is explained for previous two components, no distinct element formulations were examined. Distinct views of the connector are given in Figure 4-16.
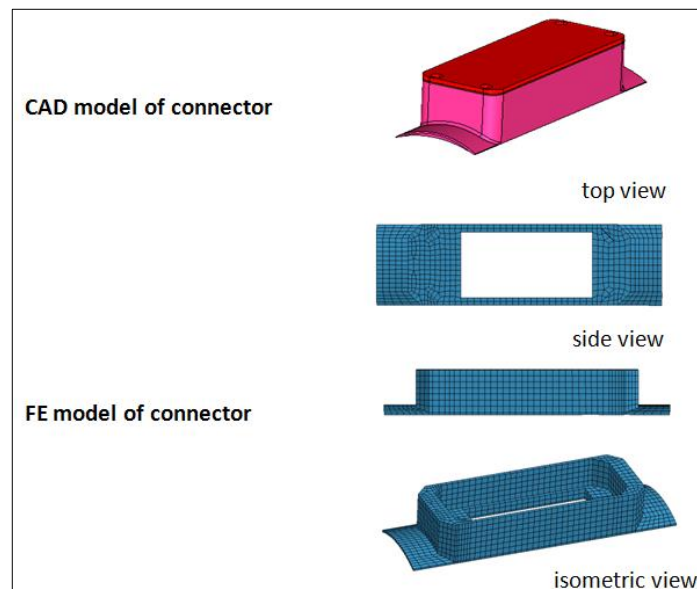

Figure 4-16 CAD and FE modeling of connector

A bilinear material model, *MAT_PLASTIC_KINEMATIC, was defined to represent the behavior of Connector made of aluminum. Density, Young modulus, Poisson ratio and yield stress value are necessary to define a bilinear material model. Classical aluminum material properties which are given in Table 4.6 were assigned to this material model.

Table 4.6 Material properties of connector

Material type	Density [kg/m^3]	Young modulus [GPa]	Poisson ratio	Yield stress [GPa]
Aluminum	2810	72	0,33	0,265

Connector has 3624 nodes and total number and types of elements were also given in Table 4.7.

Table 4.7 Types and number of elements of connector

Element type		Numbers of elements	Total
solid	hexagonal/pentagonal	2194/44	2238

Main components which are dealing with minimizing the effects of loads in case of an impact are foams thanks to their absorbing characteristics. As depicted in Figure 4-17, there is a difference between real foam cushion and simplified one. Rounded edges in original model were removed from the geometry owing to two fundamental reasons. The former reason is that simplified model lowers the run times of simulations which make analysis more effective. Possible increase in the number of elements would have cause to longer run times. The latter, it helps analyst to model foam cushions easier. This will be yeoman's service during the studies of optimization which is the topic of next chapter.
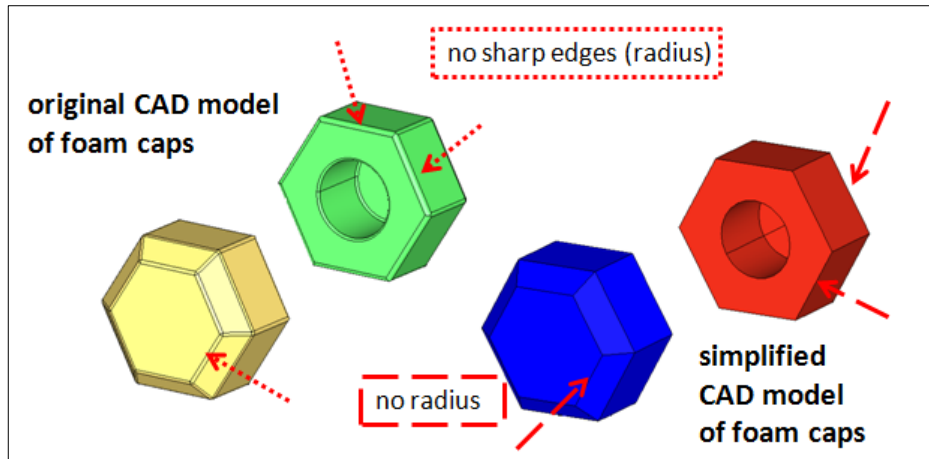
Figure 4-17 Comparison of original and simplified foam caps

Complex characteristics of foam materials make it hard to model them in FE codes. For a better representation, material models always necessitate material testing which is an expensive process. In this thesis, material characterization results of EPP and PE foams were adjusted to material models.

Expanded Polypropylene whose density is 30 kg/m^3 was used throughout experimental process, Behavior of this material was achieved to be represented thanks to *MAT_FU_CHANG material model. The following data were needed from material characterization tests to set up the card:

- Density
- Young`s Modulus
- Stress-strain curve (as a function of strain rate)
- Tensile cut-off stress (if possible)

When modeling a drop scenario, the most critical question comes into mind about material is that does characterization tests include levels of velocity that will be reached by validation tests ? As an answer to this question is that in this drop scenarios (50 cm-parallel), maximum level of velocity was at around 3 mm/ms. During material characterization process, drop tower tests did also reach up to these values (maximum 5 mm/ms). Mechanical properties of EPP are given in Table 4.8.

Table 4.8 Mechanical properties of Expanded Polypropylene

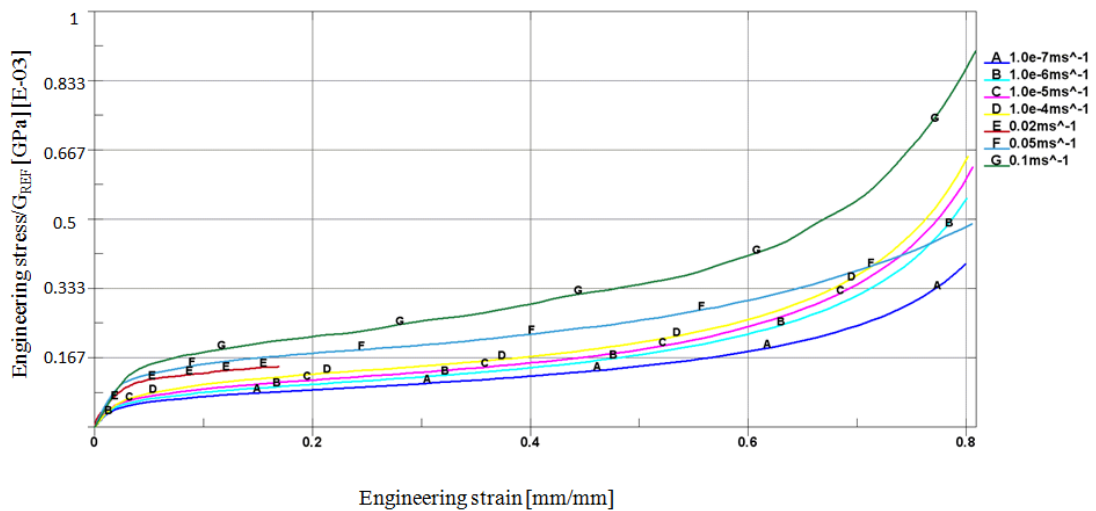| Material type	Density [kg/m^3]	Young modulus [GPa]	Dynamic relaxation moduli [GPa]	Tensile cut-off stress [GPa]
EPP	30	0,004144	0,33	0,265

Figure 4-18 Engineering stress-strain curve of EPP at different strain rates

Other than parameters given in Table 4.8, normalized stress-strain curves at different strain rates were also assigned to Expanded Polypropylene in Figure 4-18. Owing to the privacy policy of the company, the G_{REF} value in Figure 4-18 is not given.

Element types and numbers of both tail and nose foam cushions were identical and given in Table 4.9. Besides, totally there are totally 5632 nodes for each cushion.

Table 4.9 Types and number of elements of each foam cushions (tail and nose)

Element type	Numbers of elements	Total
solid hexagonal/pentagonal	5632/0	5632

4.4.2   Boundary Conditions and Contact Definitions

Drop scenario of the munition can be turned into an initial velocity problem as it is seen in the figure below. Behavior of the munition up to the impact is irrelevant, that is why it is logical to set-up an initial velocity problem. In addition, computer efficiency can also be provided by formulating such a set-up. In this set-up munition is positioned in a way that the system is slightly offset (0.5- to 1 mm) from a rigid wall with an initial velocity of 3.13 m/s. Initial velocity of the impact is calculated by Equation (4-39).

In 50 cm parallel drop scenario, initial impact velocity, v is determined by using Equation (4-39) as follows:

$$v^2 = 2gh = 2 * 9.81 * 0.5 = 3.13 \, m/s \qquad (4\text{-}63)$$
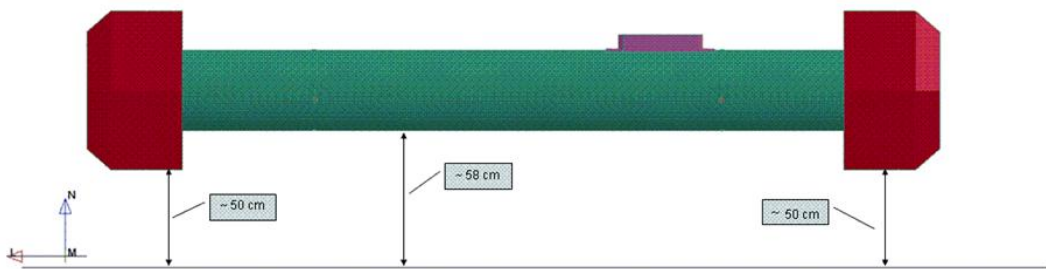

Figure 4-19 Original configuration

In Figure 4-19, original configuration of the drop scenario is depicted. This scenario is converted to an initial velocity problem as it is seen in Figure 4-20. In this figure, foam cushions (nose and tail), connector and launching tube were assigned to be at a velocity of 3.13 m/s.
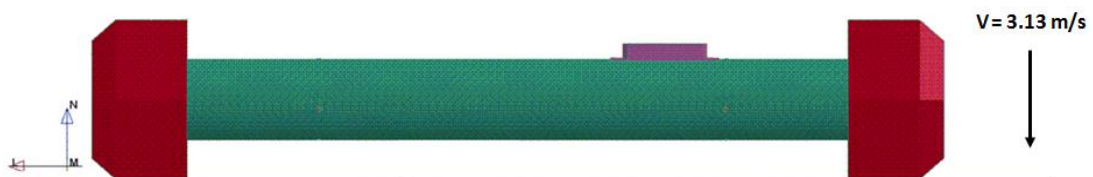
Figure 4-20 Initial velocity problem

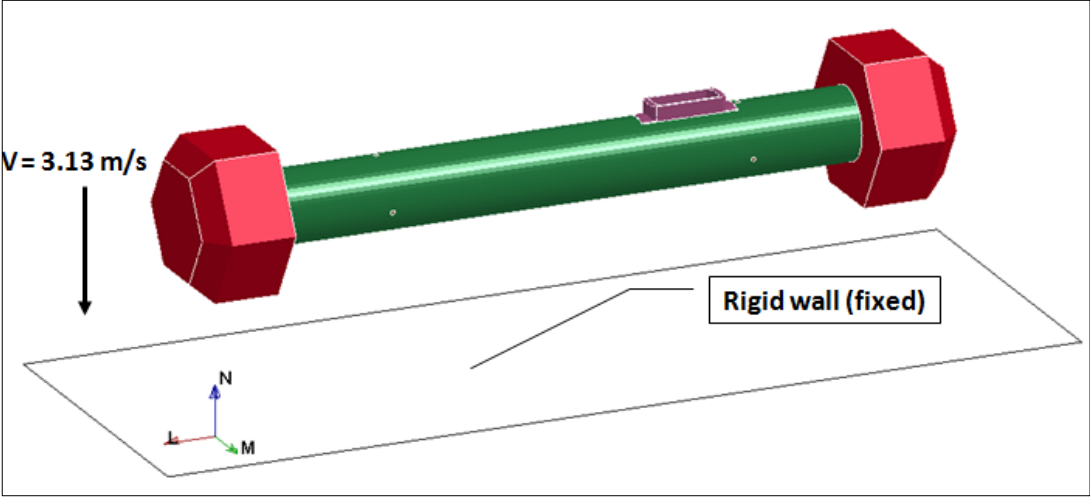A general scheme of the scenario in isometric view can be shown in Figure 4-21.

Figure 4-21 General scheme of the drop scenario

CHAPTER 5

EXPERIMENTAL RESULTS

First part of this chapter is dedicated to the quasi-static and dynamic results of the characterization tests of foams which are Expanded Polypropylene and Polyethylene. Selected foam materials were characterized for acquiring material properties that are Young Modulus and stress-strain curves for different densities and strain rates in order to use this data in validation of the drop analysis. In addition, "Force versus time" graphs were also requested to be able to use this data in validation of material characterization process.

The second part of this chapter covers the drop tests of munitions. At the very end of this chapter, trials of drop tests of munitions will be introduced. Furthermore, acceleration-time history of the final test will also be given within the comparison of its raw and filtered data.

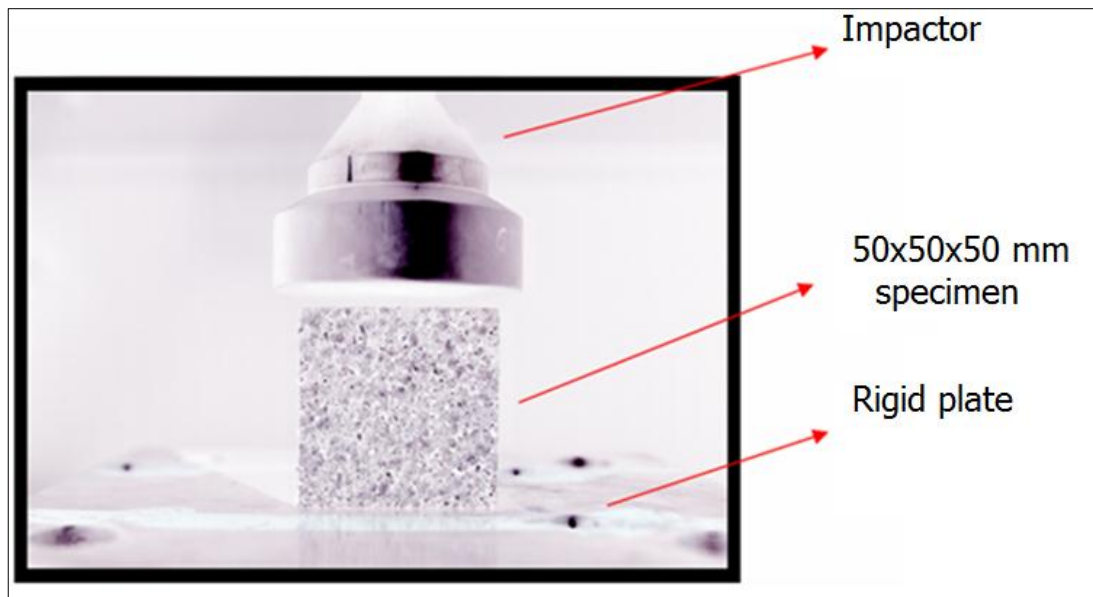## 5.1 MATERIAL CHARACTERIZATION TEST RESULTS OF FOAMS

Figure 5-1 Pre-view of a 50x50x50 mm specimen of 30 kg/m^3 EPP

As it is depicted in Figure 5-1a 50x50x50 mm EPP foam specimen is about to compress between the impactor and a rigid plate. The same figure but in detail (change by time) is given in Figure 5-2. According to Figure 5-2, impactor started to contact to foam specimen at a time t_4 and loading of foam lasted up to t_9 followed by unloading. Compression of foam came to an end when the velocity of connector was reduced to zero. At the tests conducted by İZTEK, data related to the unloading behavior of foams is not provided. For this reason, no validation of the unloading case is applicable in numerical approach.
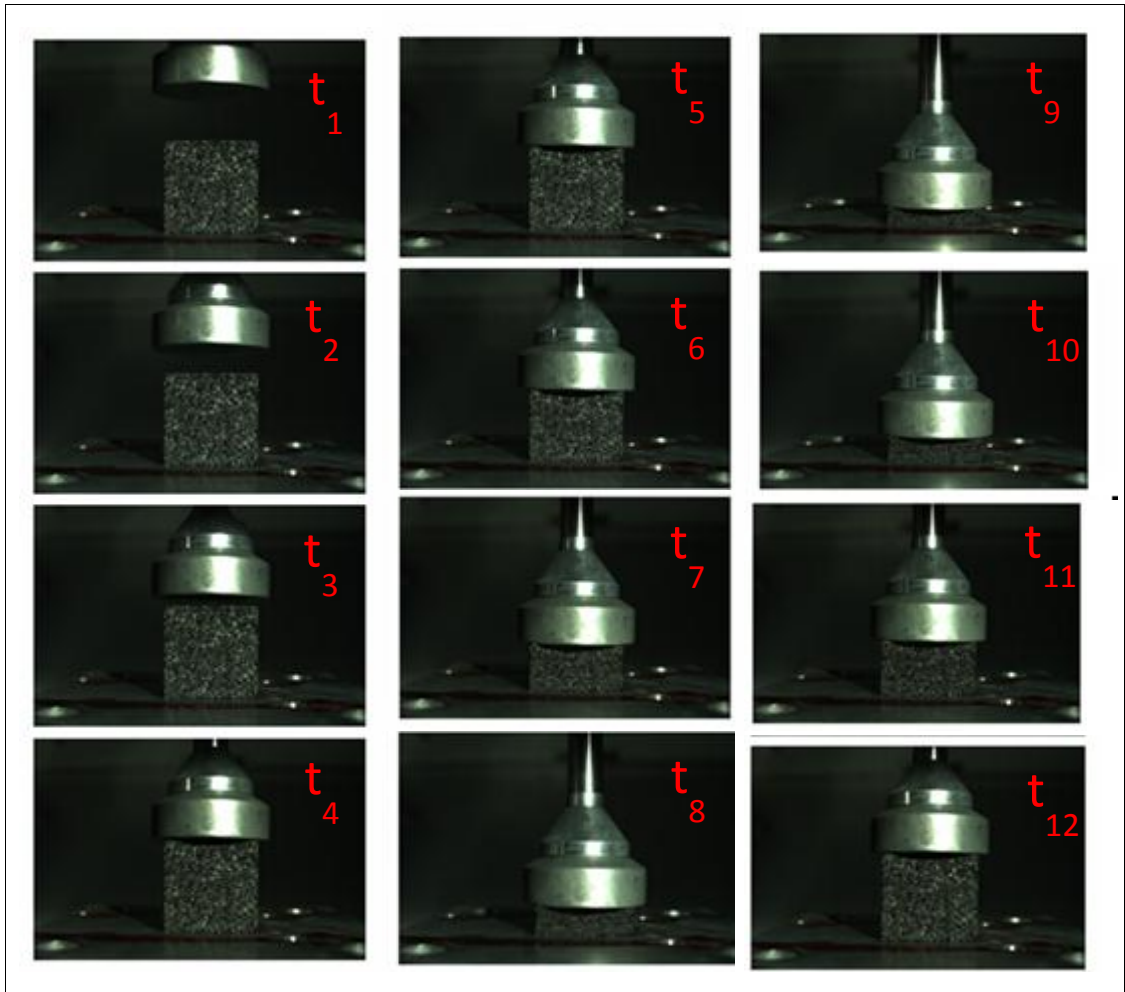
Figure 5-2 30 kg/m^3 EPP is compressed at 20 s^{-1} strain rate

Similar to EPP, PE was also compressed by rigid plates in order to get foam material property. Results of characterization tests will later be given as inputs for use of numerical approach. Test configuration of Polyethylene is depicted in Figure 5-3.
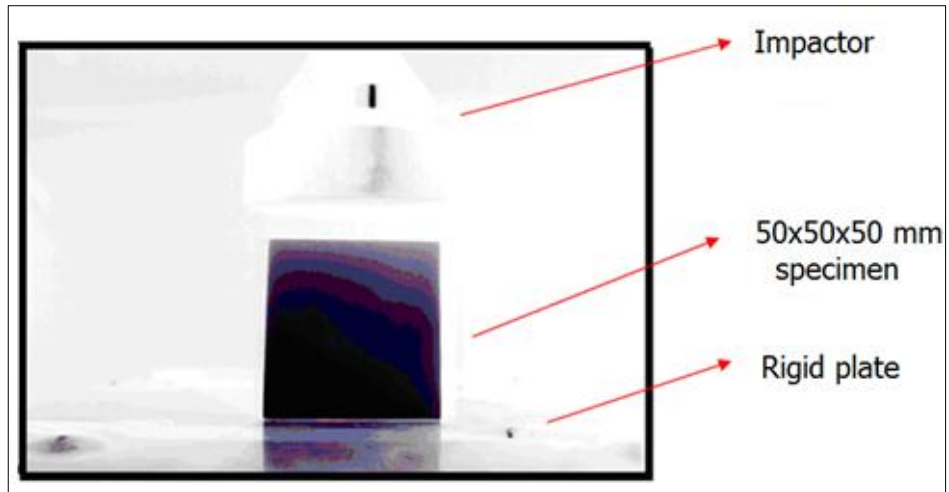
Figure 5-3 Pre-view of a 50x50x50 mm specimen of 45 kg/m^3 PE

Compression of PE foam specimen is about to begin and its change by time is given in Figure 5-4. Loading of PE specimen is shown in the figure below. Unloading behavior of foam is not given in Figure 5-4. This is because of the absence of the data related to the unloading behavior of foams. Besides, for Polyethylene material, higher strain-rates one is interested in, the more problems are encountered. That is why the highest strain-rated foam behavior is given in the figures.
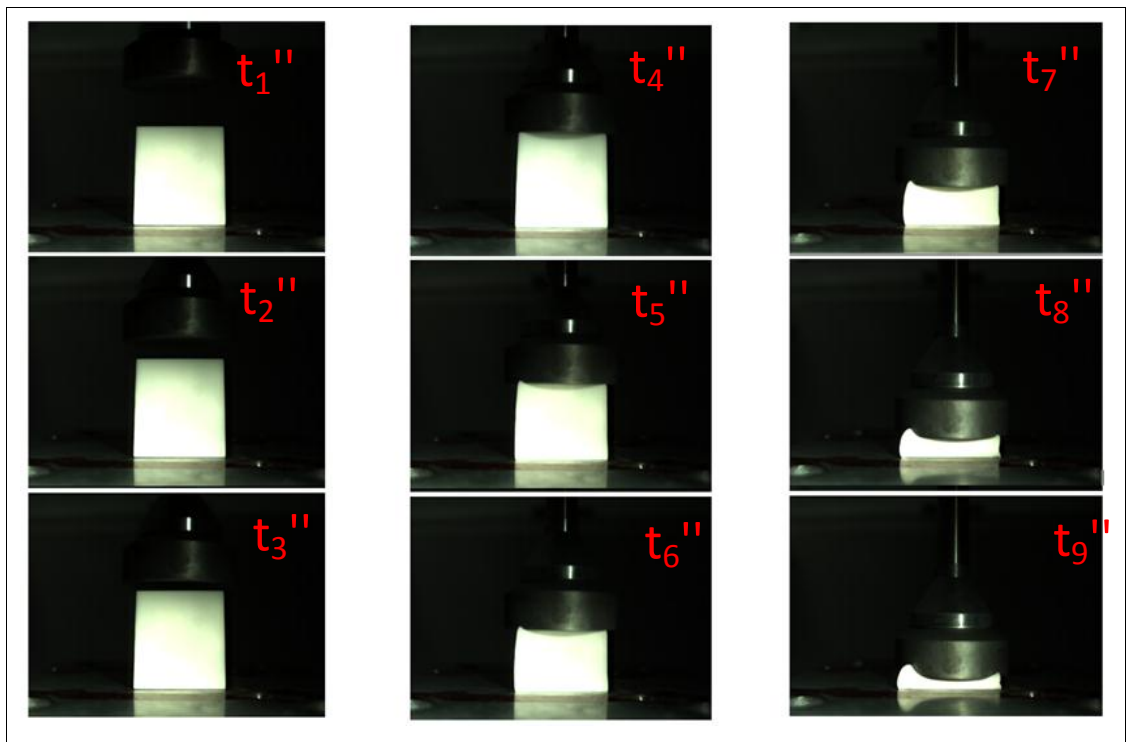

Figure 5-4 45 kg/m^3 PE is compressed at 100 s^{-1} strain rate

Results of these tests are not given in this part of the chapter. It is better to compare test results with the results of simulations on the same graph. For this reason they will be shared in Chapter.

5.2   DROP TESTS RESULTS OF MUNITIONS

In this section of the study, trials of drop tests which were used for validation of simulations will be summarized. This type of drop tests can be seen easy to conduct, however it is more complicated than it is thought to be. Unexpected difficulties were encountered throughout experimental process. Actually, problems that were encountered were not only related to conducting of the tests, but data gathering issues were also struggled.

In order to utilize for the validation of simulations that represent the experimental tests, munition with foam has exposed to 50 cm parallel drop test for ten-times. It was monitored by these tests that almost all ten drops were quite similar to each other with little changes. It should be mentioned that validation of simulations were achieved at the center of gravity. This is a classical method used for drop tests for validation process.
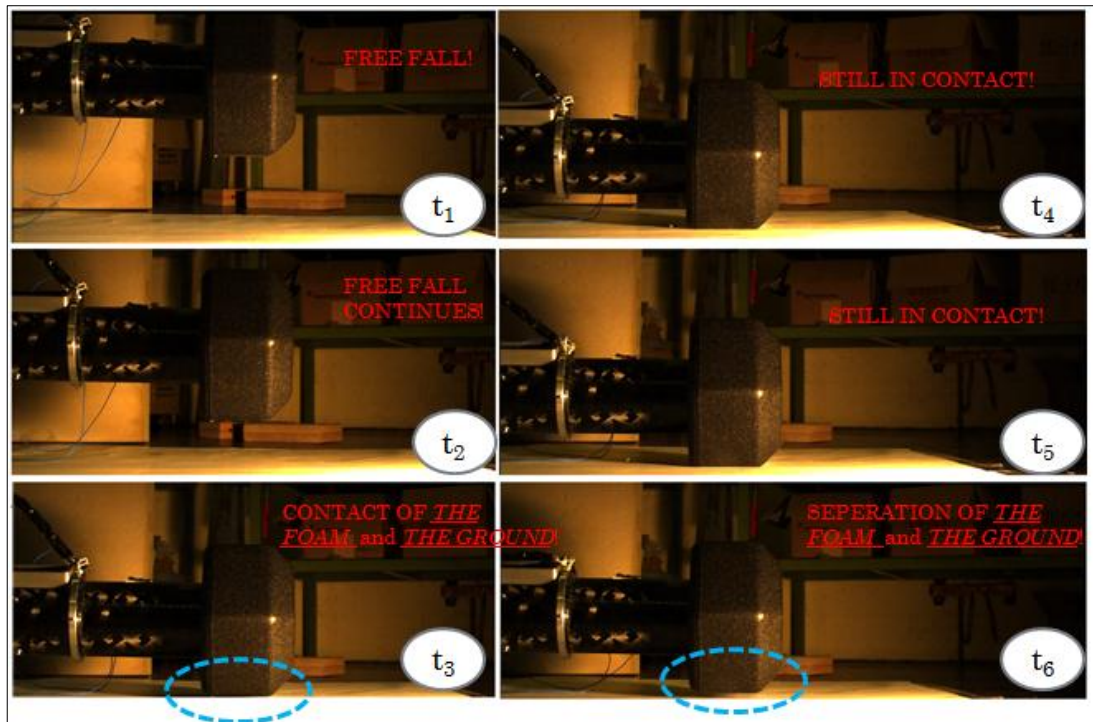
Figure 5-5 Drop test of munition at different time steps

In Figure 5-5 drop test of munition is revealed. The process starting with free fall, continued with the contact of the foam and ground. Finally, foam part separated from the ground. Acceleration time histories were recorded by accelerometers placed on previously mentioned three distinct regions on missile.

Figure 5-6 shows a typical acceleration-time curve of 50 cm parallel drop tests (at the center of gravity). It is seen in Figure 5-6 that there is a sudden change in the raw data at around 35 milliseconds. There may be a few logical explanations of such a sudden increase in acceleration data. At first it should be decided whether this change is real or not. Such an increase can be explained in a way that in addition to the actual physical data, electrical noise that superimposed on the experimental data can cause to this increase.

Such noise may be generated by electromagnetic interference, cross-talk between channels, inadvertent over-ranging of the instrument itself, nonlinearities caused by exciting the resonance frequency of the accelerometer, and over-ranging of the

instrumentation caused by setting the voltage limits of amplifiers too low, etc. Sometimes it is difficult to distinguish between electrical anomalies and good data.
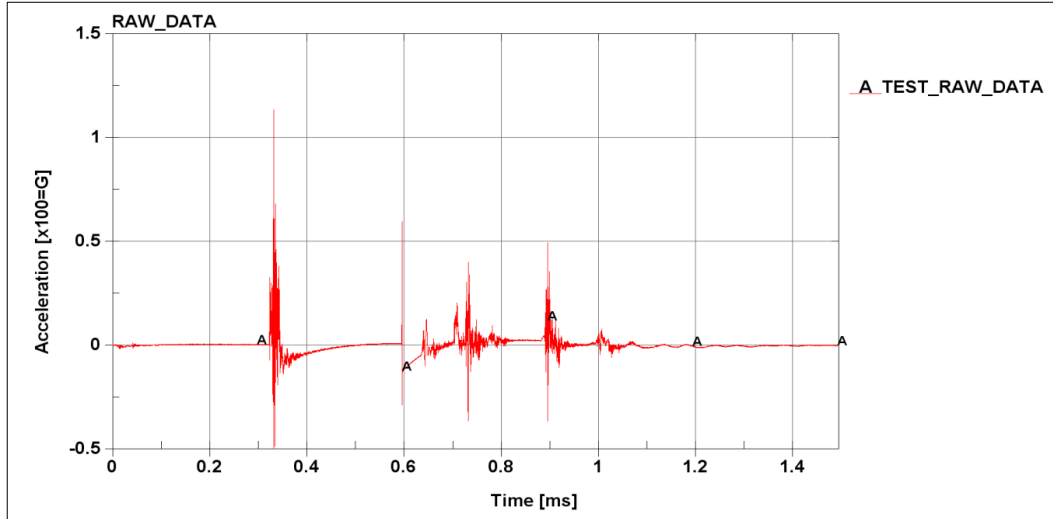

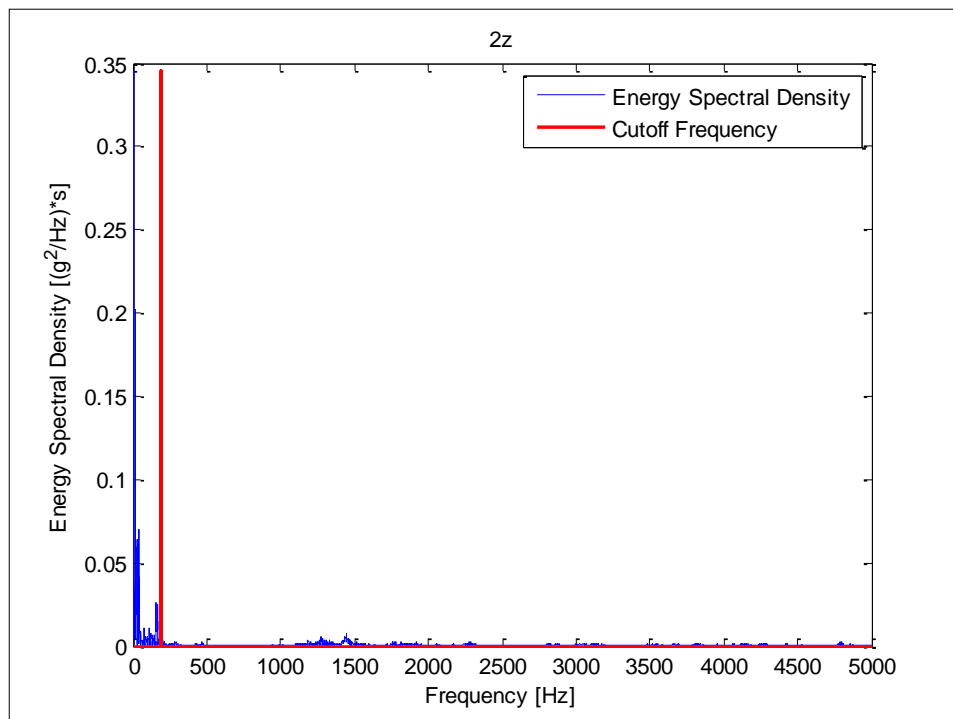Figure 5-6 Acceleration vs. time response at the COG of the missile (Raw data)

Figure 5-7 ESD-frequency response of the data at 50 cm parallel drop test

For cut-off frequency, energy spectral density method which is explained in Chapter 5 is applied. In Figure 5-7, 350 Hz is determined to be cut-off frequency level by means of the approach based on throwing away 10 % or lower values of the energy in ESD-Frequency graph. Filtered version of the curve at 350 Hz is depicted in Figure 5-8.
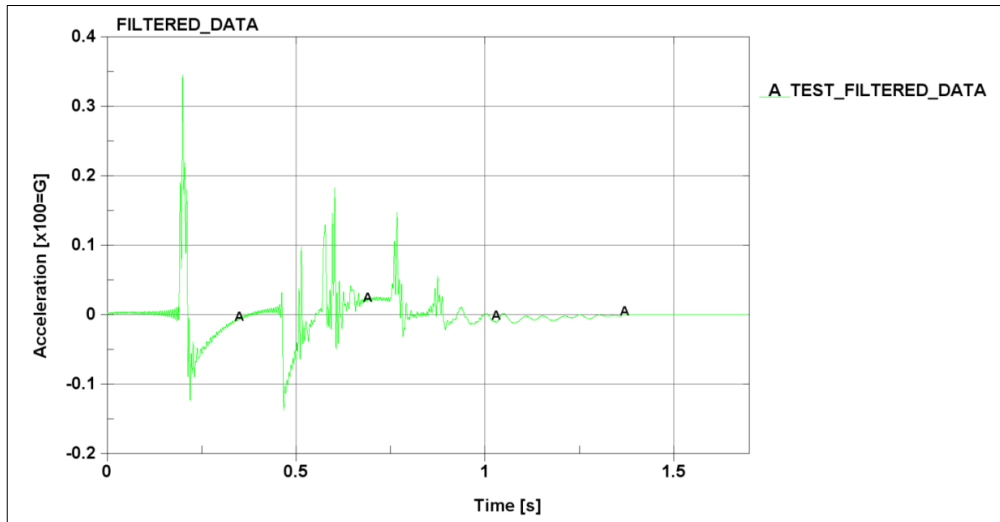

Figure 5-8 Filtered acceleration vs. time response at the COG of the missile

Comparison of the raw and filtered curves is given in Figure 5-9. Detailed explanations of filtering methods will be given in the next chapter.
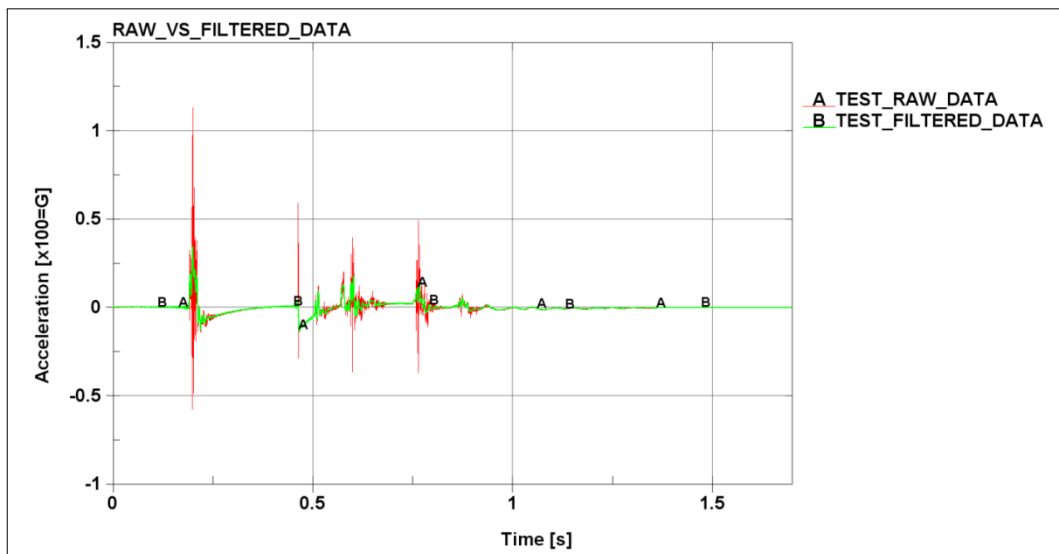

Figure 5-9 Comparison of raw and filtered responses of 50 cm parallel drop tests

CHAPTER 6

NUMERICAL RESULTS

This chapter starts with the validation analysis of the material characterization results of foams. LS-DYNA is used for the validation tool. Finite element modeling technique was also explained in detail within refinement studies. Maximum force values observed on the curves were also tabulated for comparison purposes.

6.1 RESULTS OF MATERIAL CHARACTERIZATION SIMULATIONS

Unlike the studies explained in Chapter 4, in thesis study no solid elements were preferred for the validation process. Instead, shell elements were selected for the impactor so that run time can reduce. Figure 6-1 shows the simulation scenario of the tests. In this model, initial velocity is assigned to a shell plate on which additional nodal masses are placed to provide the same weight occurred on characterization tests. Foam specimens are made of solid elements and two distinct material models, Material Model 1 (MFCF), and Material Model 2, (MMCF) were selected for Expanded Polypropylene and Polyethylene, respectively. Foam specimen was not directly supported to rigid wall. Instead, a contact algorithm is assigned with a coefficient of friction which is 0.2 - 0.3. Generally these values are suggested for the interaction of foam and steel materials. Furthermore, zero Poisson ratios are assigned to foam materials.
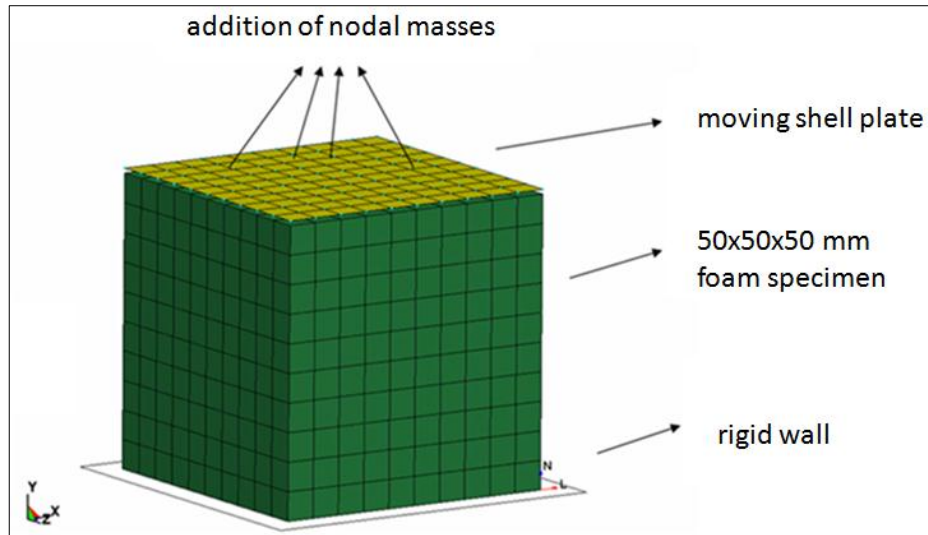
Figure 6-1 FE Model of foam

Moving shell plate and rigid wall are given the same steel properties which are: 7.85 kg/m^3, 210 GPa Young modulus and 0.3 Poisson ratio. Total number of elements and nodes are depicted in Table 6.1.

Table 6.1 Number of elements in the FE model

Element type	Element	Element number	Total
2D	Quadrilateral	400	400
	Triangular	0	
3D	Hexagonal	1000	1000
	Pentagonal	0	

In Figure 6-1, 5 mm element length is chosen for foam specimen. The reason behind this choice is directly related to the results of mesh refinement study. Refinement study is done at three distinct mesh sizes which are 25, 12.5 and 5-mm. It showed that not a notable change in force-versus time curves is observed. Although more oscillated curves were reached, similar amount of energy is dissipated (area under the force versus time curve * initial velocity). In order to picture this scene better Figure 6-2 is given.
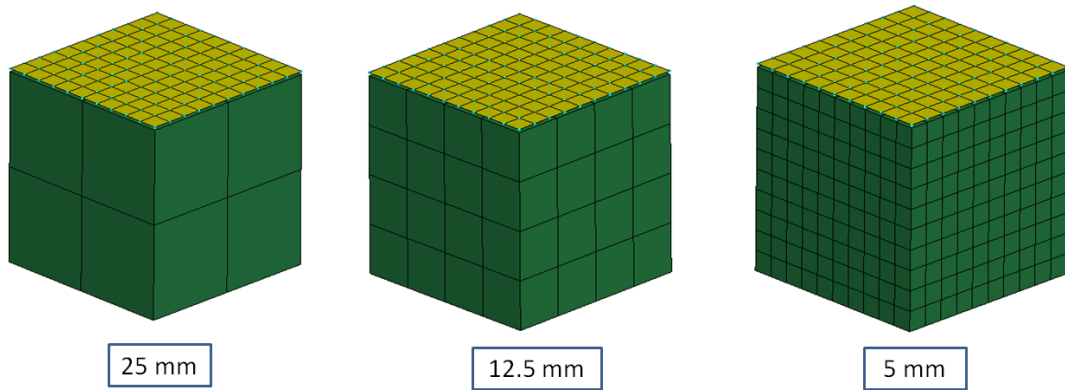
Figure 6-2 Refinement of mesh of foam specimen (EPP)

Figure 6-3 shows that the 5 mm model initially oscillates for lower mesh density up to 2 milliseconds. Pretty close match is observed starting from this point till to the end of time. By checking Figure 6-3, one may say that refinement of the mesh density does not affect the energy dissipation drastically. However, in order to make a comment on the mesh refinement study, the very beginning of the force-time curve should be examined in more detail.
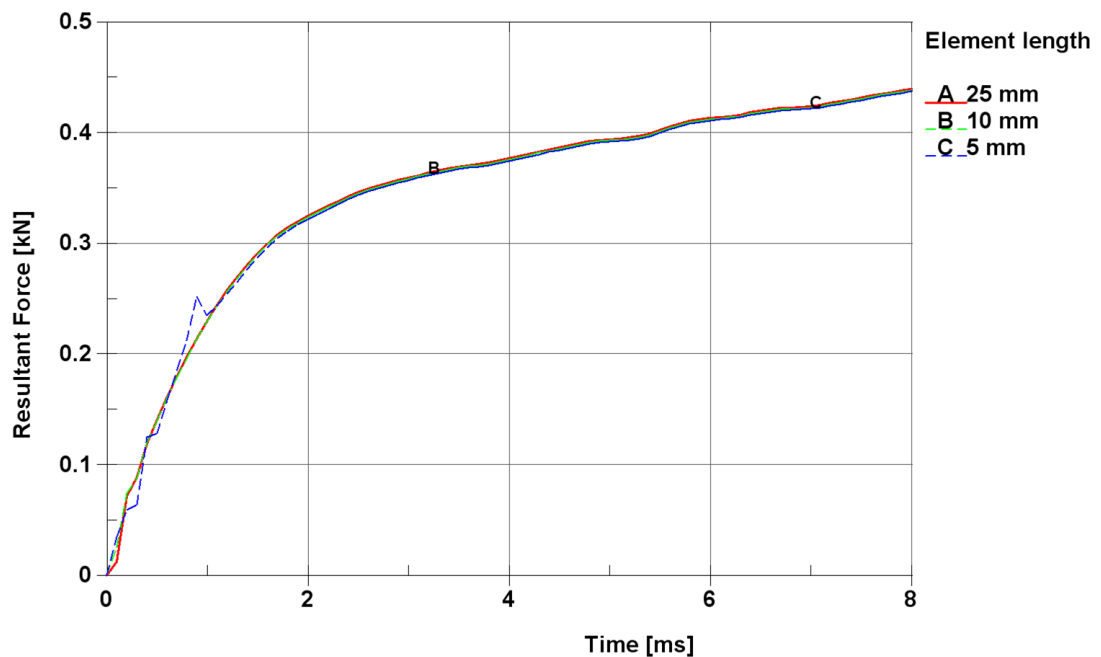

Figure 6-3 Effect of mesh refinement on force-time curve

For this reason, force-time curve is integrated in time on the interval of 0-2 milliseconds. It can be seen in Figure 6-4 that oscillation seen in Figure 6-3 does

not cause to remarkable change on impulse-time graph. However, a few iterations are done in order to get rid of this oscillation. In these iterations followings are done:

- The rigid plate (impactor) and the upper surface of the foam material are bonded to each other without any extra contact algorithm,
- The distance between the impactor and the upper surface of the foam are reduced to zero length

Although these iterations are expected to reduce the oscillation of the force-time curve of refined model, no progress is observed. It may be said that such an oscillation is possibly occurred because of the numerical instabilities.
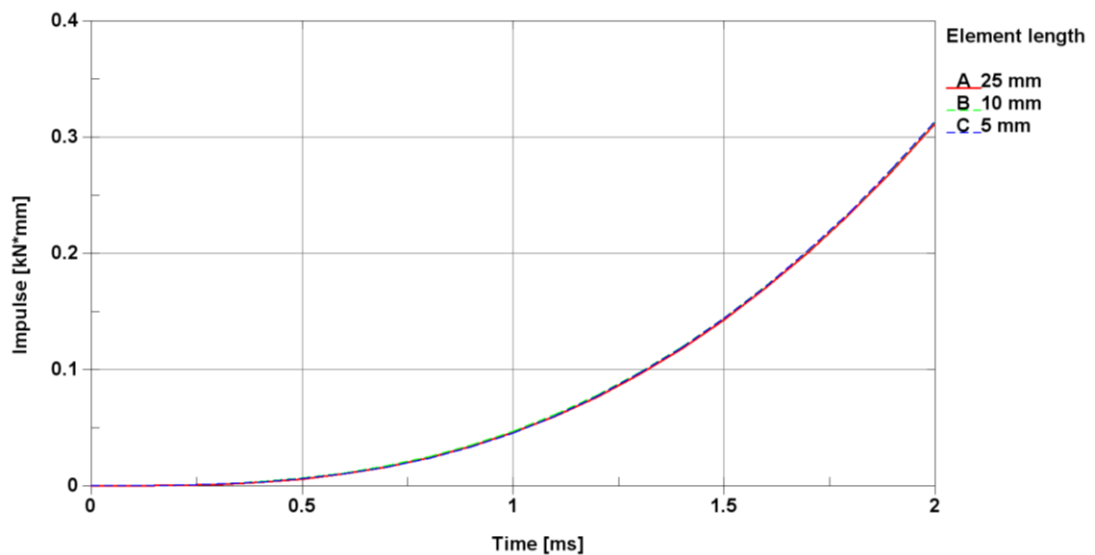

Figure 6-4 Effect of mesh refinement on impulse-time curve

It is critical to mention that in the simulation process, stress-strain curves which were obtained by material characterization process were used as input. Figure 6-5 shows the compression of 30 kg/m^3 Expanded Polypropylene foam at 1 mm/ms velocity.
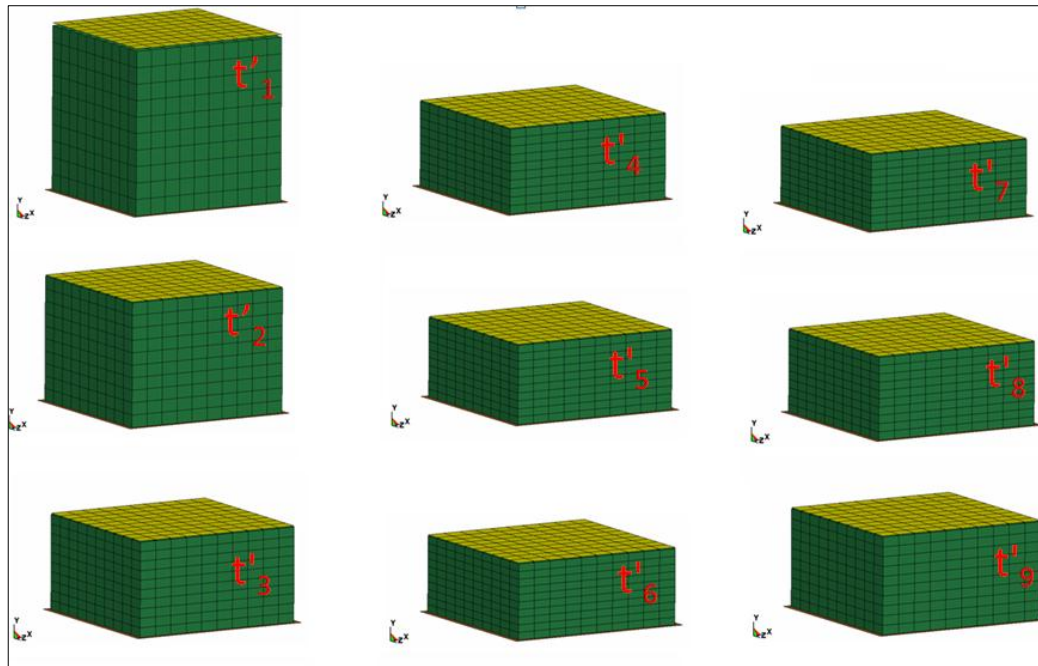
Figure 6-5 Simulation of 30 kg/m^3 EPP at a strain rate of 20 s^{-1}

As it is mentioned before, unloading behavior of EPP foam is not reached by tests, resulting in no validation is directly possible. That is why some iteration was applied to FE model by changing the parameters related to unloading behavior of foam.

For validation of Polyethylene, the same configuration of the finite element model of EPP is used. All material properties except for foam, number of elements and nodes, contact algorithms and coefficients were the same. Material Model 2 is selected for Polyethylene, while the choice was Material Model 1 for Expanded Polypropylene.

Normally, Material Model 2 is a material model for the use of irreversible foams and not commonly used for reversible materials. Although Polyethylene is a reversible material, crushable material model is preferred anyway. The reason behind this choice is based on an assumption. A big portion of the dissipated energy is provided by the loading behavior of the foam when compared to the unloading one. That is why unloading of foam can be slipped into background. Figure 6-6 shows the compression of 45 kg/m^3 Polyethylene foam at 5 mm/ms velocity. Mean element size is changed from 5 mm to 2.5 mm. Because, when strain rate is

increased, it becomes harder to simulate the scenario. Hence a precaution is taken by decreasing the mesh size.
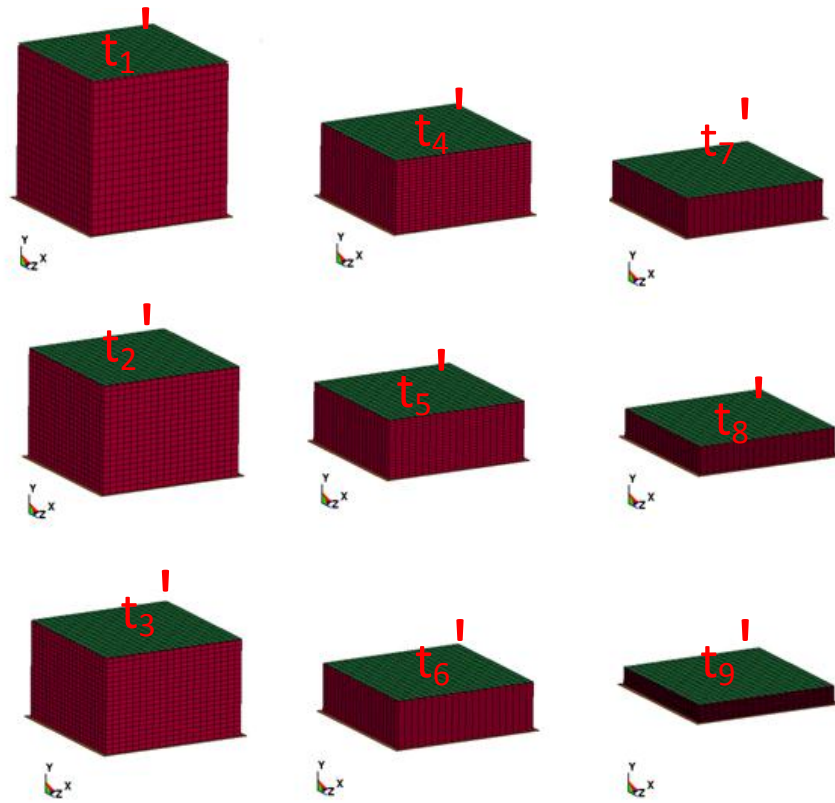

Figure 6-6 Simulation of 45 kg/m^3 PE at a strain rate of 100 s^{-1}

From now on, comparison of test and simulation is exemplified for Expanded Polypropylene and Polyethylene materials. Best way to compare them is to check the results of force-time graphs and amount of energy they absorbed.

For this reason, force-time graphs encountered in test and simulation were overlapped as it is seen in Figure 6-7. Furthermore, maximum force levels met at distinct times were also given in Table 6.2. It can be easily said that there is just a slight difference between two methods which makes the results close enough.
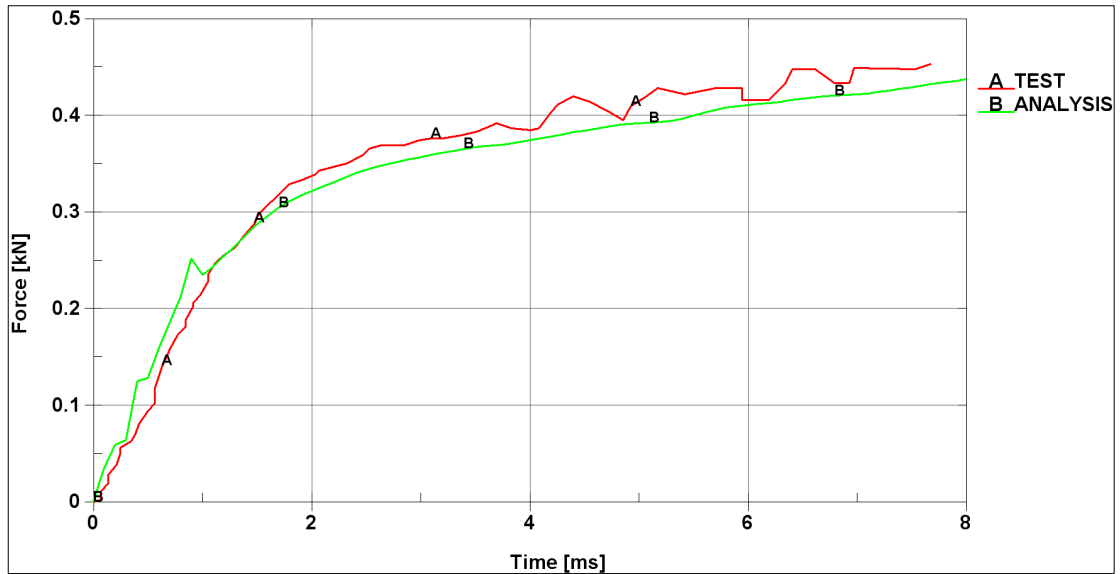
Figure 6-7 F-t comparison of test and simulation for 30 kg/m^3 EPP at 20 s^{-1}

Table 6.2 Maximum force levels of 30 kg/m^3 EPP at 20s^{-1} strain rate

Time [ms]	Maximum Force [kN] (Test)	Maximum Force [kN] (Simulation)
2	0.33	0.31
4	0.38	0.37
6	0.41	0.41
7.6	0.44	0.42

Comparison of the amount of energy which is dissipated by foams gives analyst the idea about the reliability of the results. Equation (3-1) is used for calculation of the energy absorbed by foam specimens. According to Equation (3-1), energy is directly calculated by the integral of *F (t)*dt* times initial velocity. In this case, absorbed energy has a direct relation to force-time graphs owing to the fact that initial velocity values are the same for tests and analysis.

Evidently, the more similar force-time graph for test and analysis means the closer results for absorbed energy. It can be seen in Figure 6-8 that similar trends of curves are reached. However, there is still a difference between two curves when

peak values are examined. Simulation results are a little bit lower than tests which provides analyst to be on the safe side. Otherwise, system could have absorbed more energy than it would occur in real tests. This phenomenon will probably be advantageous for analyst in case of a scenario where g levels are not low enough at the end of optimization process.

Apart from Expanded Polypropylene, Polyethylene material was also needed to be validated by simulations. The most critical point of this validation is the choice of 100 s^{-1} strain rated Polyethylene while it was 20 s^{-1} for Expanded Polyethylene. The reason behind this choice is that Polyethylene material behavior at higher strain rates is much more crucial than lower ones.

Comparison is reached by overlapping the force-time graphs. In Figure 6-8, force-time graphs of test and simulation are specified. According to Figure 6-8, a satisfactory match between two curves is seemed to be achieved. There is again a notable difference between two curves at some points.

However, trends of these two curves are quite similar to each other which mean that behavior of Polyethylene is captured well by this type of modeling. The fundamental reason of this difference is possibly because of the lack of material tests. In other words, only uniaxial compression test is applied to the specimens and it necessitates large number of material test data which are compression, tension, shear and hydrostatic in order to predict the behavior of foams better.

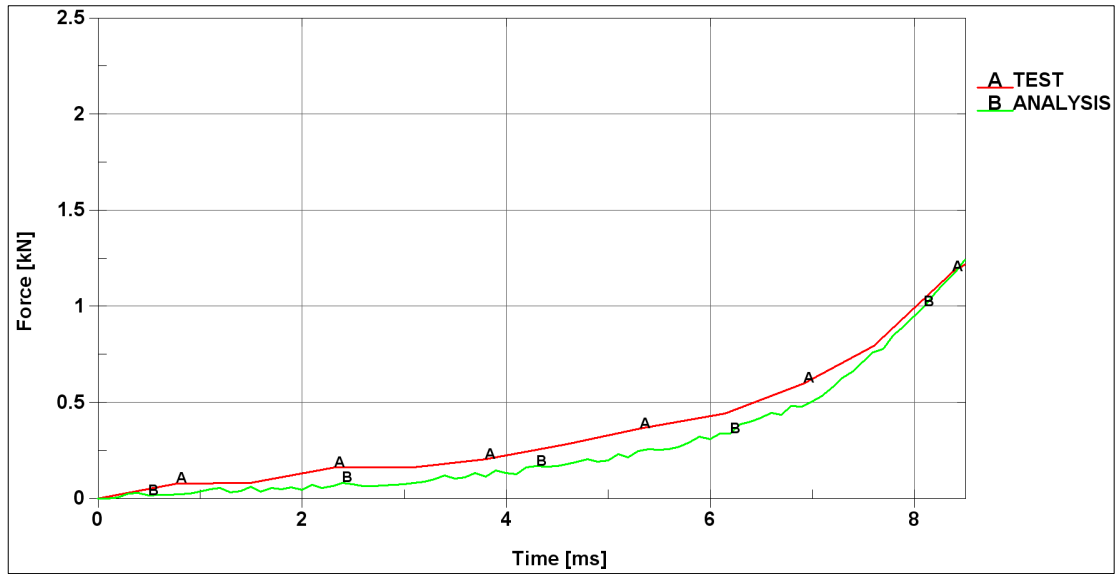Maximum values of these curves are depicted in Table 6.3.

Figure 6-8 F-t comparison of test and simulation for 30 kg/m^3 PE at 100 s^{-1}

Table 6.3 Maximum force levels of 30 kg/m^3 PE at 100s^{-1} strain rate

Time [ms]	Maximum Force [kN] (Test)	Maximum Force [kN] (Simulation)
2	0.15	0.11
4	0.25	0.15
6	0.45	0.34
8	1.01	0.96
8.4	1.25	1.24

It can be inferred from the above graphs and tables that simulation results underestimated the test results.

Generally it is possible to say that material models did show a good correlation with physical tests and simulations matched closely with test results. Although peak force levels had some deviation at some points, the nature of the curves was similar to each other. To sum up, behavior of these foams, EPP and PE, can be captured well by chosen material models.

6.2   VALIDATION RESULTS OF DROP TESTS OF MUNITIONS

As it is previously mentioned, foam parts are the most important components of the system in terms of energy absorption characteristics. In order to figure out the optimum element length, different mesh densities were examined for solid elements. Initially, 20 mm element length with default element formulation (elform 1) was selected to be starting point owing to the fact that bigger sized elements would not be reasonable when dimensions of foam caps were thought.

Distinct element lengths (20 mm, 15 mm, 5mm), formulations (elform 1, elform 2) as well as types (hexagonal, 4-node tetrahedron, 10-node tetrahedron) were examined to monitor the effects on results. In the reference [54], tetrahedron elements were also offered to be used for foam materials. That is the reason of using these types of elements for the representation of foam materials.

By observing Table 6.4, it can be concluded that maximum 10 % change in g levels is depicted. However, when the case is refinement of mesh, computational time issues came to the stage as a drawback. For instance, termination time for Model 3 (model with 5 mm element size) is twice of the termination time of Model 1 (model with 20 mm element size).

It can be concluded that computational inefficiency of the refined mesh models became an obstacle for further analysis. That is why 20 mm element sized model selected as a base model.

Table 6.4 is given for this comparison. In Table 6.4, effects of different element types on acceleration levels are tabulated. Maximum acceleration levels are given for 20-10 and 5- mm element sized models for hexagonal elements. The same scenario is thought for 4-noded tetrahedron and 10-noded tetrahedron models too. However, contact instability issues prevented some of these models for completion. That is why some other element lengths such as 15-mm are examined too. This is depicted in Table 6.4.

As seen in Figure 6-9, using distinct types of elements resulted in variations in terms of acceleration responses. According to Figure 6-9, tetrahedron element usage for foams caused to decrease in acceleration level. This type of modeling is not so often used in foam modeling.
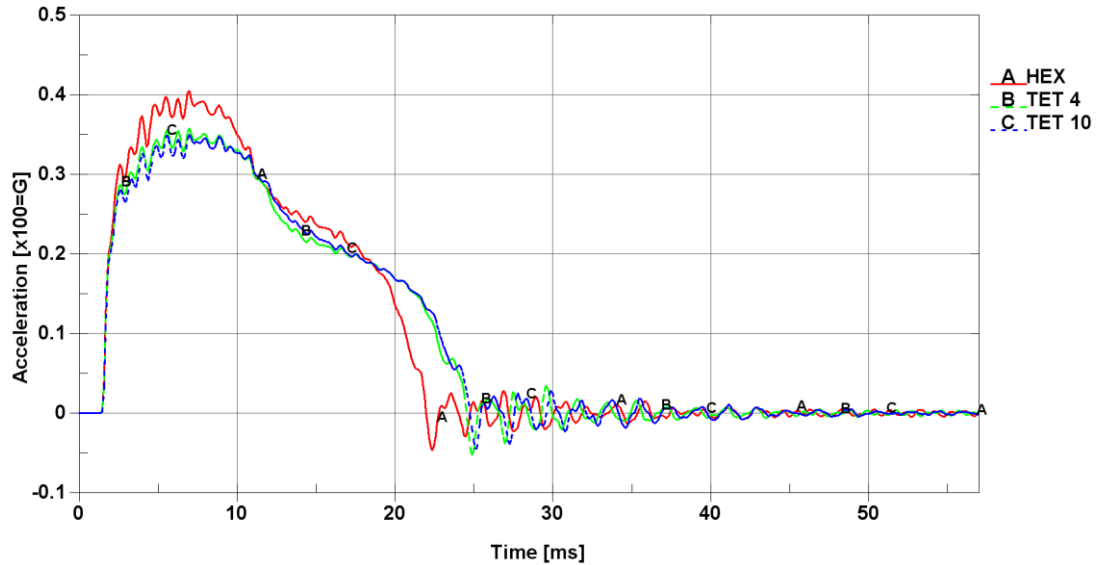

Figure 6-9 a-t responses of 3 different element types for 20 mm element length

Table 6.4 Effects of different element types and lengths on g levels

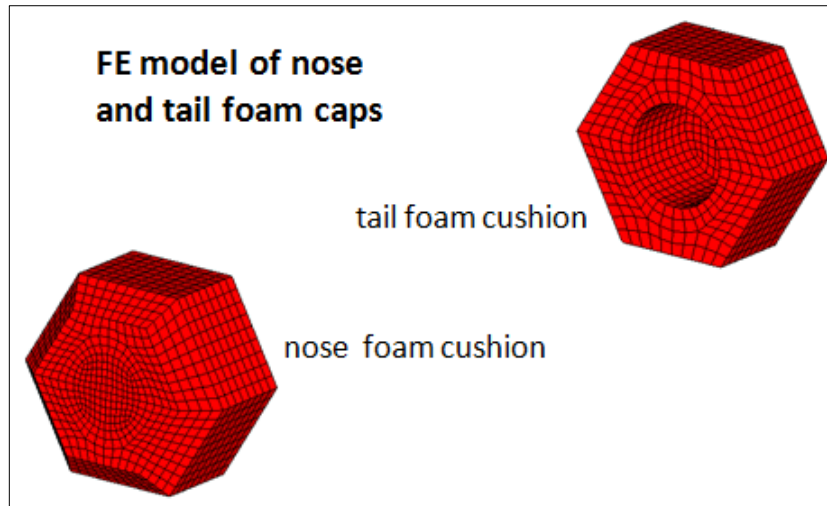| Model name	Element type	Element length [mm]	Peak Acc.-1 [g]	Peak Acc.-2 (COG)[g]	Peak Acc.-3 [g]	CPU time [hours]
Model 01	hexagonal	20	51	40	47	1.5
Model 02	hexagonal	10	47	38	45	12
Model 03	hexagonal	5	46	38	44	24.5
Model 04	4-node tetrahedron	20	47	36	42	4.5
Model 05	10-node tetrahedron	20	45	35	43	12
Model 06	10-node tetrahedron	15	44	35	42	27.5

Figure 6-10 20 mm element sized mesh of tail and nose foam cushions

As it is seen in Figure 6-10, both tail and nose foam cushions were developed to be identical. As an alternative, they can also be formed from two sections which is bonded to each other via *CONTACT_TIED_NODES_TO_SURFACE [51] card within default parameters. The main reason of this type of modeling is its being easier for analyst. Figure 6-11 shows three distinct views of these two techniques.
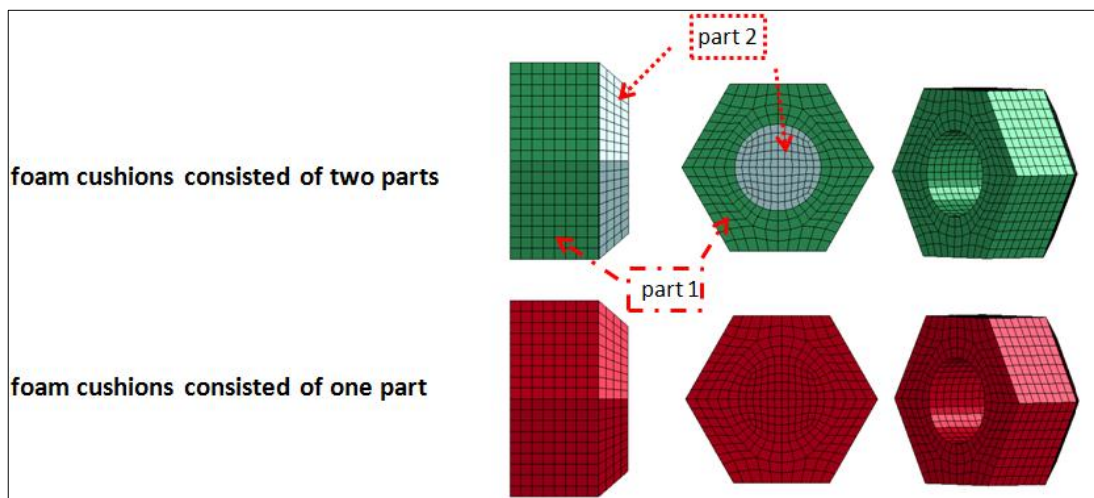

Figure 6-11 Two distinct modeling technique used on foam cushions

Still, it should be proved that not a remarkable change on the results will be monitored.

For Model 2 and Model 9, acceleration-time response of two different modeling techniques is depicted in Figure 6-12. It can be seen that both one-piece and two-piece designs give almost the same results for 10 mm element length size model. Similar scenario is observed for bigger element size (20 mm) too.
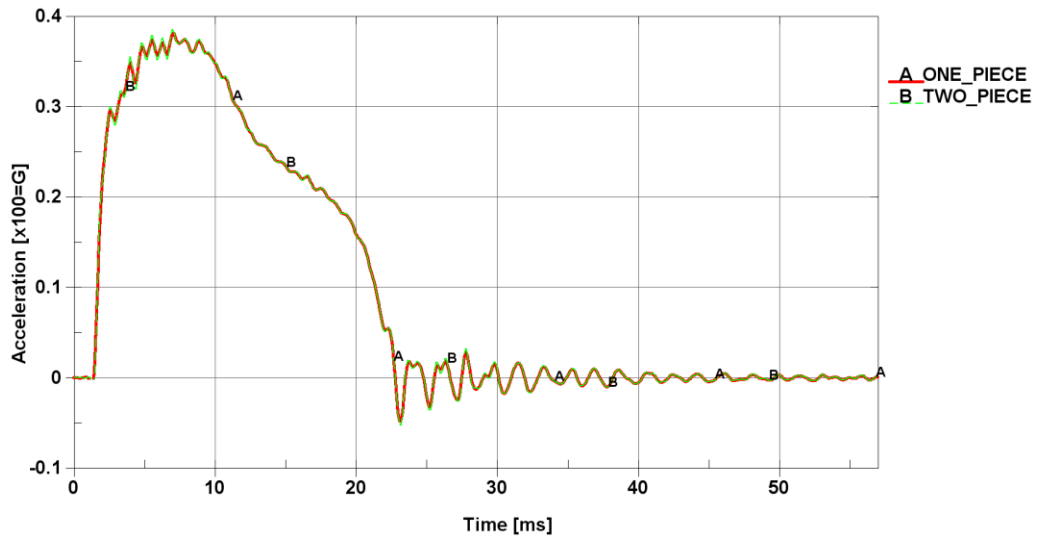

Figure 6-12 Acceleration-time graphs of two different modeling techniques

Effects of using two different techniques on foam cushions are tabulated in Table 6.5.

Table 6.5 Effects of different 2-piece designs and element lengths on g levels

Model name	Element type	Element length [mm]	Peak Acc.-1 [g]	Peak Acc.-2 (COG)[g]	Peak Acc.3 [g]
Model 01 (one-piece)	hexagonal	20	51	40	47
Model 08 (two-piece)	hexagonal	20	51	41	47
Model 02 (one-piece)	hexagonal	10	47	38	45
Model 09 (two-piece)	hexagonal	10	47	39	45

According to Table 6.5, Model 1 (one-piece) and Model 8 (two-piece) are almost reached the same results. Similar behavior is seen between Model 02 and Model 09 too. Finally it is seen that 2-piece designs (Model 08-Model 09) are not different than original designs (Model 01-Model 02) after effects on g levels were examined.
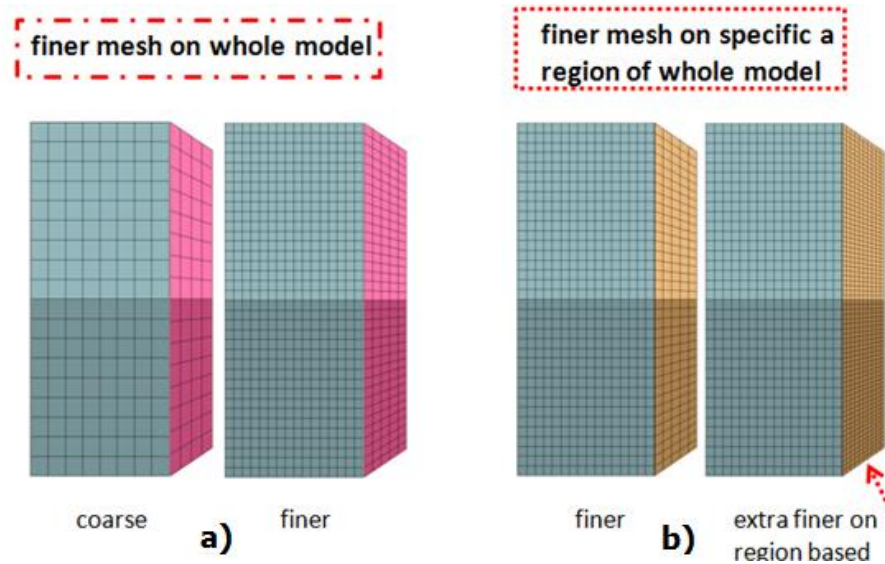

Figure 6-13 Refinement of mesh (a) on whole model (b) on region based

Figure 6-13a, a region based mesh sensitivity study is examined. As depicted in Figure 6-13b, tapered section was meshed with smaller elements than rest of the foam. Effect of mesh refinements on g levels are given in
Table 6.6.

Table 6.6 Effects of region based refinements and element lengths on g levels

Model name	Element type	Element length [mm]	Peak Acc.-1 [g]	Peak Acc.-2 (COG)[g]	Peak Acc.-3 [g]
Model 09	hexagonal	10	47	39	45
Model 10	hexagonal	10 and 5	49	39	46

Not a remarkable change was observed by applying a region based refinement. That is why it cannot be named as a big necessity.

Last but not least, Table 6.7 was given to monitor the effects of the change of element formulation. According to Table 6.7, element formulation changes did not have an outstanding effect on g levels particularly for tetrahedral formulations. Its effects on g levels can be underestimated for hexagonal element types because of computational efficiency which has a vital importance.

Table 6.7 Effects of element formulations on g levels

Model name	Element type	Element formulation	Element length [mm]	Peak Acc.-1 [g]	Peak Acc.-2 [g]	Peak Acc.-3 [g]
Model 08	hexagonal	1	20	51	41	47
Model 11	hexagonal	2	20	48	38	46
Model 05	10-node tetrahedron	16	20	45	35	43
Model 04	4-node tetrahedron	10	20	47	36	42

Another study done about foam cushions is related to contact areas of the tube and foam cushions. As it can be seen in Figure 6-14, inside surfaces of nose and tail foam cushions were bonded to the launching tube with a shrink fit. As a result, no gaps between the interior of foams and launching tube were allowed.
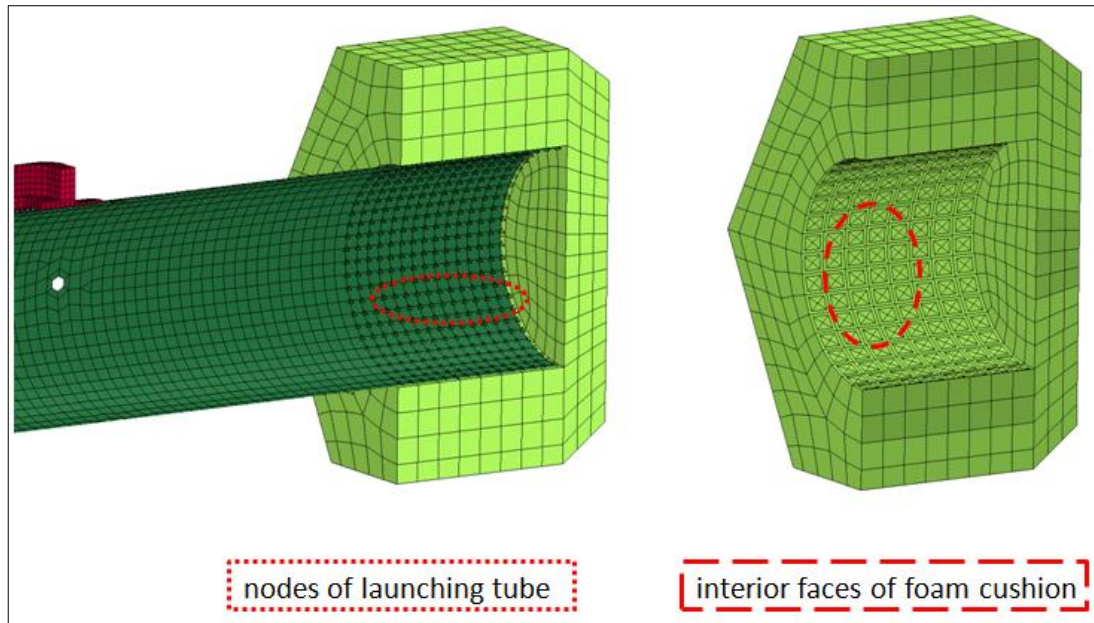
Figure 6-14 Nodes of launching tube and Interior faces of foam cushions

Contact algorithm used in this section is *CONTACT_TIED_NODES_TO_SURFACE (Contact Model 1= CTNTS) in which nodes of launching tube were shifted to the faces (or segments) of foam cushions. Consequently, both foam cushions and launching tube are going to move together. In this contact algorithm no friction is included between foam and composite launching tube due to appropriate foam-composite coefficient of friction value is unknown. However, this scenario can be accepted as a worst-case scenario owing to no friction is defined. Otherwise, dissipation of energy would have been increased due to friction.

Other two alternatives are also tried for the contact between the interior surface of the foam and the outer surface of the launching tube. As a first alternative, bottom side of the tube and foam were bonded to each other with Contact Model 1, while the upper side is released to move free. Alternative 1 for the contact definition is depicted in Figure 6-15.
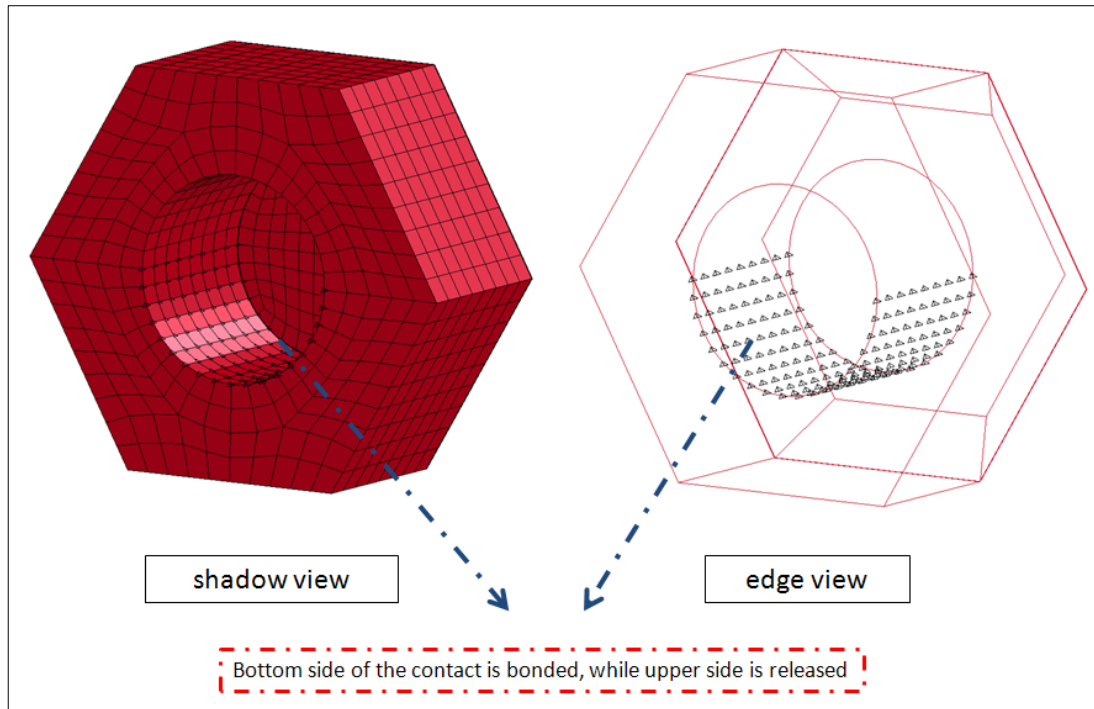
Figure 6-15 Alternative 1 for the contact between foam and tube

In Alternative 2, no bonding between the launching tube and the foam was defined. Instead, *CONTACT_AUTOMATIC_SURFACE_TO_SURFACE (Contact Model 2= CASTS) is used with and/or without coefficient of friction. A drawback of this type of usage is that foam cushions can slide over the launching tube surface. This is possibly the most similar scenario in which drop tests were met. However, sliding of the foam caps on tube results in the change of the position of the foams. Consequently, foam materials deform much more than expected which cause to hourglass problems.

As a result of these distinct types of contact definitions, just ignorable changes (maximum 1 g) on acceleration levels were encountered. In analysis, Contact Model 1 with full surface bonding is preferred.

Similar to the relation between foam cushions and launching tube, connector and launching tube were also defined to move together. Again, Contact Model 1 is defined within the same parameters used between foam and launching tube. No absorption of energy is in question when connector is the case so that not much

attention is given. Connection of launching tube and connector is shown in Figure 6-16.
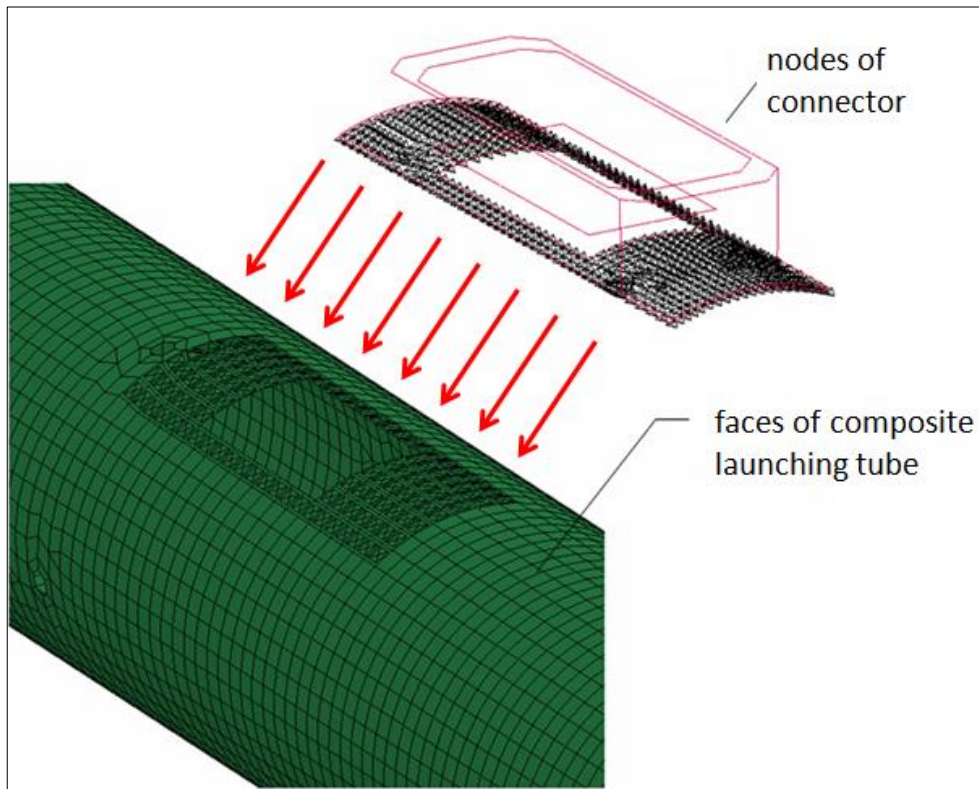

Figure 6-16 Nodes of connector and faces of launching tube

In Figure 6-17, summary of both connector-tube and tube-foam contacts were given. Furthermore, it should be emphasized that critical elements at the area of contact were developed within good aspect ratio so that better behavior is possible to be seen. In Figure 6-17, these critical areas are shown.
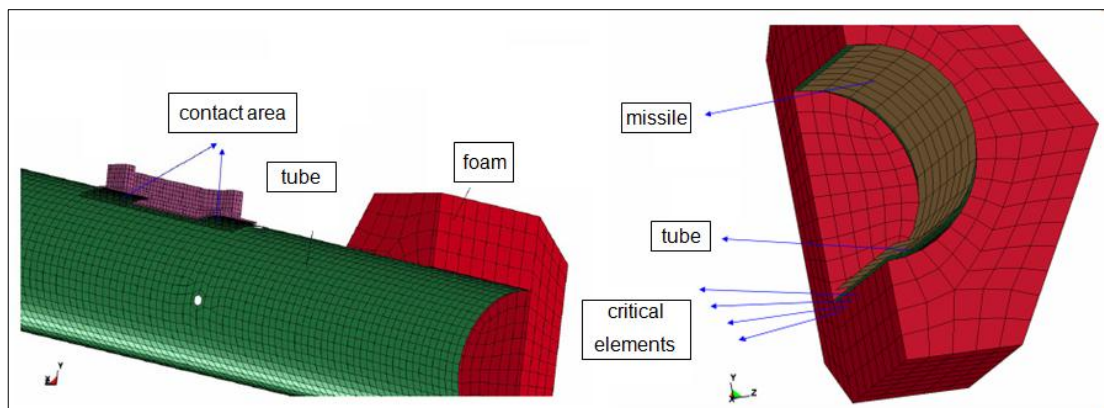

Figure 6-17 Summary of contacts and critical elements

In order to represent the scenario of experimental process, relation between launching tube and missile should also be true. If no connection were defined between the tube and the missile, missile would slide inside the launching tube. In drop tests, bolts were used to prevent sliding of missile. In simulations, no bolts were modeled; instead the nodes around the holes were connected to the nodes of the missile as it is seen in Figure 6-18.
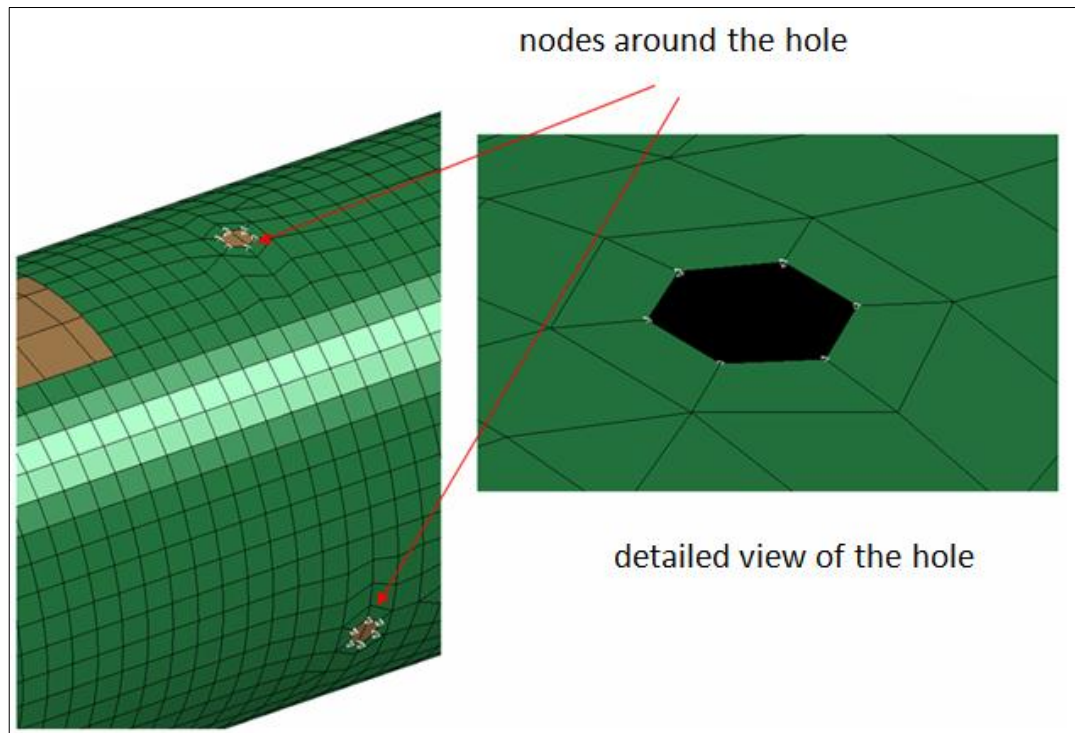

Figure 6-18 Nodes around the hole and detailed view of hole

In this section of the thesis, energy diagrams, load encountered at the center of gravity, velocity-time graph and displacement seen on the foam cushions will be given. Prior to examining energy graphs, it is expected that most of the energy will be dissipated by polymeric foam cushions. According to Figure 6-19, amount of energy dissipated by composite launching tube was too low when compared to foams. As depicted in Figure 6-19, no energy dissipation is expected from missile owing to rigid modeling.
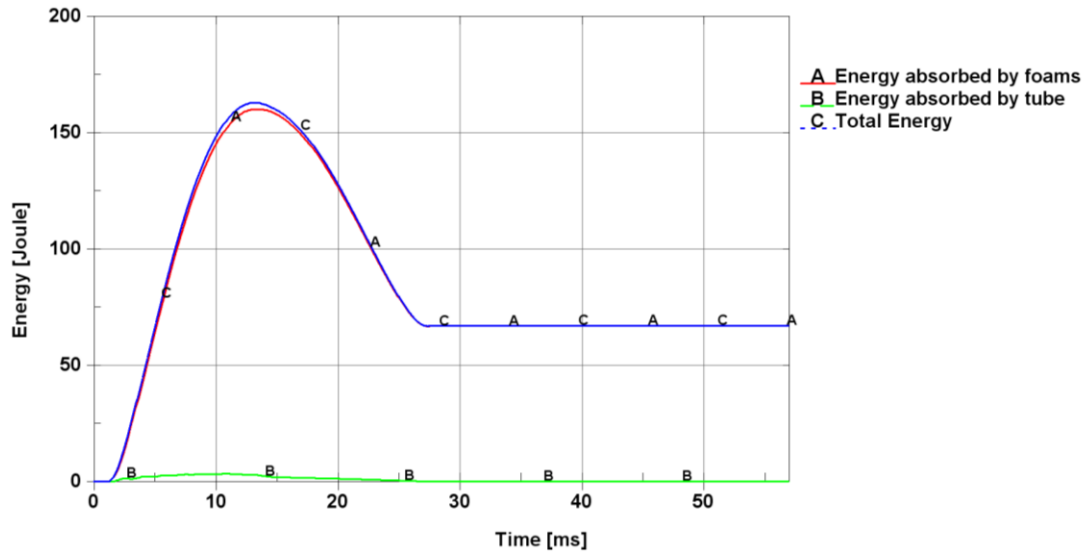
Figure 6-19 Energy diagram comparison of foams and composite launching tube

Amount of energy absorbed by tubes seems not to be changed whether launching tube is modeled with composite material model or not. In Figure 6-20, it can be supposed that amount of energy absorbed by tubes is drastically changed by different modeling.
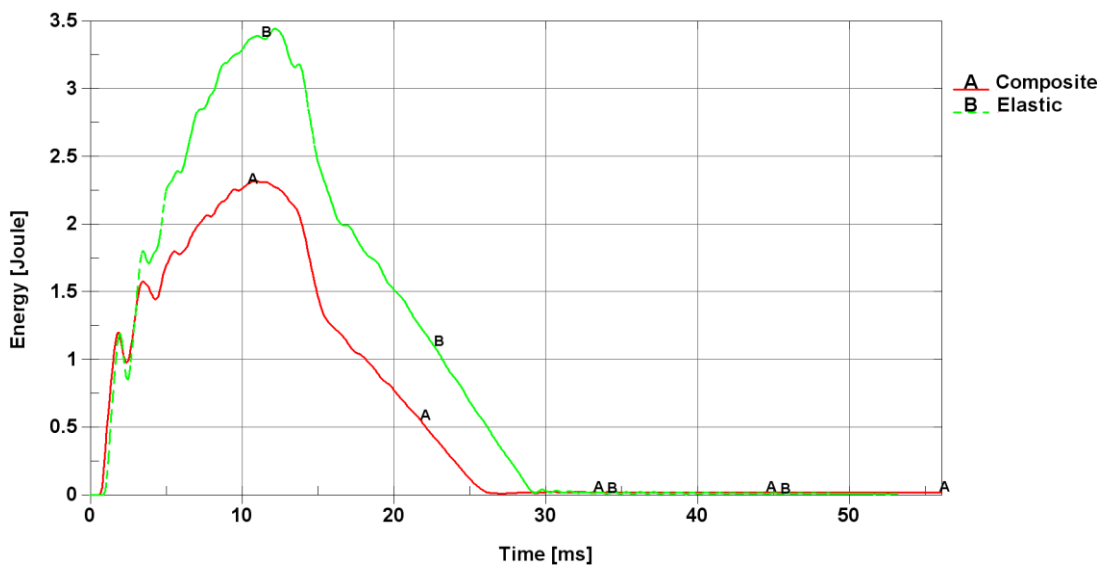

Figure 6-20 Comparison of the energy absorption of both model

For a better interpretation, ratio of the energy absorbed by composite and elastic modeling is compared with total absorption. This is depicted in Figure 6-21.
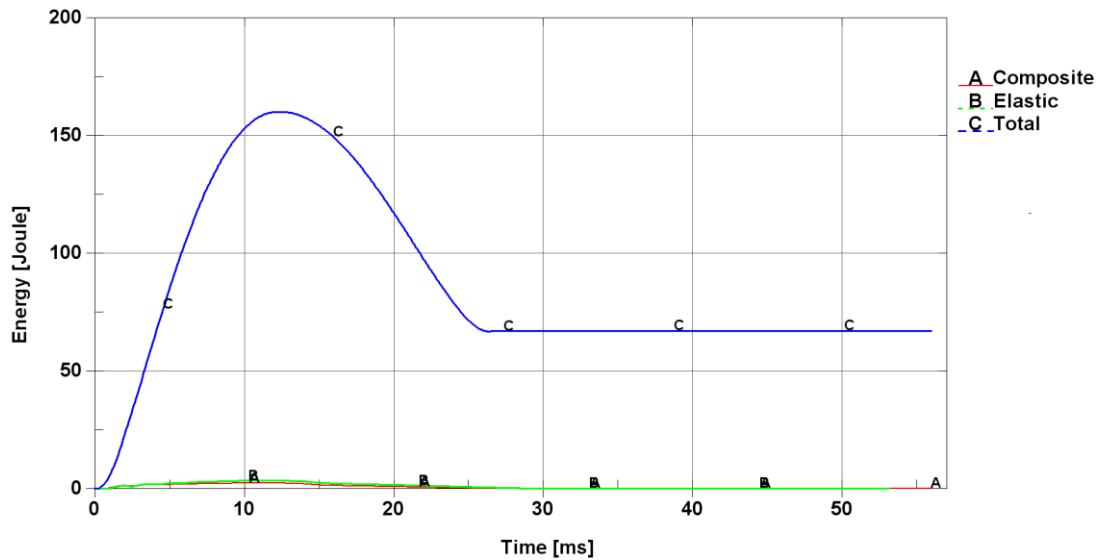
119

Figure 6-21 Total energy absorption vs. both model

Amount of energy dissipated by tube is too low when compared to the total dissipated energy. This expression says that different modeling technique of the launching tube does have a minor effect.
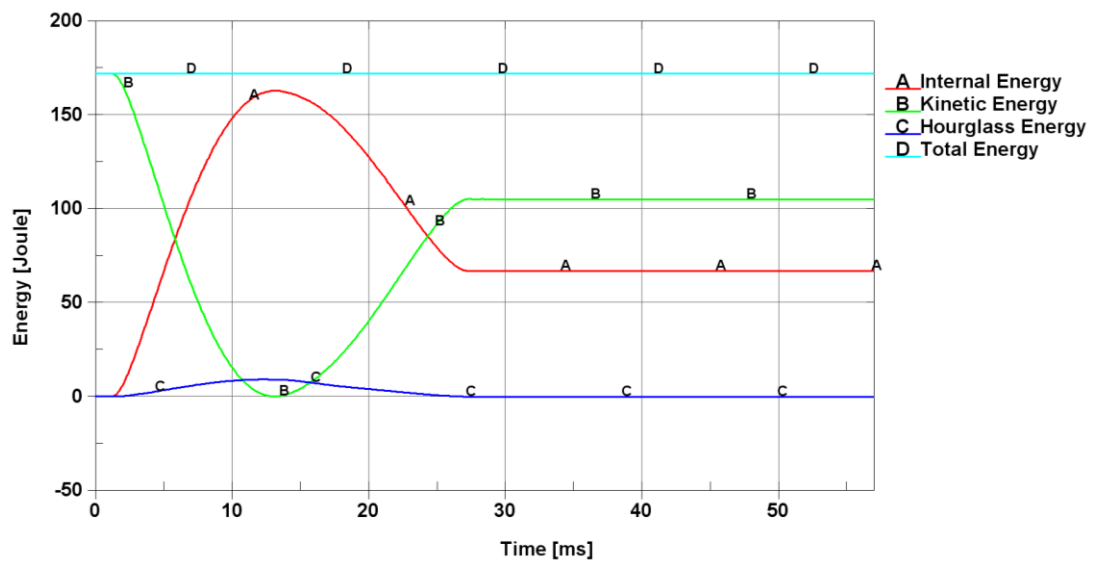

Figure 6-22 Kinetic-internal-hourglass and total energy diagrams

In Figure 6-22, hourglass energy seems to be lower than 10 % of total energy which is desirable. In addition, total energy curve is constant which means no energy was produced within the system. Kinetic energy was reduced while internal

energy was increasing and vice versa. This shows that internal energy-kinetic energy transition was also as expected.

Another output that is needed to be checked is velocity-time graph. What is expected to be seen in this graph is that rebound velocity of the munition should be lower than initial velocity. This expectation was proved by Figure 6-23 and less than 3.13 m/s velocity were occurred.
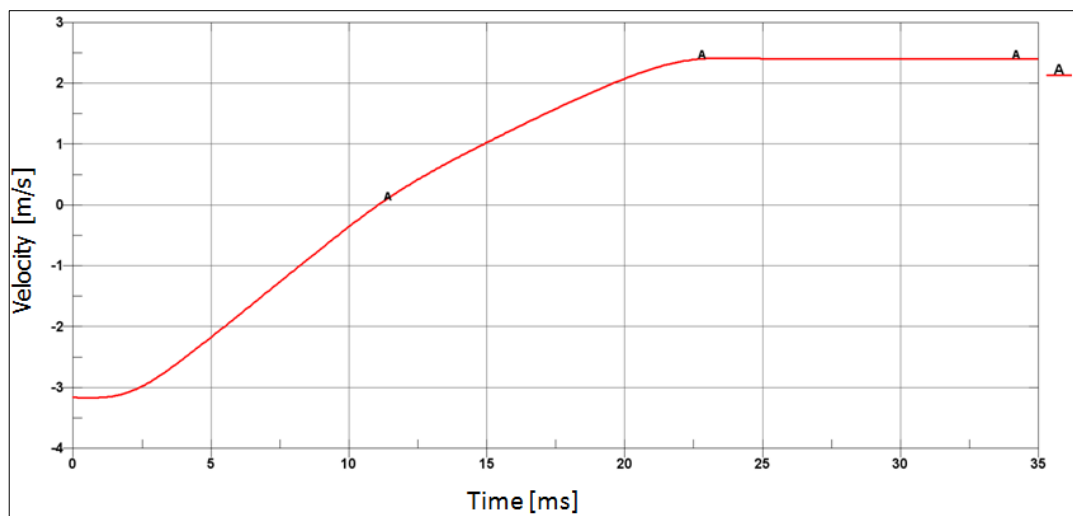

Figure 6-23 Velocity-time graph

At the very beginning of the graph, no change of initial velocity is seen for a few milliseconds. This is probably because of the fact that no contact of foam cushion within the ground has happened yet. After impact, velocity was started to reduce sharply up to a point that crush of foam has ended. Whole system began to move against gravity after velocity was decreased to zero. This elevation lasted up to a rebound height which is lower than starting one. Then, the system was continued to move with a constant velocity owing to no gravity was defined in the model. Since area of interest in this scenario is totally related to the crush of foam cushions which provide energy absorption, late behavior of the mechanism was not paid attention.

In Figure 6-24, 50 cm parallel drop simulation unfiltered acceleration-time history of the center of gravity of the munition is depicted. As it can be seen in detailed view

of the same figure, maximum load seen at COG is at around 40 "g". However, when filtering is applied to the same graph, lower "g" values will be encountered.

An answer to the question "why acceleration data in FE code should be filtered?" is given the reference [51]. According to the reference, acceleration data (both test data and simulation) usually contain high-frequency oscillations. These oscillations are not noise. High frequency modes are often present as well as the low frequency modes. And the magnitude (or amplitude) of the high-frequency modes are often so large that they will prevent you from seeing the "main" acceleration curve, if they are not filtered out. It is my understanding that if you are about to compare acceleration curves from test and simulation you should sample both cases with the same frequency and also apply the same filter to the raw data in both cases (test and simulation).
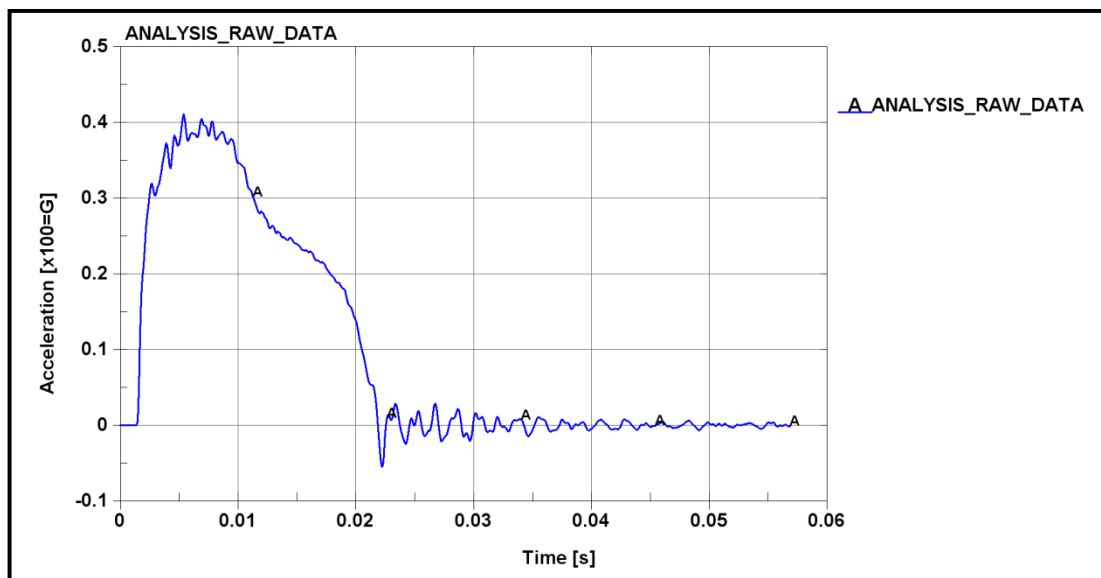

Figure 6-24 Unfiltered acceleration-time response of the munition at COG

As an illustration of the effect of the filter frequency, all filtered acceleration-time histories were plotted in the same figure. In Figure 6-25, acceleration responses were filtered using six different cut-off frequencies which are 100-, 200-, 300-, 350-, 600- and 1000-Hz.
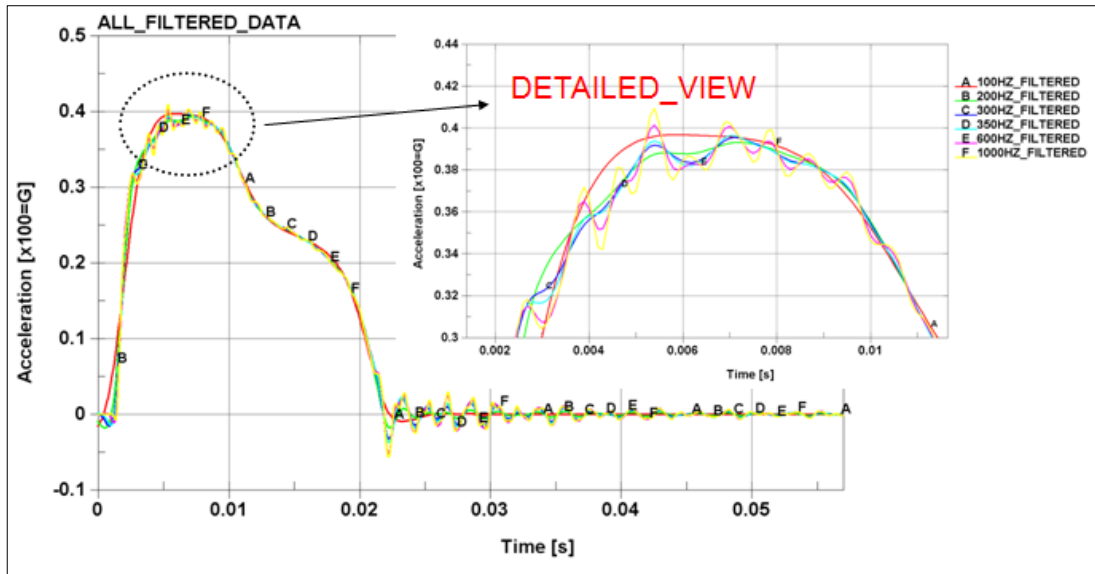
Figure 6-25 Acceleration-time history of COG at six different frequencies

In Figure 6-26, three out of six filter frequencies which are mid frequencies were extracted from the figure and then compared to the raw data.

Figure 6-26 A-t responseof the data for three major frequencies

As a result, 350 Hz is selected to be a cut-off frequency due to the fact that the same frequency was also used in drop tests. As shown in Figure 6-27, peak acceleration was reduced a bit and reached to a value of 38-g.

Figure 6-27 Comparison of raw and filtered acceleration-time histories
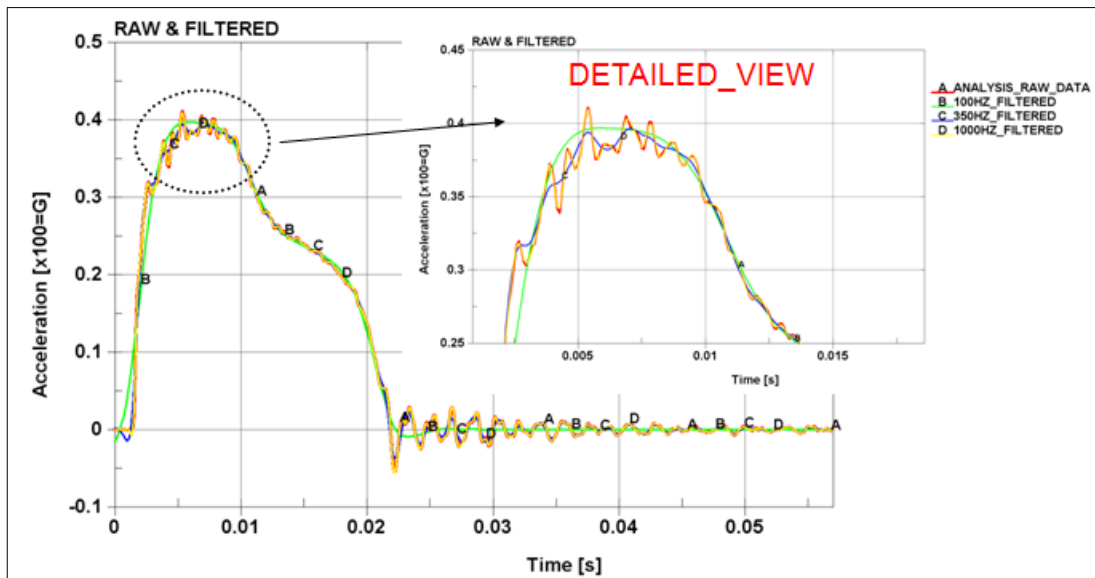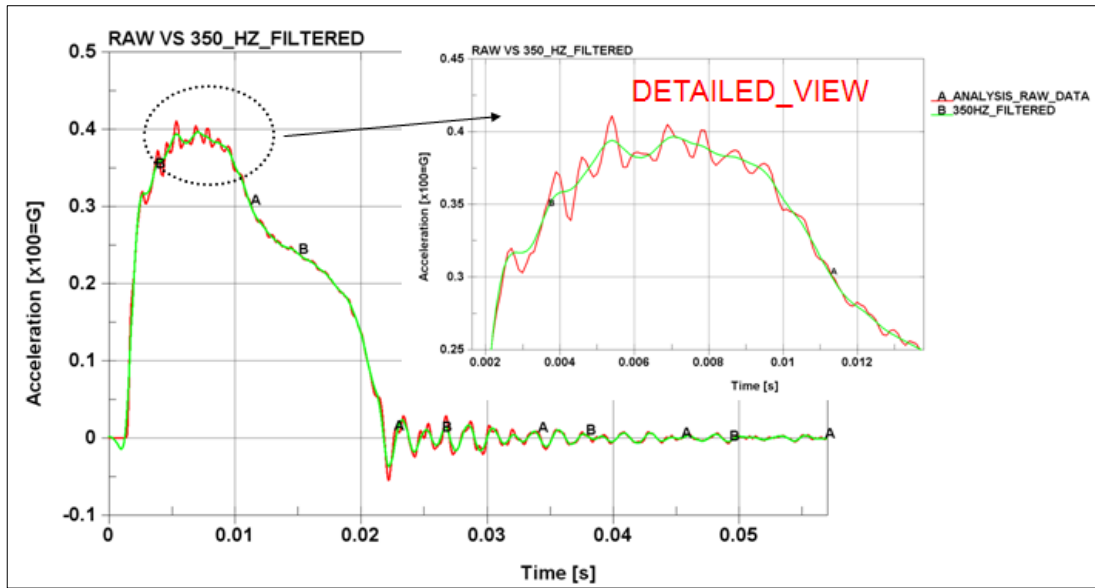
Comparison of test and numerical analysis will be shown in Figure 6-28 so that a better conclusion can be made. Owing to the fact that test data was recorded longer times a detailed view of the impact moment was also given in the same figure.
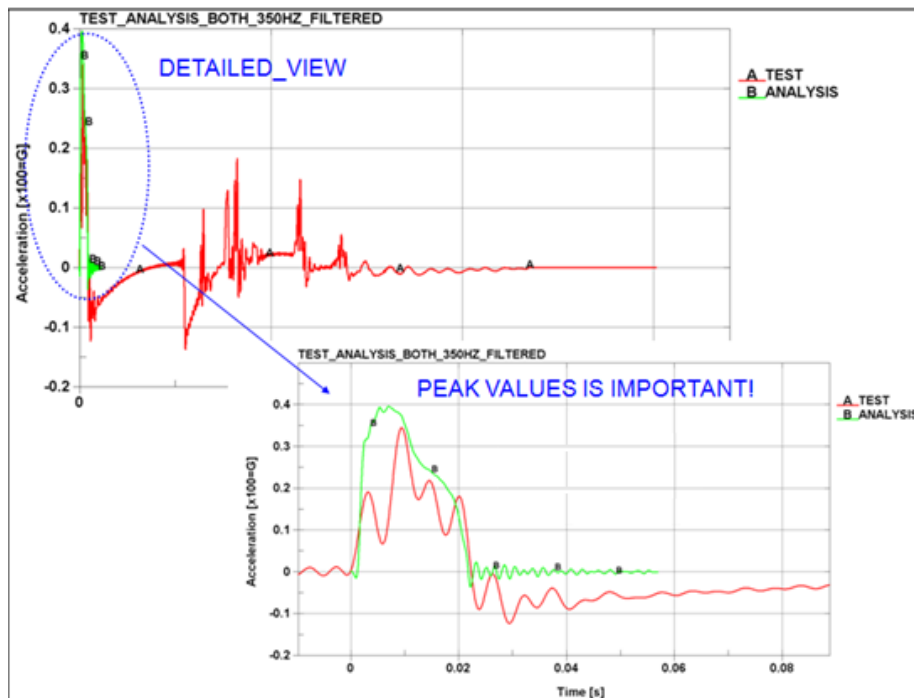

Figure 6-28 Comparison of filtered acceleration-time history of test and analysis

124

It is also seen in the same figure that acceleration curve of simulation is pretty smooth when compared to test data which is more fluctuated as expected. This is probably because of modeling techniques of the missile. Owing to the rigid modes of the missile not much oscillation was observed during the simulation as it does in the tests. Whereas, peak data observed in both test and simulation is close enough to each other, 35-38-g, respectively. This slight difference is tolerable and according to the graph, it is inevitable that test and analysis results matched well. Finally, there have been no more obstacles to go further study which is optimization of the geometry of the foam.

6.3   PARAMETRIC STUDY ON FOAM GEOMETRY

Validation studies showed that measured "g" levels are not low enough for system to keep structural integrity. Hence, load levels should be reduced to tolerable values which will be accomplished by optimization studies. Starting from this point of the study, no experimental process will be applied. Instead, computer based studies will pioneer us to reach this target. By doing so, less time will be needed and lower budget will be utilized to finalize the study compared to experimental ways.

Material types, densities and dimensions of foam cushions are three major design parameters. Other than Expanded Polypropylene which was used during validation process, Polyethylene and combination of both PE and EPP also came to the stage. 30 kg/m^3 EPP was only option during validation process whereas, different material densities for EPP and PE were also used throughout optimization process thanks to material characterization tests. Two fundamental differences between PE and EPP can be listed as follows:

- Although PE can absorb more energy than EPP with the same density, it deforms much more then EPP,

- EPP can come back to its original position faster than PE when rebounding of the material is considered.

Finite element model used in validation process had a slight distinction whose effect on energy absorption is minimal prior to optimization process. Other than the

connector (Connector 2) which took part in FE model during validation process, another connector (Connector 1) was added to FE model. Although addition of new connector did not affect absorption characteristics of foam cushions, it brought a limitation to the system. In case of an impact, no contact between Connector 1 and the ground will be allowed.
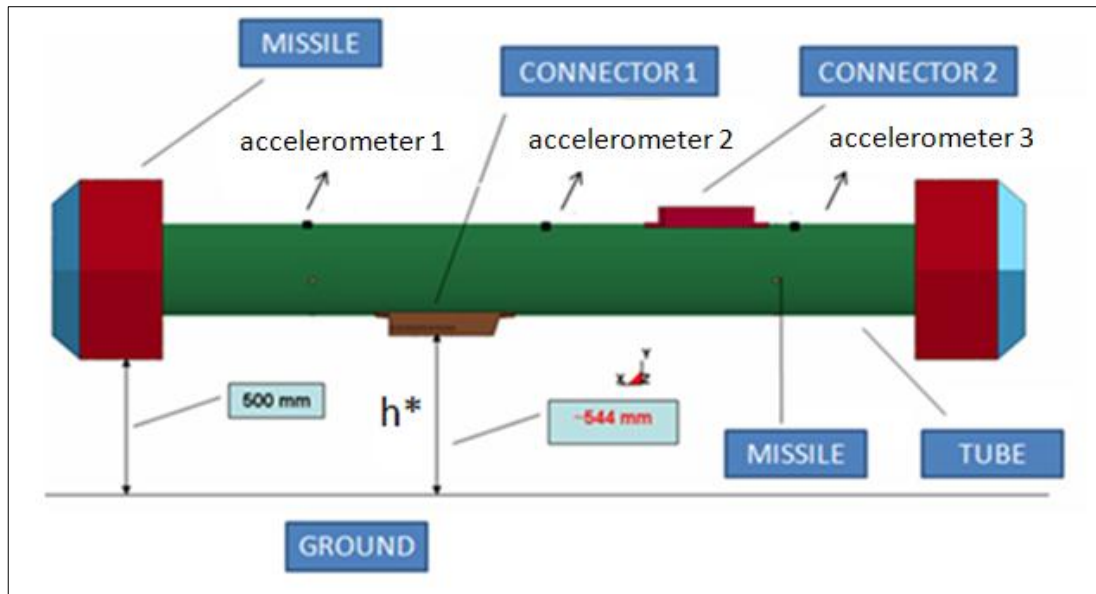

Figure 6-29 Components, accelerometers and a general view of new model

A new-model was developed within the beginning of parametric study. Apart from addition of Connector 1, positioning of accelerometers and drop height were also depicted in Figure 6-29. In the same figure, "h^1" is also defined as the vertical displacement between Connector 1 and the ground at the time of maximum crush. This distance is tried to be maximum during optimization studies owing to the fact that too low "h^1" values will be a threat for the system.

One more development used in the optimization models is that foam cushions were developed as two or three pieces, then bonded together with the *CONTACT_TIED_NODES_TO_SURFACE algorithm whose detail was given in previous chapters. The main goal of this approximation, shown in Figure 6-30, is to save time to develop distinct FE models. Negligible effect on energy absorption was monitored with this simplification.
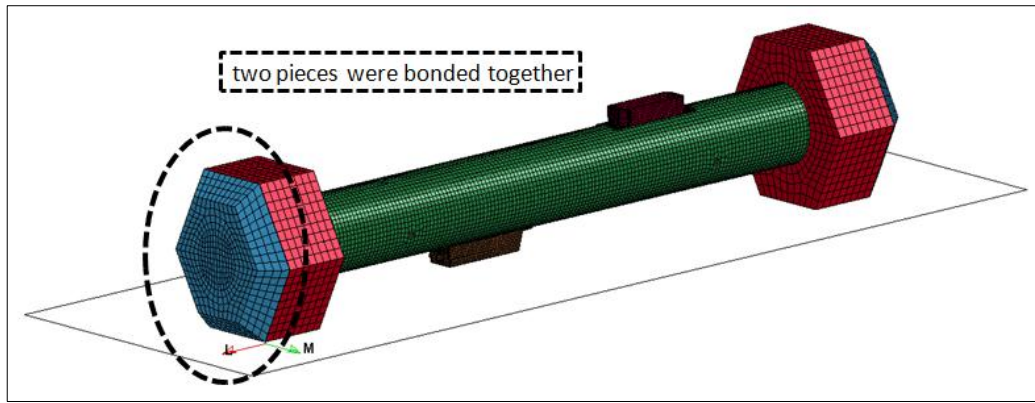
Figure 6-30 Simplification on modeling foam cushions

A base model, as shown in Figure 6-31, was developed with the same dimensions of foam cushions which were used in tests with the addition of Connector 1. Later, results of both test and FE model were discussed. No comparison of h distance is done owing to the fact that system had no Connector 1 in validation tests.
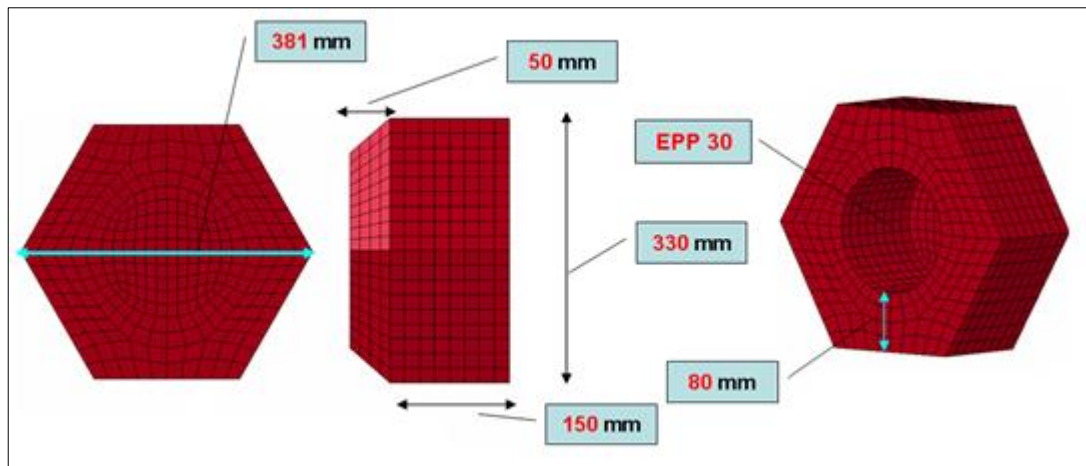

Figure 6-31 Base-model with its dimensions and material type

Table 6.8 Test and base model comparison in terms of h and acceleration

VARIATIONS	h^1 [mm]	Acceleration-COG [g]
TEST	-	35
BASE MODEL	27.5	40

h^1 =vertical displacement between Connector 1 and the ground at the time of maximum crush

127

As it can be seen in Table 6.8, peak acceleration values are close to each other with a slight deviation than can be accepted as tolerable in drop scenarios. It should also be mentioned that no comparison of accelerometers other than COG was made. Yet, only COG acceleration levels were validated during this process.
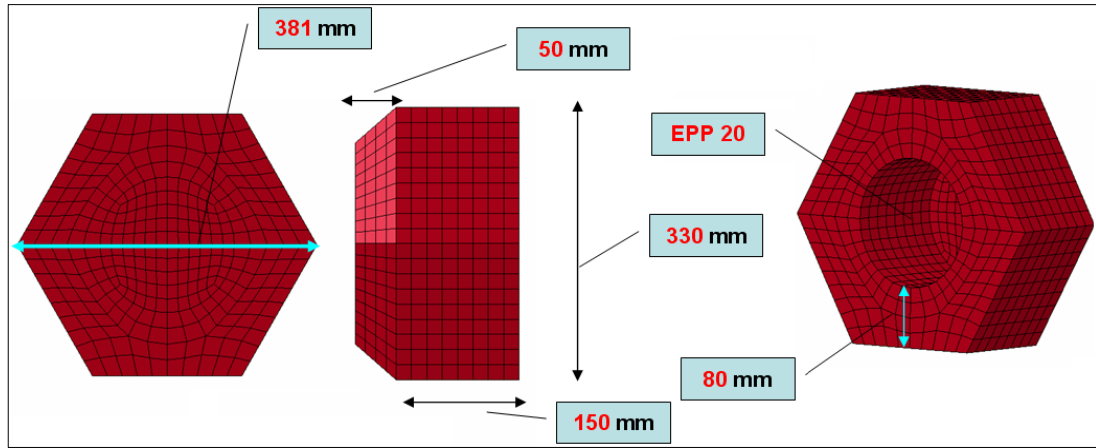

Figure 6-32 Model 1 with its dimensions and material type

As shown in Figure 6-32, only difference between the Base model and Model 1 is material density. Dimensions of the base model remained same while, density changed from 30 kg/m^3 to 20 kg/m^3.

Table 6.9 Base model and Model 1 comparison in terms of h and acceleration

VARIATIONS	h^1 [mm]	Acc-1 [g]	Acc-2 (COG)[g]	Acc-3 [g]
BASE MODEL	27.5	51	40	47
MODEL 1	22.8	37	32	42

As it is depicted in Table 6.9, "g" levels were achieved to be reduced while, bottom surface of Connector 1 approached to the ground 5 more millimeters.

Similar to Model 1, Model 2 had the same dimensions of based model as seen in Figure 6-33. One major distinction of Model 2 from previous two designs was using a combined design of Expanded Polypropylene with two different densities which are 30 kg/m^3 and 20 kg/m^3. More than 80% of the total volume of foam cushion

was formed with denser material, while 20 mm thick interior surface of the cylinder was thought to be 20 kg/m^3 EPP material.

Moreover, in contrast to the first two models, Model 2 was developed within three-piece design which was mentioned before.
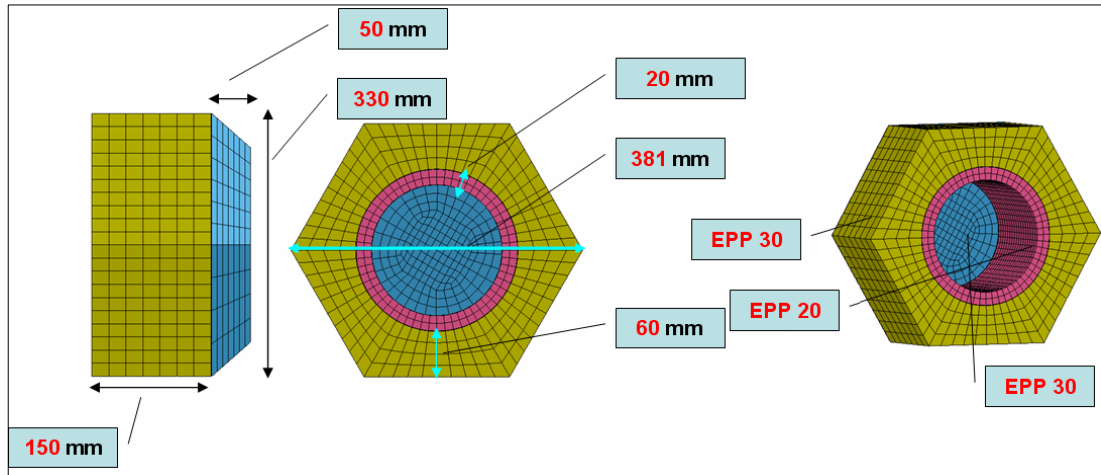

Figure 6-33 Model 2 with its dimensions and material type

According to the values in Table 6.10, not a big change was achieved in terms of acceleration by Model 2.

Table 6.10 Base model and Model 2 comparison in terms of h and acceleration

VARIATIONS	h^1 [mm]	Acc-1 [g]	Acc-2 (COG)[g]	Acc-3 [g]
BASE MODEL	27.5	51	40	47
MODEL 2	27	49	39	48

Because of the fact that not a good progress was achieved by Model 2, similar approach with a little change was repeated for Model 3 as depicted in Figure 6-34. This time, a part of the interior volume of foam cushion was formed with 45 kg/m^3 Polyethylene which is a more deformable material than EPP, while rest of the foam was 45 kg/m^3 Polypropylene.

20 mm thick PE material was expected to absorb non-ignorable amount of energy when compared to the previous model. Three-piece design of foam cushions was again applied for simplicity.
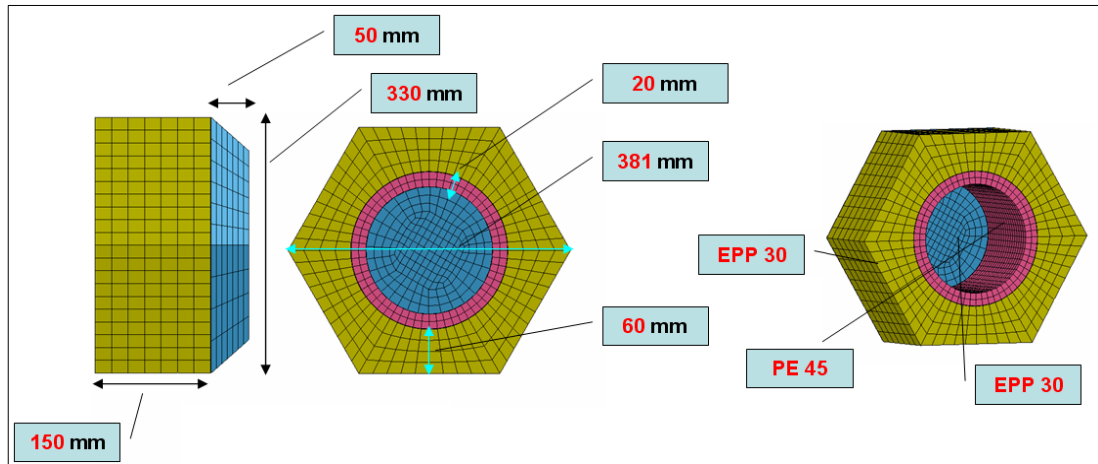

Figure 6-34 Model 3 with its dimensions and material type

As expected, a considerable reduction of load levels was accomplished by Model 3. According to Table 6.11, approximately 10 g decrease was monitored at the center of gravity of the model.

On the other hand, distance between Connector 1 and the ground were also at appropriate levels.

Table 6.11 Base model and Model 3 comparison in terms of h and acceleration

VARIATIONS	h^1 [mm]	Acc-1 [g]	Acc-2 (COG) [g]	Acc-3 [g]
BASE MODEL	27.5	51	40	47
MODEL 3	22.4	38	31	36

Model 4 is shown in Figure 6-35 and was developed with the same approximation applied to Model 3 thanks to the reduction rate of load levels seen in this model. Totally same FE model with Model 3 was utilized in Model 4 except that surrounding 30 kg/m^3 EPP was altered to 20 kg/m^3 EPP.
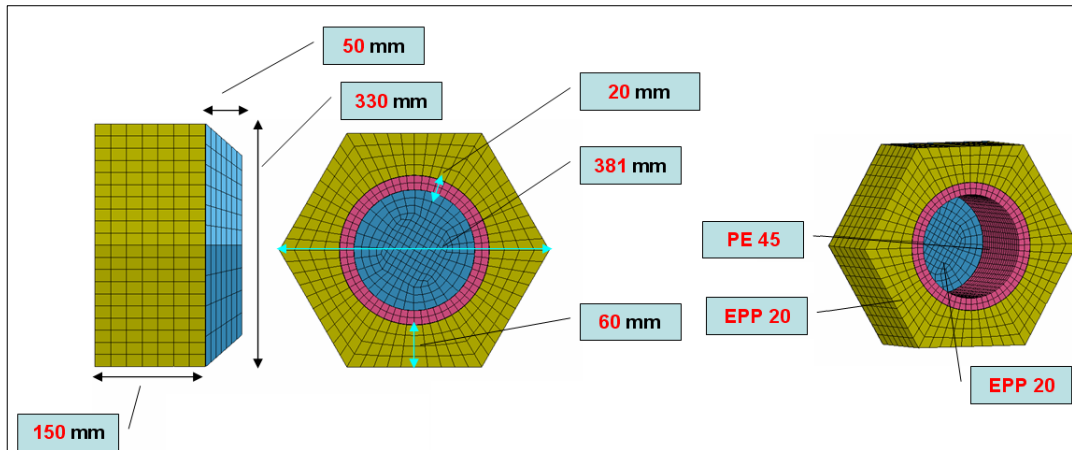
Figure 6-35 Model 4 with its dimensions and material type

Table 6.12 shows that reduction of load rates reached to remarkable values while, "h" distance was also at around 20 millimeters which is acceptable.

Table 6.12 Base model and Model 4 comparison in terms of h and acceleration

VARIATIONS	h[1] [mm]	Acc-1 [g]	Acc-2 (COG)[g]	Acc-3 [g]
BASE MODEL	*27.5*	*51*	*40*	*47*
MODEL 4	*18,7*	*33*	*27*	*33*

Starting from Model 5, dimension changes were also applied to the models. Thickness of the foam cushions in axial direction was reduced from 150 mm to 120 mm, while this was from 381 mm to 358 mm in radial direction. As it is shown in Figure 6-36, foam cushions were formed only by 20 kg/m^3 EPP. Similar to the most of the previous models, three-piece design was preferred.
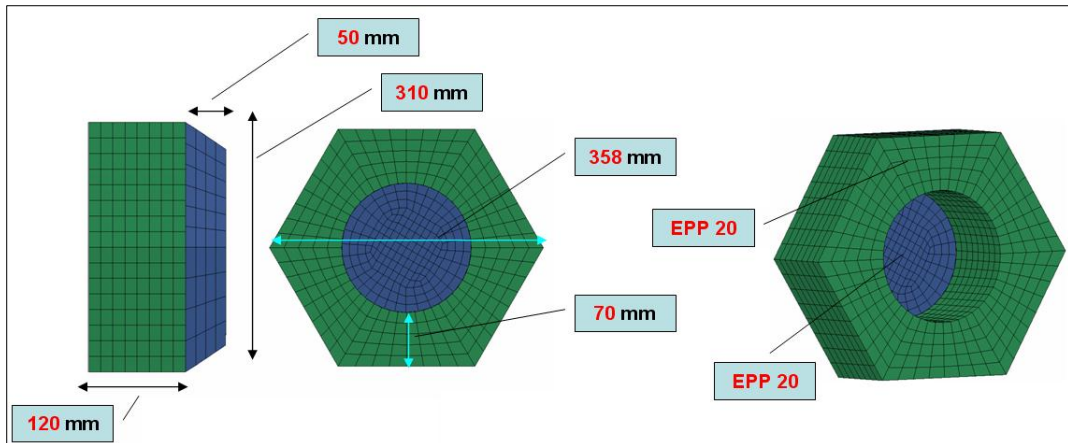
131

Figure 6-36 Model 5 with its dimensions and material type

As it is depicted in Table 6.13, pretty low acceleration values were reached by Model 5 as it is achieved by Model 4. However, bottom surface of Connector 1 was approached to the ground much more than previous models. Only 10 mm separates these two surfaces from each other.

Table 6.13 Base model and Model 5 comparison in terms of h and acceleration

VARIATIONS	h^1 [mm]	Acc-1 [g]	Acc-2 (COG)[g]	Acc-3 [g]
BASE MODEL	27.5	51	40	47
MODEL 5	9.8	32	28	39

In Model 6, both combination of materials and dimension changes were applied to obtain better results. Thickness of the foam cushions in axial direction was reduced from 150 mm to 120 mm, while tapered section of it was reduced from 50 mm to approximately 29.5 mm by remaining taper angle the same. Radial change in foam cushions was the same with Model 5, from 381 mm to 358 mm.

Furthermore, 25 mm thick interior cylindrical surface of the foam was formed by 65 kg/m^3 PE, while 20 kg/m^3 EPP was used for the rest of the foam cushion.

As it is easily depicted in Figure 6-37, a finer mesh is applied to the model. This was an obligation to be done because of the excessive distortion of the foam elements.

Thanks to the mesh sensitivity study performed at the very beginning of this chapter, it is possible to say that not a remarkable effect on energy absorption will be expected.
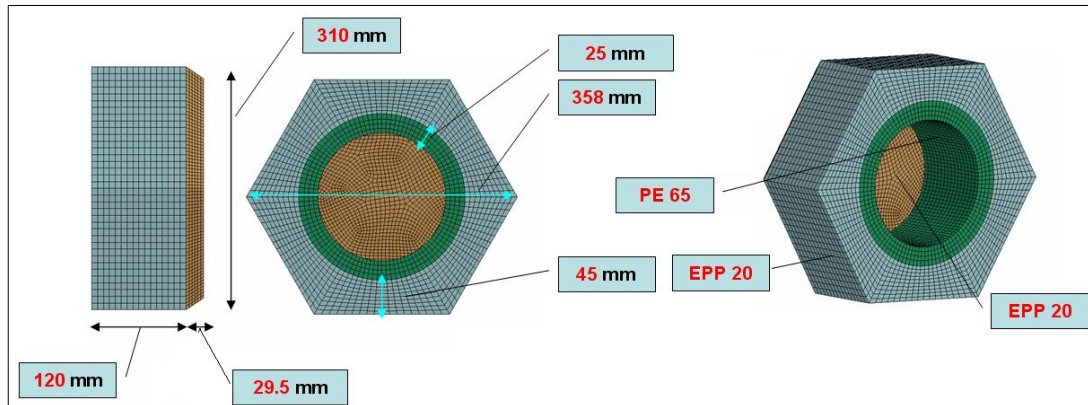

Figure 6-37 Model 6 with its dimensions and material types

Up to now, the lowest values of acceleration responses was achieved by Model 6 whereas, the lowest values of h distance was also seen in the same model.

Table 6.14 Base model and Model 6 comparison in terms of h and acceleration

VARIATIONS	h^1 [mm]	Acc-1 [g]	Acc-2 (COG)[g]	Acc-3 [g]
BASE MODEL	27.5	51	40	47
MODEL 6	4.3	28	23	35

Considering the results of Model 6 shown in Table 6.14, distance, "h", needs to be increased. Usage of either a denser material for the interior section of the foam or a lighter material for the surrounding section of the foam could have helped to manage this. By picking the second alternative, 30 kg/m^3 EPP instead of 20 kg/m^3 one were selected for the surrounding part of the foam in Model 7 as shown in Figure 6-38.
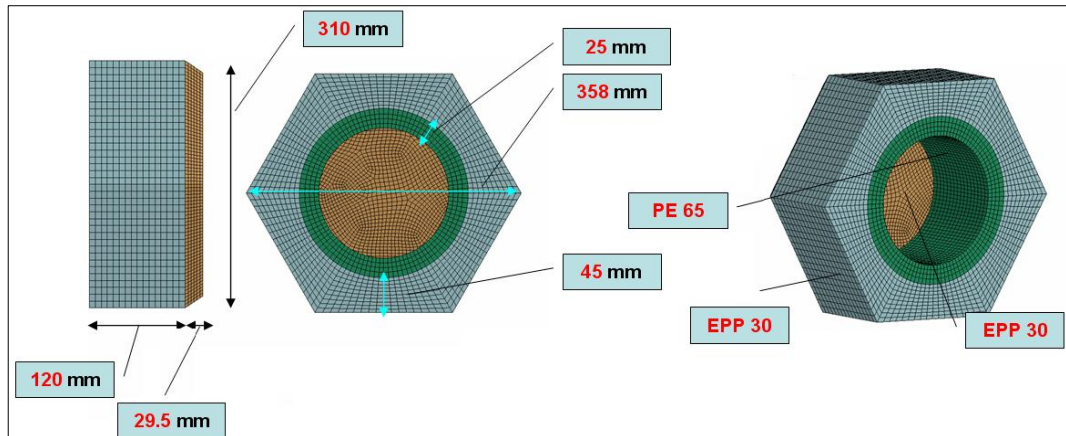
Figure 6-38 Model 7 with its dimensions and material types

As shown in Table 6.15, increase in `h` distance is achieved, while g levels were again reached to critical levels.

Table 6.15 Base model and Model 7 comparison in terms of h and acceleration

VARIATIONS	h^1 [mm]	Acc-1 [g]	Acc-2 (COG)[g]	Acc-3 [g]
BASE MODEL	27.5	51	40	47
MODEL 7	10.6	40	29	42

By considering the first alternative mentioned in Model 7, interior section of the foam cushion were developed within 45 kg/m^3 PE instead of 65kg/m^3 PE as depicted in Figure 6-39.

Other than above mentioned material change, no dimension altering will be applied to the model.

According to the values take part in Table 6.16, it is easy to say that Model 8 cannot be presented as an option as a result of optimization studies owing to the closeness of the Connector 1 to the ground.
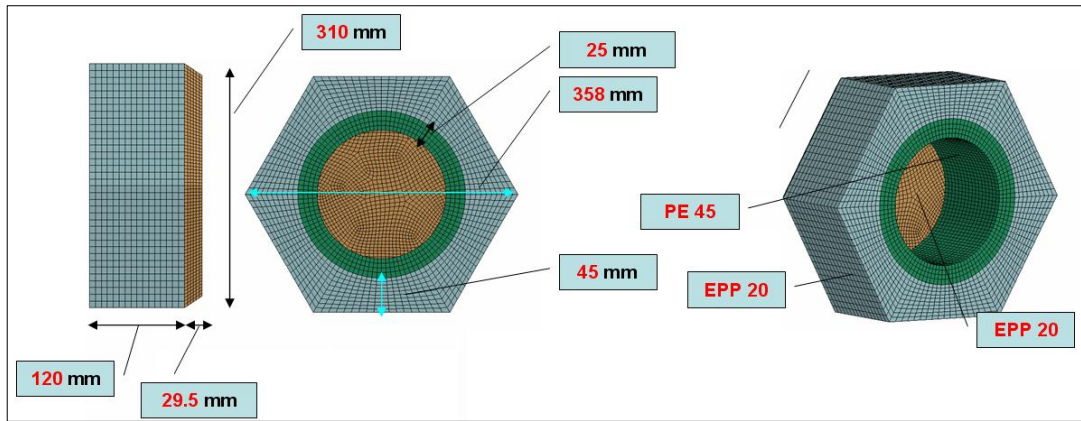
Figure 6-39 Model 8 with its dimensions and material types

Table 6.16 Base model and Model 8 comparison in terms of h and acceleration

VARIATIONS	h^1[mm]	Acc-1 [g]	Acc-2 (COG)[g]	Acc-3 [g]
BASE MODEL	27.5	51	40	47
MODEL 8	2.8	42	21	30

Thickness of the foam cushions in axial direction was reduced from 150 mm to 120 mm, while tapered section remained the same. In radial direction this change is from 381 mm to 340 mm. As it is shown in Figure 6-40, foam cushions were formed only by 20 kg/m³ EPP.

In Table 6.17, it was shown that not a remarkable reduction was observed in terms of acceleration levels. Moreover, Connector 1 was reached to the closest distance to the ground too. Only 2 millimeters separates Connector 1 from the ground. In case of a possible contact within the ground would have increased the load levels up to critical values. That is why Model 9 was elected with these dimensions and material type from the alternatives.
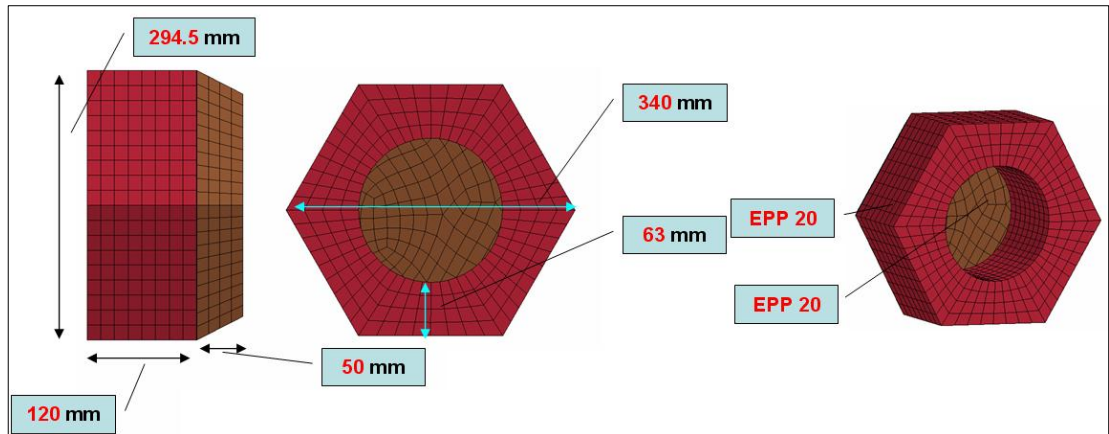
Figure 6-40 Model 9 with its dimensions and material types

Table 6.17 Base model and Model 9 comparison in terms of h and acceleration

VARIATIONS	h[1] [mm]	Acc-1 [g]	Acc-2 (COG)[g]	Acc-3 [g]
BASE MODEL	27.5	51	40	47
MODEL 9	2.2	32	29	40

Model 10 was developed with the same dimensions of Model 9. In other words, similar reductions in axial and radial directions were applied to the Model 10. As seen in Figure 6-41, a two-piece design of EPP30 foam cushions was again selected for simplicity.

In Table 6.18, peak acceleration values were seen at the center of gravity and at three different accelerometer locations. Neither a remarkable decrease in terms of acceleration nor a notable increase in distance, "h", was observed when compared to Model 9.
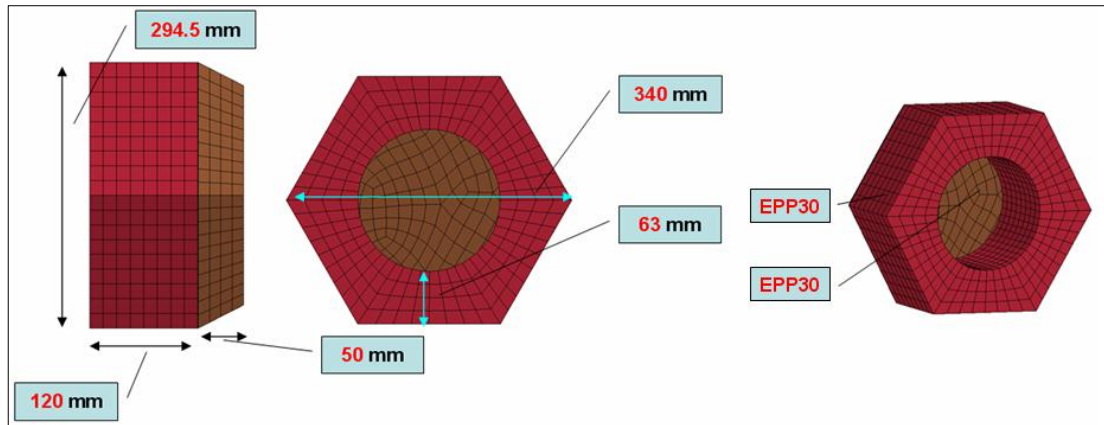
Figure 6-41 Model 10 with its dimensions and material types

Table 6.18 Base model and Model 10 comparison in terms of h and acceleration

VARIATIONS	h^1 [mm]	Acc-1 [g]	Acc-2 (COG)[g]	Acc-3 [g]
BASE MODEL	27.5	51	40	47
MODEL 10	7,2	44	36	44

Apart from the 10 models, some other alternative designs were also developed as seen in Figure 6-42. Some of them were also reached notable results in terms of acceleration responses. However, a common pitfall about these designs was the potential manufacturing difficulties. Moreover, the jeopardy of the usage of these designs can also be another drawback that should not be underestimated. A summary of these designs is given in Table 6.19.

Table 6.19 Summary of the alternative models in terms of h and acceleration

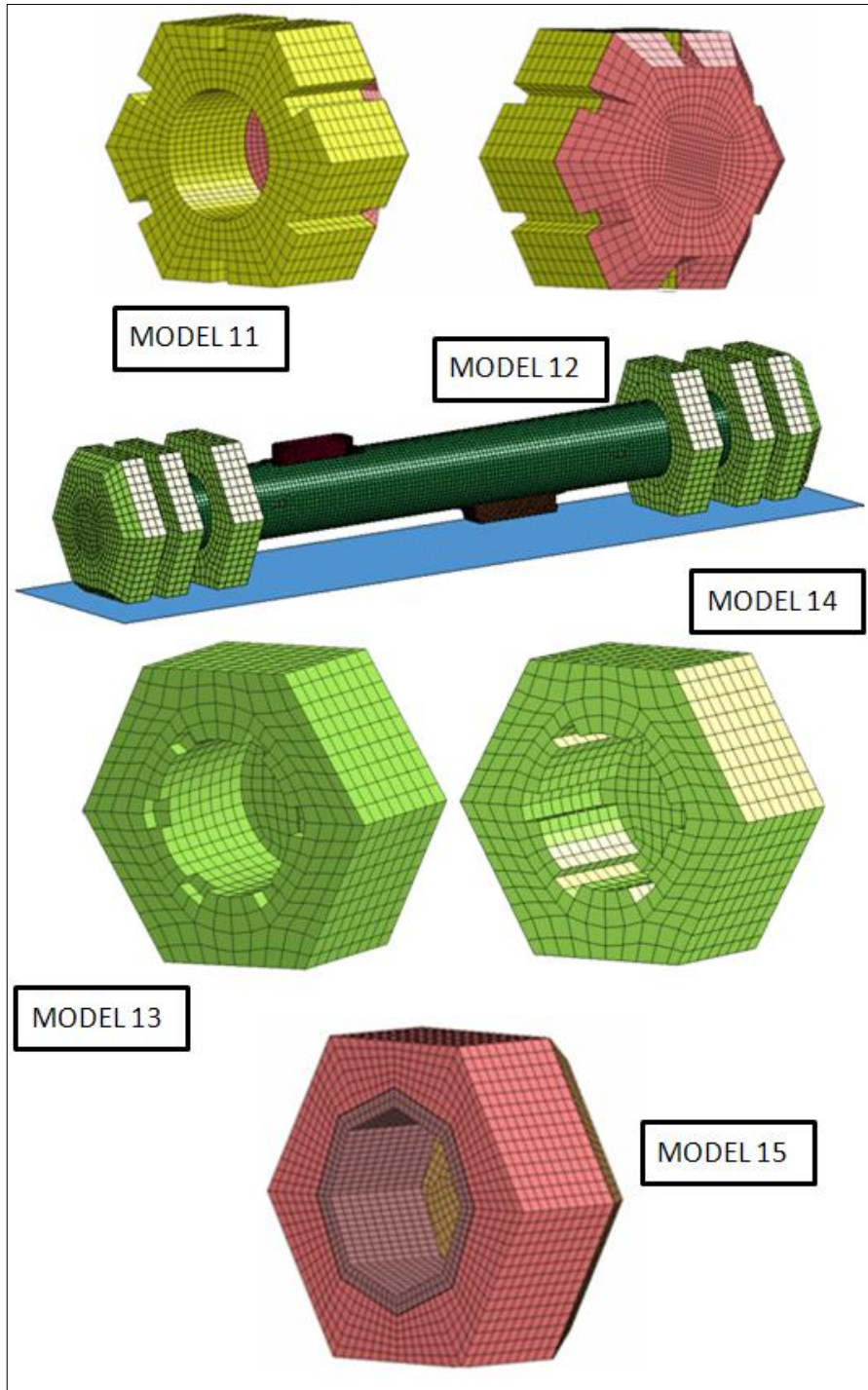| VARIATIONS	h^1 [mm]	Acc-1 [g]	Acc-2 (COG)[g]	Acc-3 [g]
BASE MODEL	27.5	51	40	47
MODEL 11	26	38	35	44
MODEL 12	7	52	45	56
MODEL 13	6	47	41	49
MODEL 14	5	46	40	48
MODEL 15	10	33	25	35

Figure 6-42 Alternative designs

According to summary of the results given in Table 6.20, some models may be seemed problematic in terms of h distance. In other words, vertical displacement between Connector 1 and the ground have been reached to critical values which is

not desirable. Model 6, Model 8 and Model 9 were elected considering the threat they may have cause to in case of a drop scenario.

Although h distance is not challenging for some models which are Model 2, Model 3, Model 7 and Model 10, g levels of these designs were not satisfactory.

Table 6.20 Summary of results of the ten models in terms of h and acceleration

VARIATIONS	h[1] [mm]	Peak acceleration [g]			
		Acc-1	Acc-2	Acc-3	Acc-COG
Base Model	27,5	51	40	47	40
Model_1	22,8	37	32	42	32
Model_2	27	49	39	48	39
Model_3	22,4	38	31	36	31
Model_4	18,7	33	27	33	27
Model_5	9,8	32	28	39	28
Model_6	4,3	28	23	35	23
Model_7	10,6	40	29	42	29
Model_8	2,8	42	21	30	21
Model_9	2,2	32	29	40	29
Model_10	7,2	36	44	36	44

---

[1] vertical displacement between Connector 1 and the ground at the time of maximum crush
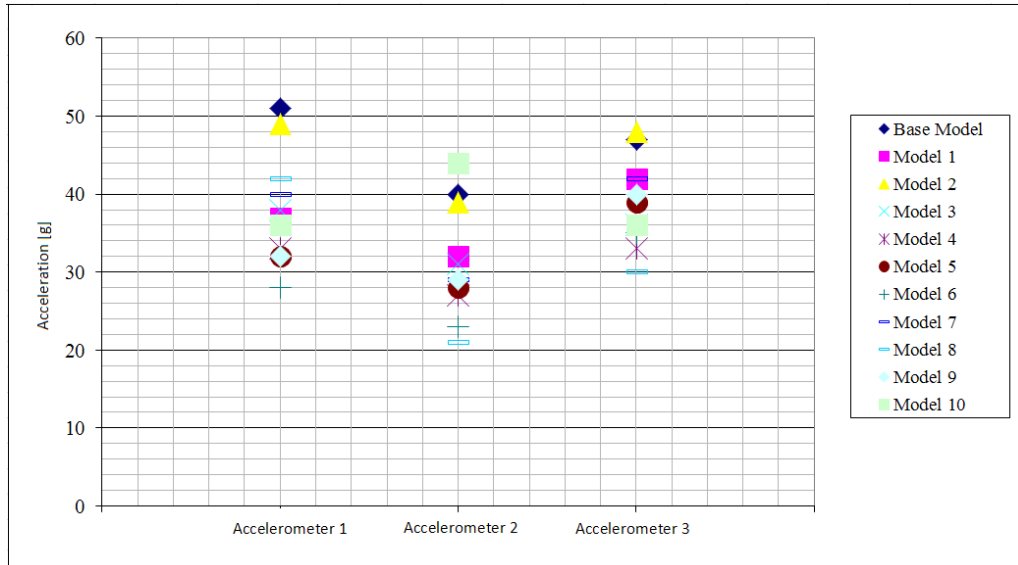
Figure 6-43 Comparison of results of the ten models in terms of acceleration

Peak acceleration values of ten distinct models and base model are compared in Figure 6-43. In addition to acceleration values, vertical displacements between Connector 1 and the ground at the time of maximum crush is also compared in Figure 6-44. It is depicted in Figure 6-44 that all ten models achieved reducing the levels of displacement when compared to Base model.
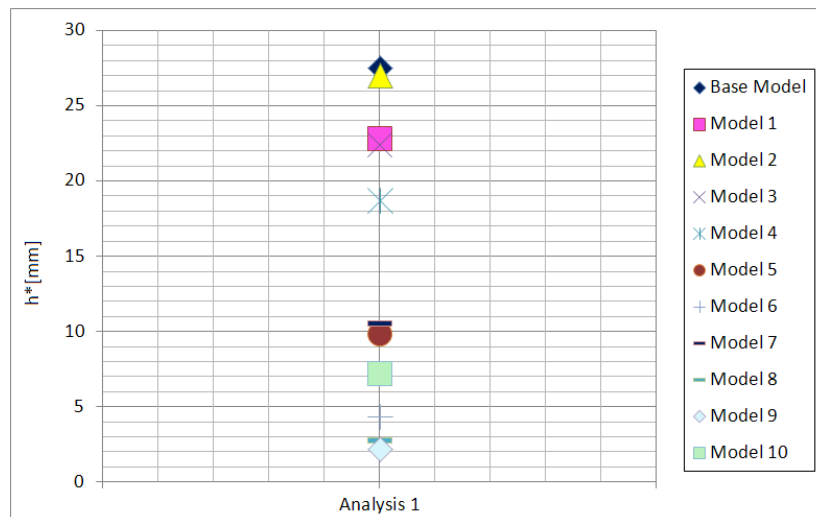
Figure 6-44 Comparison of results of the ten models in terms of h^1

As it can be inferred from Table 6.20 and Figure 6-43, only three designs which are shown in Figure 6-45 may fulfill the expectations. In Figure 6-45, referred dimension is belongs to the base model.
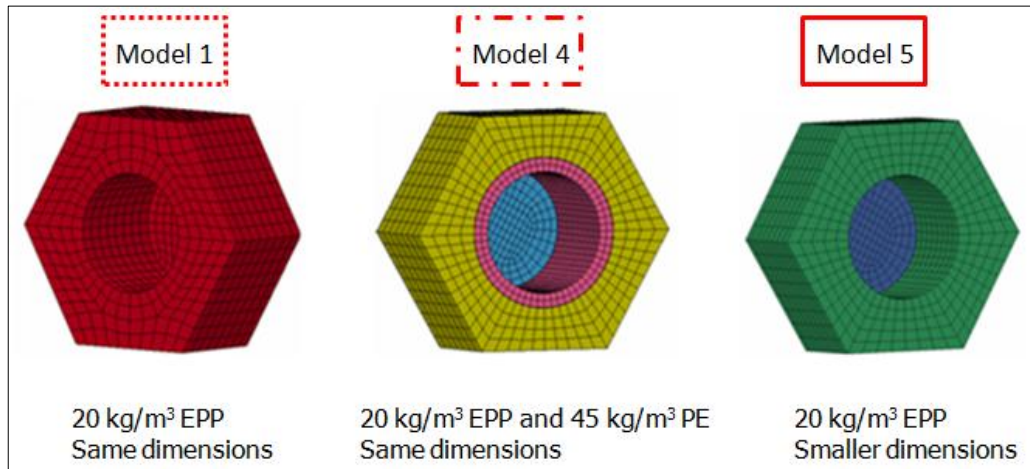
Figure 6-45 Best 3 models out of 10 distinct designs

Table 6.21 Best 3 models out of 10 different models

VARIATIONS	h^1 [mm]	Peak acceleration [g]			
		Acc-1	Acc-2	Acc-3	Acc-COG
Base Model	27,5	51	40	47	40
Model_1	22,8	37	32	42	32
Model_4	18,7	33	27	33	27
Model_5	9,8	32	28	39	28

Peak acceleration values of the best 3 options and the vertical displacement between Connector 1 and the ground at the time of maximum crush is given in Table 6.21.

Considering all the three models which are the best options of optimization process, Model 4 seems to be the best alternative. However, selected design consists of two distinct polymeric foams which are Expanded Polypropylene and Polyethylene as seen in Figure 6-45. Combination of these two materials may cause troubles when

their gluing was thought. In other words, gluing of these two polymeric materials can be problematic.

Bearing in mind that jeopardy, Model 4 would not also be a perfect choice. From the last two alternatives, Model 1 and Model 5, lower g levels were reached by Model 5. In addition, h distance was also not seemed to be troublesome. However, manufacturing of Model 5 seemed to be luxurious compared to the fabrication of Model 1. Yet, Model 1 has the same dimensions of the model which was used in validation tests. Tendency shifted from Model 5 to Model 1 thanks to the potential usage of the same mold utilized in the tests. It should be noted that only difference between these two designs was the geometrical dimensions.

In the light of above mentioned factors, h and g levels were evaluated again. Finally, Model 1 is preferred over Model 5. In Figure 6-46, final decision is shown with its dimensions and material type.
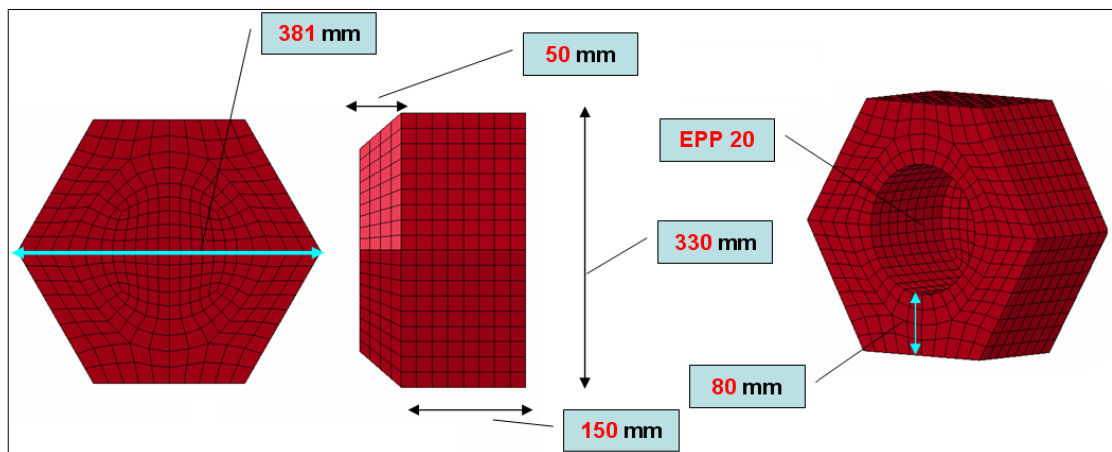
Figure 6-46 Final model dimensions and material type

CHAPTER 7

FINAL TEST RESULTS

7.1 FINAL TESTS

Final drop tests which are using optimized shaped foam cushions will be summarized here. Difficulties met at validation process were not repeated because of the experience gained during these tests. The 500-g *PCB 356B21* three axis accelerometers were preferred. Besides, system has dropped onto a concrete ground on which a white cover sheet is placed. By means of this strategy, better pictures were tried to be taken by high speed camera. Figure 7-1 shows the scenario of the final tests which repeated ten times to get more consistent results.
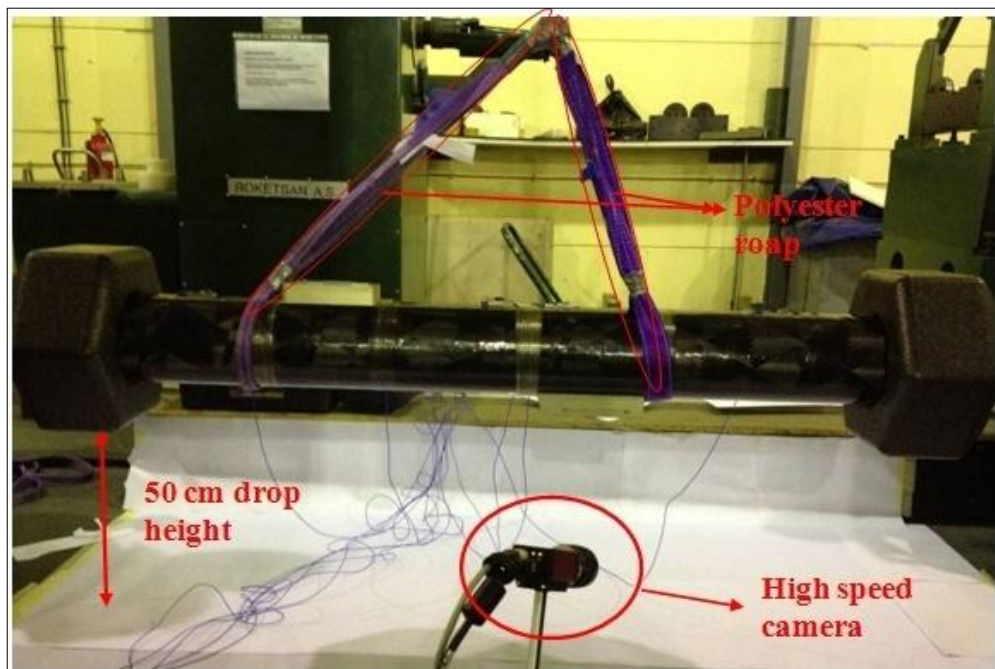
Figure 7-1 Final drop test view with optimized foam cushions

Prior to final tests, the missile and launching tube interaction has been changed. Previous scenario had 8 bolts as previously mentioned to hold the missile tube and the launching tube together. Instead, only one pin was used for this mission in final tests.

This change forced the FE analysis model to update too. For this reason Figure 7-2 is developed.
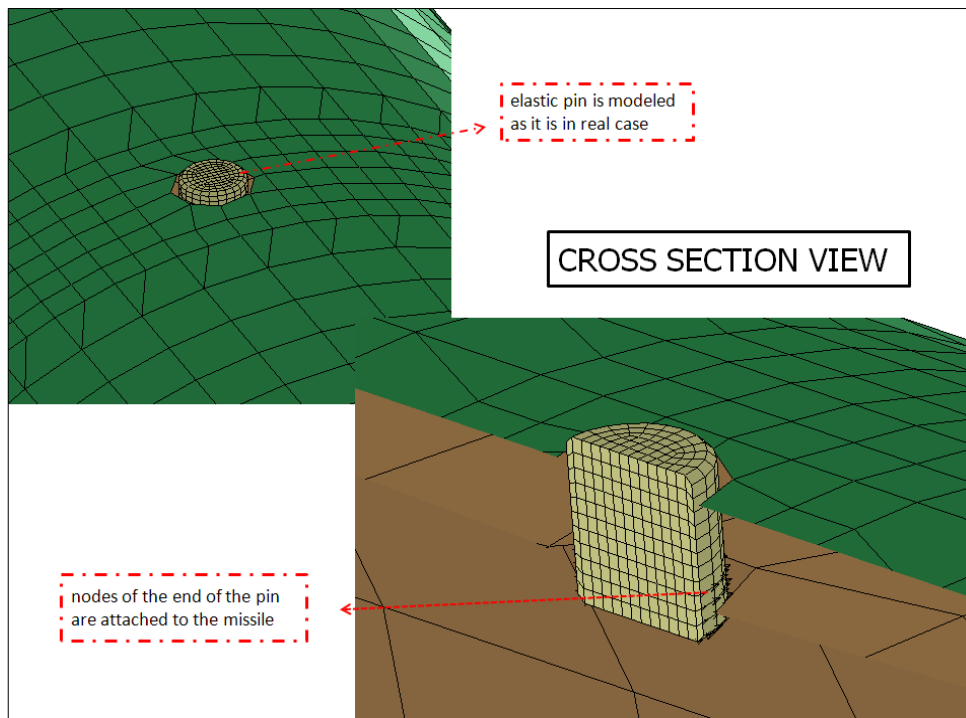
Figure 7-2 Updated connection of the missile and launching tube connection
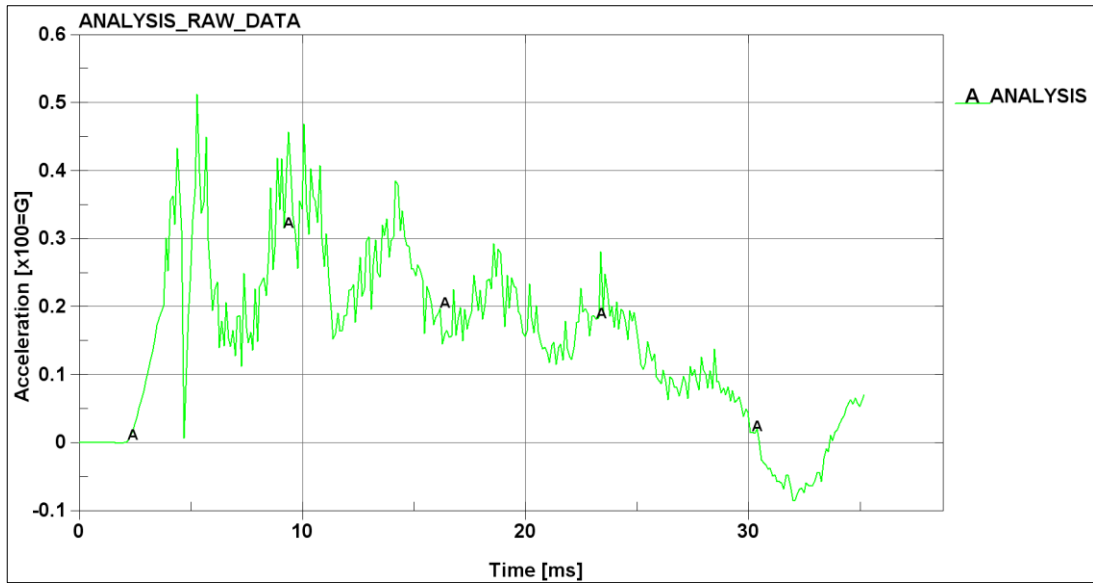
Figure 7-3 Acceleration vs. time response of the missile at COG

Figure 7-3 is obtained from the numerical simulations. According to Figure 7-3, a more oscillated data is reached when compared to Figure 6-24, which is the raw data of the validation analysis. Fundamental reason of this fluctuation is possibly due to the interaction of the launching tube and the missile. In the validation process, the missile and the launching tube were connected to each other within 8 bolts, while just one but thicker pin has this mission in final configuration.
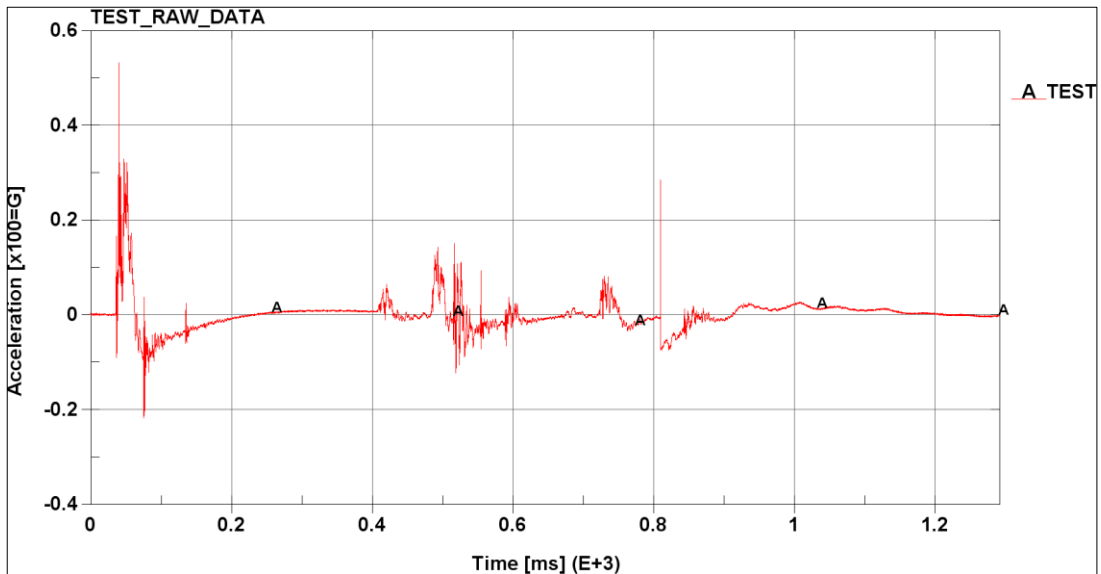
Figure 7-4 Acceleration vs. time response at the COG of the missile (Raw data)

Drop tests are repeated for 5 times. Similar behaviors are observed during all five tests in terms of acceleration responses. Figure 7-4 is given for the representation of five tests. However, results of all five tests with filtered versions are given in APPENDIX A.

Another important comment on final tests is that sudden peaks that seen in the raw data are relatively low when compared to the validation tests. It is thought that accelerometer connection to the missile cannot cause to such a difference. Because such peaks are depicted in both glued and bolted versions. Connection of the missile and the tube is the major change that is seen in final tests. For this reason, It is thought that connection of the missile and the tube has the most notable effect on aforementioned peaks.
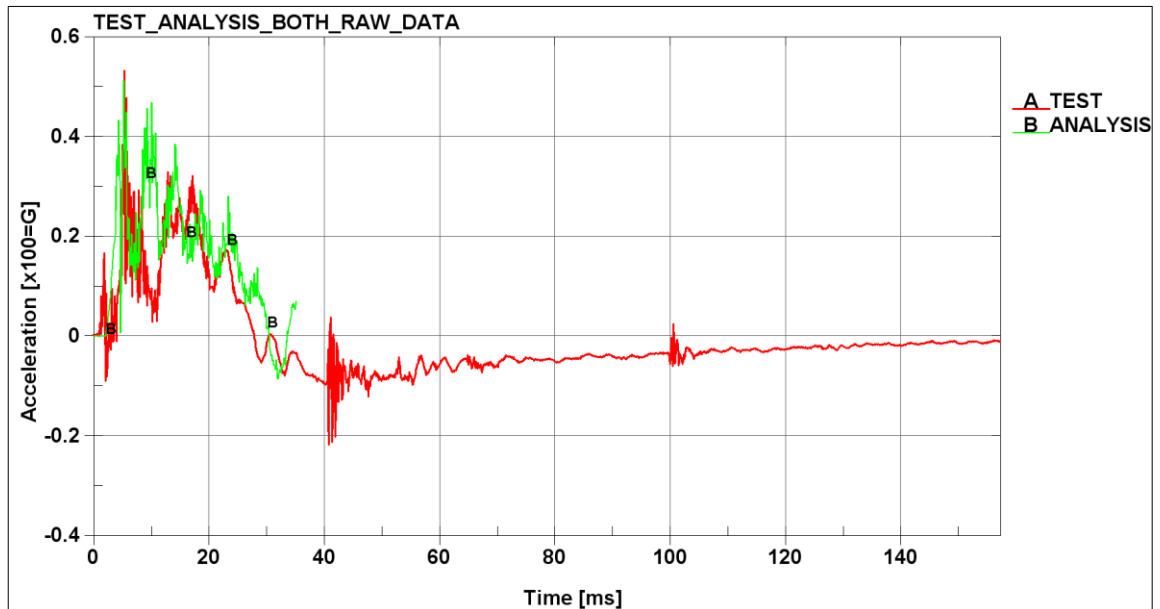
Figure 7-5 Comparison of raw data of both final test and analysis at COG

Both test and analysis raw data were overlaid to monitor whether the tendency of these two curves are similar to each other or not. Figure 7-5 shows that an outstanding match is reached between test and analysis raw data.

146
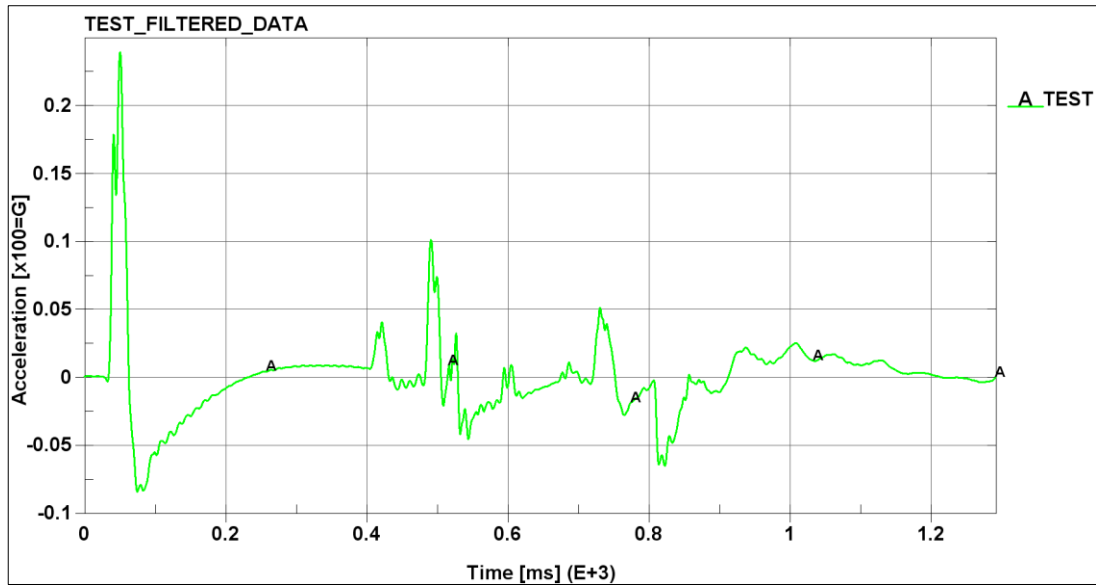
Figure 7-6 Acceleration vs. time response of the missile (108 Hz. Filtered data)

Raw and filtered data measured at the center of gravity of the missile were shown in Figure 7-4 and Figure 7-6. Approximately 40-g values were reduced to the levels of 25-g's after getting rid of the noise that takes part in the system. This is succeeded in by filtering action. The cut-off frequency value (108 Hz.) is selected considering the ESD method. The method used for filtering and the ESD of the signal is given in Figure 7-7.

10 % of total ESD energy is determined as a limitation point so that signal data which has lower energy than this limit is necessary to be filtered. In order to monitor the deviation of filtered data, 5 % and 15 % of total ESD energy are also examined in the context of the thesis. Detailed explanation of such a comparison is given in APPENDIX C.
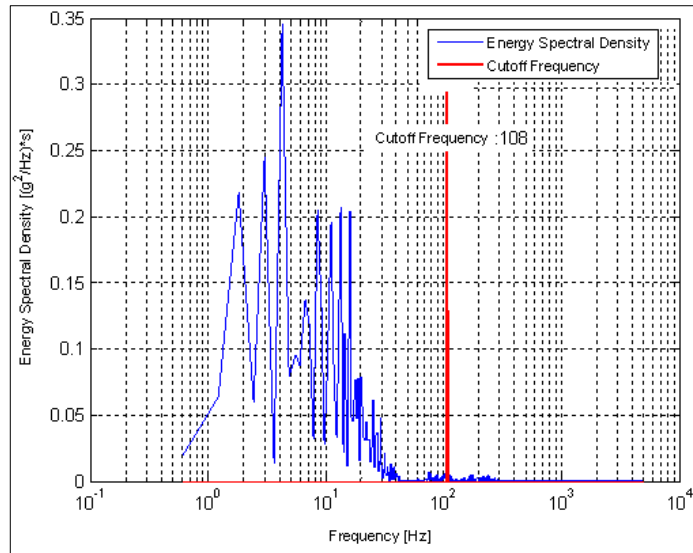
Figure 7-7 ESD-frequency response of the data at 50 cm final drop test

In Figure 7-8, acceleration-time history of 50 cm final drop tests is depicted. As previously explained, acceleration data is measured from the center of the gravity of the models with the addition of optimized shaped foam cushions.

As also seen in validation results, more oscillated curve of test results have been reached. Fluctuation of the curve of simulation is not as much as the curve of test. In addition to the closeness of the peak values of these two curves, quite similar trends of them proved that study accomplished in success.
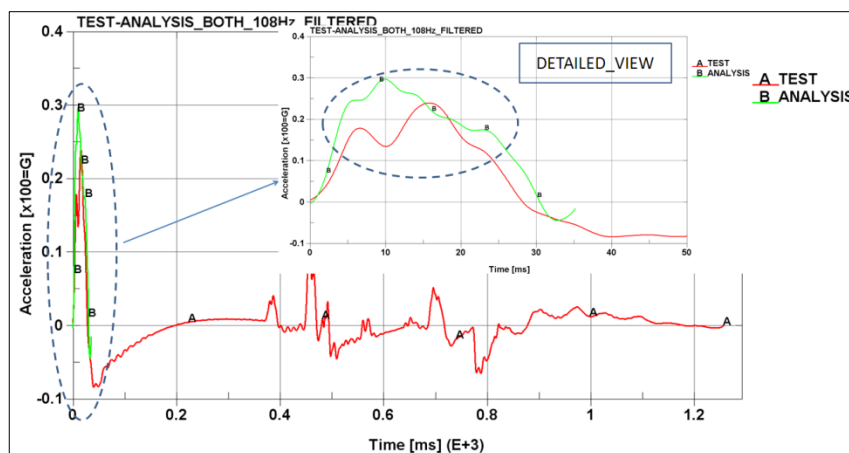
Figure 7-8 Final drop tests of munition with optimized foam cushions

CHAPTER 8

CONCLUSION

Material characterization process is the opening section of the study. Prior to this process, research was performed in order to gain the sufficient information to make characterization study to start. Characterization tests were performed by quasi-static compression test and drop tower test mechanism at distinct strain rates for various densities regarding the polymeric characterization standards. Results of these tests were used as input parameters for numerical validation of material models. LS-DYNA, was utilized for numerical studies during the study.

Minimizing the load levels that are encountered by drop cases was the major task of the thesis. In order to model drop case scenarios in FE codes, material modeling capabilities of the code should be robust enough. Besides, this capability is directly affected by the usage of material characterization results. For this reason, possessing relevant material properties have a remarkable influence on the results of simulations.

Determining initial geometry of the foam was also a critical step to go on further tasks. Therefore, similar systems were investigated to have an idea about the geometric shape of the foam caps. Cylindrical and rectangular shaped designs were eliminated due to the drawbacks of these models. Hexagonal shaped foam caps were determined to be the best option for the protection of munitions.

After the integration of foam caps into the system, drop tests of munitions were ready to be conducted. During tests, problems were encountered due to the lack of experience on this topic. Accelerometer selection, data acquisition technique and

difficulties of arranging parallel drop scenario were challenging tasks. However, drop tests were completed well after more than a few trials. Acceleration responses of the munition were recorded during tests in order to validate the same scenario in numerical approach.

This transition, from experimental approach to numerical one, was possibly the most significant section of the thesis. Yet, the rest of the study was continued in simulation based works till the final tests. Validation of the drop tests of munition with the initial foam caps began with finite element modeling of the components of the system. Throughout this process, all sub-segments of the model were developed obeying the general rules of finite element modeling. Special care was taken particularly for the foam modeling which is the hardest part of the thesis. This is mainly because of the high deformable characteristics of foam materials. Apart from the mesh sensitivity study, different element types were also investigated during validation process. Finally, a close match of acceleration-time curves was reached between test and analysis.

Parametric study on foam geometry started with the completion of the validation of drop tests. Geometric parameters of initial foam geometry, as well as different types of foam materials having different densities were two principal parameters to minimize the acceleration level and to control distance between the ground and the connector. For this purpose, ten different models that possess various changes were developed. Apart from above mentioned ten models, some other alternative designs having some downsides were developed too. Manufacturing difficulties and probable usage problems prevented these alternatives from being a final alternative. Out of ten candidates, the best 3 models were selected to be the final model. However, two out of best three models were elected considering the cost effects and manufacturing troubles.

Final selected model is then again validated by final tests. As previously declared in Chapter 7, final tests had some changes when compared to previous ones. However, by applying these changes to the final model, it has been seen that a brilliant match between tests and simulations were reached.

Eventually, conclusions of the thesis can be listed as follows:

- Experimental method is a trustworthy but costly process for drop scenarios. Furthermore, the time consumed for conducting experimental tests is also much more than numerical method.

- Here, crucial point is the accuracy of the numerical analysis. With correct assumptions and experience, it is possible to reach similar results with experimental tests.

- Material properties are the major factor on the reliability of the results of numerical simulations. For this reason, the more reliable material data the analyst has, the better results are reached.

- Material modeling is another critical point of the thesis. Appropriate material models representing the exact behaviors of materials should be selected as it is achieved in this thesis. Otherwise, accuracy of the results will not be satisfactory.

- Apart from material modeling, simplifications and assumptions made in the numerical model have also significant effects on the results. Here, experience has a big role on the correct modeling of the scenario.

- With this study, it is shown that iterative numeric simulations can replace with experimental tests. Hence, cost expenditure cane be decreased and less time is consumed.

- Main goal of the thesis which is lowering the effects of drop scenario on munitions is achieved. Appropriate foam geometry is determined considering the manufacturing and cost effects.

REFERENCES

[1] Gibson, L.J., Ashby, M.F., *Cellular solids, Structures and Properties*, Cambridge, Cambridge University Press, 1997.

[2] Dalia, A.T., *Foam modeling and application to sabot impact*, M.Sc. in Structures, Crashworthiness and Impact, Cranfield University, School of Engineering, 2007.

[3] Quellet S., Cronin D., Worswick D., *Compressive response of polymeric foams under quasi-static, medium and high strain rate conditions*, Polymer Testing 25, pp. 731–743, 2006.

[4] *Polyform*, http://polyform.com/pages.php?page=fabrication_process, last visited June 2012.

[5] Droste, A., Rottger. J, *Crash Performance Increase with Structural BETAFOAM*, Dow Automotive, 6th LS-DYNA Anwenderforum, Frankenthal, 2007.

[6] Campbell, B.M., *A Numerical Side Impact Model to Investigate Thoraric Injury in Lateral Impact Scenarios*, M.Sc. Thesis, University of Waterloo, Canada, 2009.

[7] Reid J.D., Faller R., Holloway J., Rohde J. and Sicking D., *New Energy-Absorbing High-Speed Safety Barrier,* Transportation Research Record 1851, National Research Council, pp. 53-64, 2003.

[8] Neumayer, D., Chatiri, M., and Höermann, M., *Drop test simulation of a cooker including foam packaging and pre-stressed plastic foil wrapping,* 24th CADFEM Users Conference, Stuttgart, Germany, October 25-27, 2006.

[9] Mills, N.J., Masso-Moreu Y., *Finite Element Analysis Finite Element Analysis (FEA) Applied to Polyethylene Foam Cushions in Package Drop Tests*, Packaging Technology and Science, Vol. 18, No. 1., pp. 29-38, January 2005.

[10] Jackson, K.E., Fasanella, E.L., *Development of an LS-DYNA Model of an ATR42-300 Aircraft for Crash Simulation*, 8th International LS-DYNA Users' Conference, Dearborn, Michigan, May 2-4, 2004.

[11] Jackson, K.E., Fasanella, E.L., *Crash Simulation of a Vertical Drop Test of a B737 Fuselage Section with Overhead Bins and Luggage*, Proceedings of the Third Triennial Aircraft Fire and Cabin Safety Conference, Atlantic City, NJ, October 22-25, 2001.

[12] Fasanella, E.L., Jackson, K.E., *Best Practices for Crash Modeling and Simulation*, Technical Report NASA/TM-2002-211944, Langley Research Center, Hampton, VA 2002.

[13] Ayyıldız, A., *Buzdolabı düşürme testinin sonlu elemanlar metodu yardımıyla nonlinear analizi ve deney sonuçlarıyla karşılaştırılması*, M.Sc. Thesis, Ege University, 2006.

[14] Wang, Y.Y., Lu, C., Li, J., Tan, X.M., Tse, Y.C., *Simulation of Drop Impact Reliability for Electronic Devices*, Finite Elements in Analysis and Design 41, pp. 667-680, Elsevier, 2005.

[15] Posch W., Sageder A., *Borealis Polypropylene Helping to Shape the Future of White Good Industry,* BIAS, 2002.

[16] Wang, H.L., Chen, S.C., Huang, L.T., and Wang. Y.C., *Simulation and Verification of the Drop Test of 3C Products*, 8th International LS-DYNA Users Conference, Dearborn, Michigan, May. 2-4, 2004.

[17] Schwer, L.E., Kennedy, J.M., *A Validation Case Study: Steel Billet Drop Tests and Simulations as Reported in NUREG/CR-6608*, 6th International LS-DYNA Conference, Dearborn, Michigan, April 9-11, 2000.

[18] Hsu, H., Hsian, B., *Applications of LS-DYNA in Electronic Products*, 7th International LS-DYNA Users Conference, South Michigan, 2004.

[19] Low K.H., Yang A., Hoon K.H., Zhang X., Lim J.K.T., Lim K.L., *Initial study on the drop-impact behavior of mini Hi-Fi audio products*, Advances in Engineering Software 32, pp. 683-693, 2001.

[20] Minnicino, M., *XM982 155-mm Artillery Projectile Container Support System, Finite Element Model Development and Analysis*, ARL-TR-3619, September 2005.

[21] Kellas, S., *Quasi-Uniform High Speed Foam Crush Testing Using a Guided Drop Mass Impact*, NASA/CR-2004–213009, 2004.

[22] Zhang, J., Kikuchi, N., Li, V., Yee, A., and Nusholtz, G., *Constitutive modeling of polymeric foam material subjected to dynamic crash loading*, International of Impact Engineering, Volume 21, Issue 5, pp. 369, 398, May 1998.

[23] Avalle, M., Belingardi, G., Montanini, R., *Characterization of polymeric structural foams under compressive impact loading by means of energy absorption diagram*, International Journal of Impact Engineering, Volume 25, Issue 5, pp. 455-472, May 2001.

[24] Campbell, B.M., Cronin, D.S., Salisbury, C.P., *High Rate Characterization of Automotive Seat Foams*, Society of Experimental Mechanics Conference, Springfield, MA, 2007.

[25] De Vries D.V.W.M., *Characterization of polymeric foams*, Eindhoven University of Technology, July, 2009.

[26] Reid, J.D., Bielenberg, R.W., *Modeling Crushable Foam for the SAFER Racetrack Barriers*, 8th International LS-DYNA Users Conference, Dearborn, Michigan, May. 2-4, 2004.

[27] Slik,G., Vogel, G., and Chawda, V., *Material Model Validation of a High Efficient Energy Absorbing Foam*, 5[th]LS-DYNA Forum, Ulm, Germany, 2006.

[28] Burr, S.T., Vogel, G.D., *Material Model Development for Impact Analysis of Oriented Polypropylene Foam Structures*, SAE World Congress, Detroit, Michigan, March 5-8, 2001.

[29] Müllerschön, H., Dangel, A., Karajan, N., Hummel, A., Wrai, A., Wust, A., *Modeling of Plastics for Crash Simulation of Fuel Tanks,* 3rd LS-DYNA Anwenderforum, Bamberg, 2004.

[30] Hassan, J., Schuser, P., and Frederick, G., *Polyurethane Material Models for Simulating Leg-Form Impact in Explicit Transient Dynamics,* 6th International LS-DYNA Users Conference, Dearborn, MI, April 2000.

[31] Croop, B., Lobo, H., *Selecting Material Models for the Simulation of Foams in LS-DYNA*, 7th European LS-DYNA Users Conference, Salzburg, 2009.

[32] Carney, K., Melis, M., Fasanella, E.L., Lyle, K.H., Gabrys, J., *Material Modeling of Space Shuttle Leading Edge and External Tank Materials For*

Use in the Columbia Accident Investigation, 8th International LS-DYNA Users Conference, Dearborn, Michigan, May. 2-4, 2004.

[33] Mines, R.A.W., *Strain Rate effects in crushable structural foams*, Applied Mechanics and Materials Vols. 7-8, pp., 231-236, 2007.

[34] Ozturk U.E., Anlas G., *Finite Element Analysis of expanded polystyrene foam under multiple compressive loading and unloading*, Materials and Design 32, pp. 733-780, 2011.

[35] ASTM D1621, *Standard Test Method for Compressive Properties Of Rigid Cellular Plastics,* United States of America, 2000.

[36] Walter P.L., *Selecting Accelerometers for and Assessing Data from Mechanical Shock Measurements,* Technical Note, 2008.

[37] Aszkler C., *Acceleration, Shock and Vibration Sensors,* PCB. Piezoelectronics, Inc.

[38] Data Processing Vehicle Safety Workgroup, *Crash Analysis Criteria Description Version 1.6.2.*,2005.

[39] Yahoo Groups, *http://tech.groups.yahoo.com/group/LSDYNA/message/9409*, last visited September 2012.

[40] Yahoo Groups, *http://tech.groups.yahoo.com/group/LSDYNA/message/27191*, last visited September 2012.

[41] MIL-STD-810F, *Environmental Engineering Considerations and Laboratory Tests*, Department of Defense, United States of America, January 2001.

[42] Graf, T., *Advanced FEM Analysis with LS-DYNA-Theoretical Basics*, Dynamore GmbH, 2009.

[43] Hallquist, J.O., *LS-DYNA Keyword User's Manual*, Version 971, Livermore Software and Technology Corporation, Livermore CA, May 2007.

[44] Serifi, E., Hirth, A., Matthaei, S., Müllerschön, H., *Modeling of Foams using Mat83-Preparation and. Evaluation of Experimental Data*, 4th European LS-DYNA Conference, Ulm, Germany, May 22-23, 2003.

[45] Jackson, K.E., *Predicting the Dynamic Crushing Response of a Composite Honeycomb Energy Absorber Using Solid-Element-Based Models in LS-DYNA*, 11st International LS-DYNA Users Conference, Dearborn, Michigan, June. 6-8, 2010.

[46] Vezina, M., Firoozrai. A., *Drop Test into Water and Wave Impact Simulations of a Novel 7-Meter Plastic Boat with LS-DYNA*, 11st International LS-DYNA Users Conference, Dearborn, Michigan, June. 6-8, 2010.

[47] Description of Sample Problems, Introduction to features in LS-DYNA, Livermore Software and Technology Corporation, 2001.

[48] Hallquist, J.O., *LS-DYNA Theory Manual,* Version 971, Livermore Software and Technology Corporation, Livermore CA, May 2006.

[49] Sambamoorthy, B., Tuhin, H., *Characterization and component level correlation of energy absorbing Polyurethane foams using LS-DYNA Material Models*, 3rd European LS-DYNA Conference, Paris, France, June 18-19, 2001.

[50] Reid, J.D., Bielenberg, R.W., *Modeling Rebound of Foam Backed Racetrack Barriers*, 10th International LS-DYNA Users Conference, Dearborn, Michigan, June. 8-10, 2008.

[51] Graf, T., *Advanced FEM Analysis with LS-DYNA-Material Modeling Notes,* October, 2008.

[52] Soden P.D., Hinton M.J., Kaddour A.S., *Lamina Properties, Lay-up Configurations and Loading Conditions for a Range of Fibre-Reinforced Composite Laminates,* Composite Science and Technology 58, pp. 1011-1022, 1998.

[53] Yahoo Groups, *http://tech.groups.yahoo.com/group/LSDYNA/message/33372*, last visited July 2012.

[54] Hirth, A., Du Bois, P., *From Complex 3D-Foam Parts to Ready LS-DYNA Input data in Less Than One Hour,* Examples from Occupant Simulation at Daimler Chrysler, 2001.

[55] Graf, T., *Advanced FEM Analysis with LS-DYNA-Contact Modeling Notes*, October, 2008.

APPENDIX A

ENERGY SPECTRAL DENSITY METHOD

Here, a more detailed explanation which is directly taken from reference [41] is given. The ESD estimate, the properly scaled magnitude of the Fourier Transform of the total shock, is computed at a uniform set of frequencies and displayed as a two dimensional plot of amplitude versus frequency. In determining the ESD estimate, it is important that the Fast Fourier Transform block size is selected such that all the shock event is contained within the block; but excessive noise beyond the effective duration, T_e, of the shock be removed by zero-padding the transform block, i.e., replacing noise data values by zeros. The ESD description is useful for comparing the distribution of energy within the frequency band among several shocks. Figure A-2 displays the ESD estimate for the shock time history of Figure A-1. For an ESD estimate, the percentage of normalized random error in the ordinate is 100%. By either (1) averaging n adjacent ESD ordinates or (2) averaging n independent, but statistically equivalent ESD estimates, the percentage of normalized random error can be decreased by $1/n$.
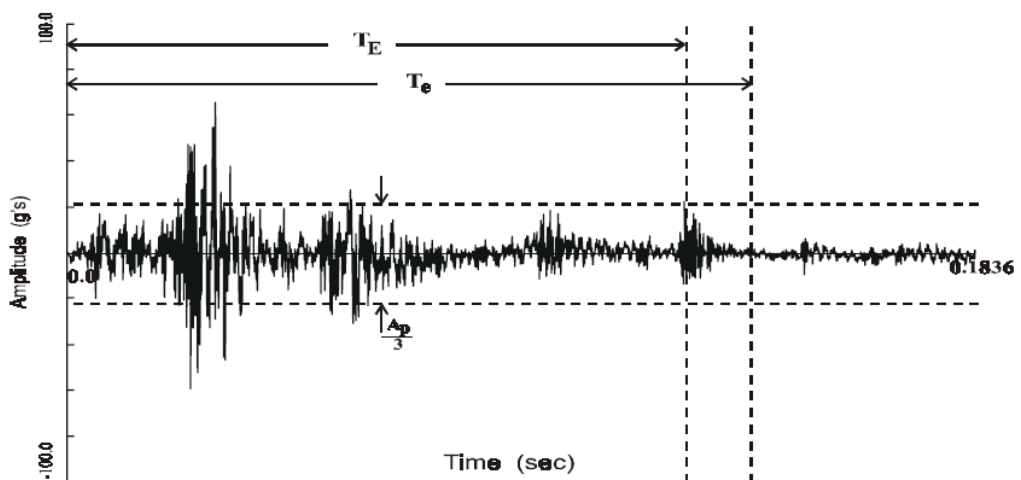

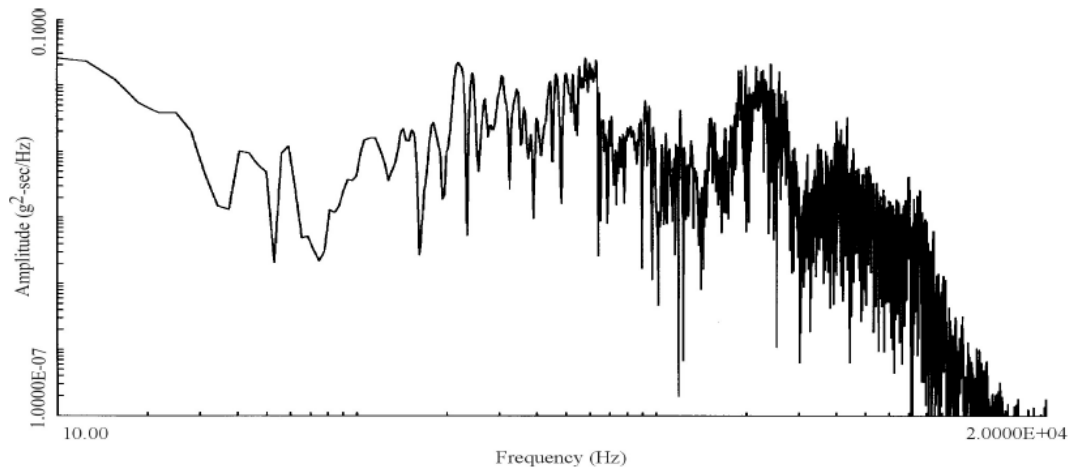
Figure A-1 Sample shock response acceleration maximax SRS.

Figure A-2 Sample shock response acceleration ESD estimate.

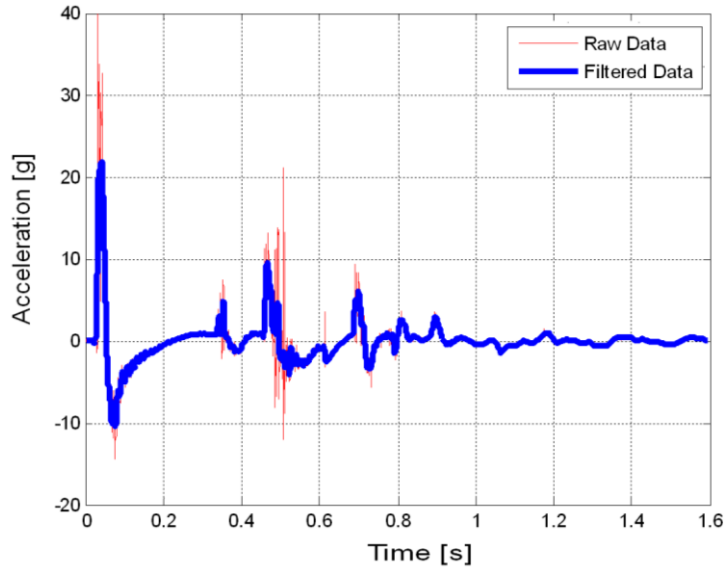# APPENDIX B

EXPERIMENTAL RESULTS
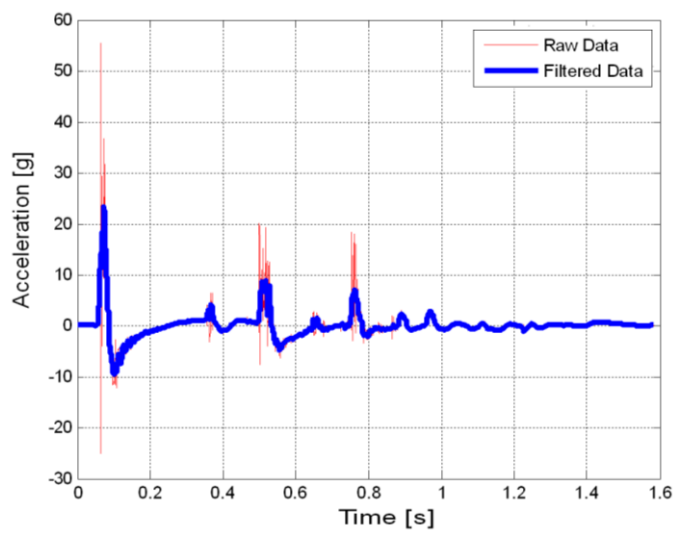

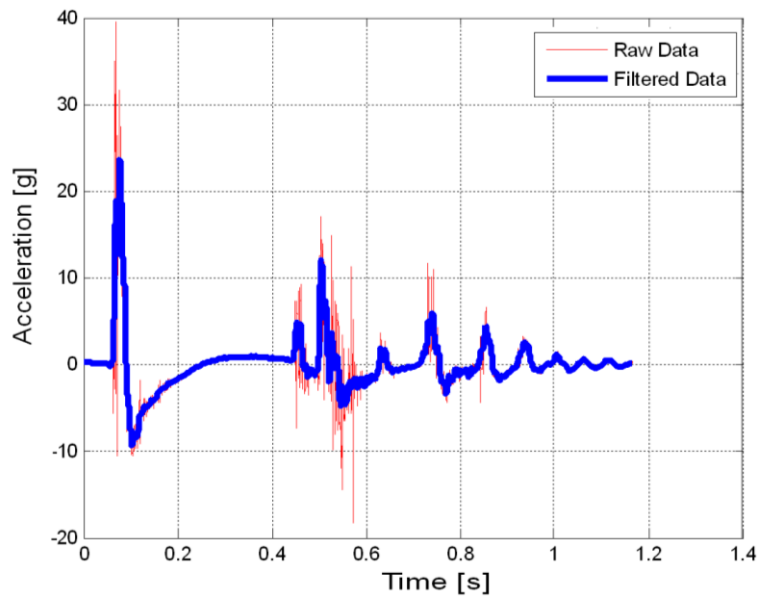Figure B-1 Final drop test number 1

Figure B-2 Final drop test number 2
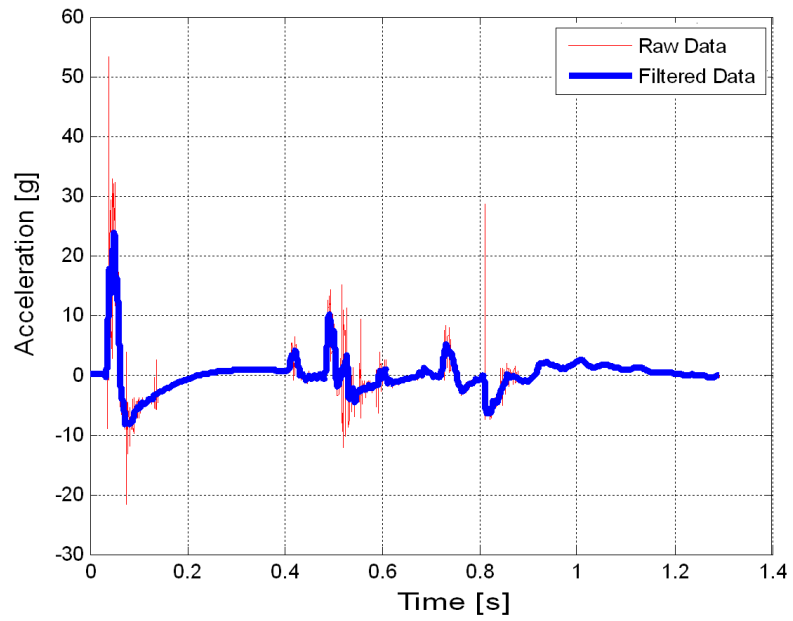
Figure B-3 Final drop test number 3

Figure B-4 Final drop test number 4
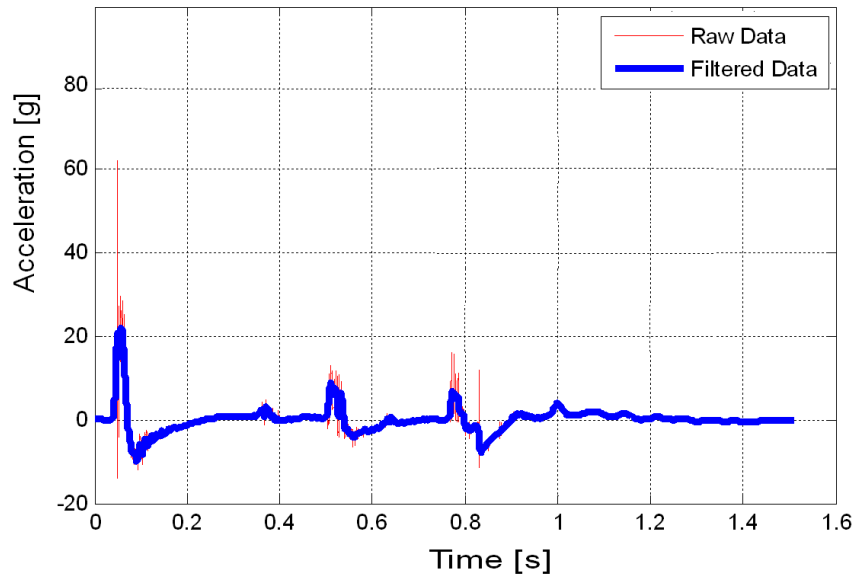
Figure B-5 Final drop test number 5

APPENDIX C

COMPARISON OF DIFFERENT ESD APPROACHES

In this thesis limitation point is determined to be 10 % of total ESD so that signal data which has lower energy than this limit is necessary to be filtered. In the context of the thesis, a study related to different ESD approach is examined too. 5 %, 10 % and 15 % is selected as limitation point. Later, cut-off frequencies and peak acceleration values are compared.

Table C-1 Comparison of cut-off frequencies and peak accelerations

Limitation point	Cut-off frequency [Hz.]	Peak Acceleration [g]
5%	141.6	24.6
10%	108	23.5
15%	43.9	20.3

According to Table C-1 increasing limitation point resulted in decreasing cut-off frequencies as expected. It is also seen in Table C-1 that higher limitation point (15 %) resulted in decreasing the peak acceleration. This is not a desired scenario due to the fact that lower cut-off frequencies often cause to miss the peak acceleration values. On the other hand, lower limitation point (5 %) caused to a minor effect on g levels (1 g). With this study it is shown that 10 % is a logical choice for limitation point.